# STUDY OF THE CHEMISTRY OF THE CARBON FUEL CELL

# ELECTROLYTE AT NEAR CRITICAL CONDITIONS

A THESIS SUBMITTED TO THE GRADUATE DIVISION OF THE
UNIVERSITY OF HAWAIʻI AT MĀNOA IN PARTIAL FULFILLMENT
OF THE REQUIREMENTS FOR THE DEGREE OF

MASTER OF SCIENCE
IN

MECHANICAL ENGINEERING

AUGUST 2012

By
Maider Legarra Arizaleta

Thesis Committee:

Michael J. Antal Jr, Chairperson
Beei-Huan Chao
Lloyd Hihara
Gérard Nihous

# ACKNOWLEDGEMENTS

First and foremost, I'd like to thank my advisor and mentor Dr. Antal for his patience, guidance, generosity, and support through the past two years. It is an honor to be one of his graduate students. I'd also like to acknowledge Lloyd Paredes for providing assistance in the Laboratory.

I'm also grateful to my lab mates Ashley Blitz who started the project and Daniel Kahoonei who ran part of the experiments with me. And finally to Zsuzsanna Czégény for providing the TG-MS analysis.

# TABLE OF CONTENTS

**ACKNOWLEDGEMENTS** ..... i

**LIST OF TABLES** ..... iv

**LIST OF FIGURES** ..... viii

**NOMENCLATURE** ..... ix

**CHAPTER 1. INTRODUCTION AND OBJECTIVE** ..... 1

1.1 Hydrogen Fuel Cells ..... 1

1.2 Direct Carbon Fuel Cells ..... 2

1.2.1 Direct Carbon Fuel Cells with Coal as the Carbon Anode ..... 3

1.2.2 Direct Carbon Fuel Cells with Biocarbon as the Carbon Anode ..... 3

1.3 Objective ..... 4

**CHAPTER 2. LITERATURE REVIEW** ..... 5

2.1 History of Direct Carbon Fuel Cells (DCFC) ..... 5

2.2 Electrolyte ..... 6

2.2.1 Molten Carbonate Fuel Cell (MCFC) ..... 6

2.2.2 Molten Hydroxide Fuel Cell ..... 8

2.2.3 Hybrid Direct Fuel Cell (HDCFC) ..... 10

2.3 Carbon ..... 12

2.3.1 Biocarbon ..... 12

2.4 Aqueous Alkaline Fuel Cell ..... 13

2.5 Bicarbonate/Carbonate chemistry ..... 15

**CHAPTER 3. FUEL CELLS DESIGNS** ..... 20

3.1 First Design ..... 20

3.1.1 Results ..... 23

3.2 Second design ..... 25

3.2.1 Results ..... 26

3.3 Third and fourth design ..... 27

**CHAPTER 4. ELECTROLYTE** ..... 32

4.1 pH and Solubility of the $H_2O$-Hydroxide system ..... 41

4.1.1 Solubility ..... 41

4.1.2 pH ..... 43

4.1.3 Validation of the pH model ..... 45

4.2 pH and Solubility of the H2O-Carbonate system ..... 48
4.2.1 Solubility ..... 48
4.2.2 pH ..... 50
4.2.3 Validation of the pH model ..... 53
4.2.4 Carbonate with a CO2 atmosphere ..... 56
4.3 Boiling point ..... 60
**CHAPTER 5. STUDY OF THE CARBONATE/BICARBONATE CHEMISTRY. ANALYSIS OF THE FINAL EXPERIMENTAL SOLUTION** ..... 63
5.1 Summary of previous work in the Lab ..... 65
5.1.2 Temperature to prevent the formation of the crystals ..... 63
5.2 Determination of the equilibrium constant of the potassium bicarbonate decomposition reaction ..... 65
5.2.1 Apparatus ..... 65
5.2.2 Procedure ..... 66
5.2.3 Reactions and Assumptions ..... 67
5.3 Analysis of the final solution. Calculation of the conversion and equilibrium constant ..... 75
5.3.1 Measure of the final pH ..... 76
5.3.2 TG-MS of the dried crystals ..... 89
5.3.3 Titration of the sample ..... 91
**CHAPTER 6. STUDY OF THE CARBONATE/BICARBONATE CHEMISTRY. THERMODYNAMIC PROPERTIES OF THE BICARBONATE DECOMPOSITION REACTION** ..... 114
6.1 Estimation of the thermodynamic properties with Van't Hoff plot ..... 114
6.2 Comparison with literature thermodynamic data.
6.2.1 Craig, N.C. and Barner and Scheuerman ..... 119
6.2.2 Report Bureau of Mines ..... 124
6.2.3 SUPCRT92 ..... 138
**CHAPTER 7. CONCLUSIONS** ..... 140
7.1 Further work ..... 142

# LIST OF TABLES

**CHAPTER 2. LITERATURE REVIEW**

2.1 Aqueous Alkaline Biocarbon Fuel-Cell Chemical Reactions and Thermodynamics at NTP ..... 14

**CHAPTER 3. FUEL CELLS DESIGNS**

3.1 Conditions and results of the biocarbon fuel cell using a Ni heating plate ..... 23

3.2 Conditions and results of the biocarbon fuel cell using a Ti heating plate..... 24

3.3 Conditions and results of the SS biocarbon fuel cell ..... 26

**CHAPTER 4. ELECTROLYTE**

4.1 Equilibrium constants (extrapolated to zero ionic strength)..... 34

4.2 Solubility in water with the temperature, under 1 atm pressure, units in g/100 g $H_2O$ . 42

4.3 Solubility in mol /$L_{H2O}$ at 20 °C . The solubility of CsOH is given at 30 °C ..... 42

4.4 Solubility of carbonates in water with the temperature, under 1 atm pressure, units in g/100 g $H_2O$ ..... 49

4.5 Solubility of carbonates in water in mol /$L_{H2O}$ at 20 °C ..... 49

4.6 Solubility of bicarbonates in water with the temperature, under 1 atm pressure, units in g/100 g $H_2O$ ..... 49

4.7 Solubility of bicarbonates in water in mol /$L_{H2O}$ at 20 °C ..... 50

4.8 Solubility of carbon dioxide in water at S.T.P/g $H_2O$ with pressure from 12 to 40°C..... 58

**CHAPTER 5. STUDY OF THE CARBONATE/BICARBONATE CHEMISTRY. ANALYSIS OF THE FINAL EXPERIMENTAL SOLUTION**

5.1 Moles of the species before and after the bicarbonate decomposition for case #1 ..... 73

5.2 Moles of the species before and after the bicarbonate decomposition for case #2 ..... 74

5.3 Moles of the species before and after the bicarbonate decomposition for case #3 ..... 75

5.4 Experimental pH of mixtures of potassium carbonate/bicarbonate representing the products of reaction 5.3 at different conversions beginning with a 1 molal initial potassium bicarbonate solution ..... 78

5.5 Experimental pH of mixtures of potassium carbonate/bicarbonate representing the products of reaction 5.3 at different conversions beginning with a 0.1 molal initial potassium bicarbonate solution ..... 78

5.6 Calibration form for the 1st electrode ..... 84

5.7 Calibration form for the 2nd electrode..... 84

5.8 Bicarbonate and Carbonate concentrations of reaction $2HCO_3^-(aq) \leftrightarrow CO_3^{2-}(aq)+CO_2(aq)+H_2O$ for different conversions given an initial 1M bicarbonate solution and accuracies of bicarbonate and carbonate concentrations using the pH –conversion model..... 87

5.9 Determination of the effect of cooling. Set of experiments #1 ..... 88

5.10 Experiment conditions and final pH and conversion. All the experiments have been cooled down by immersion in a bucket of cool water. The initial concentration of the bicarbonate of all experiments is 1M. The final solution of all experiments is colorless. Set of experiments #2..... 89

5.11 Experiment conditions and final pH and conversion. All the experiments have been cooled down by immersion in a bucket of cool water. The initial concentration of the bicarbonate of all experiments is 0.1M. The final solution of all experiments is colorless. Set of experiments #3..... 90

5.12 Mass composition from TG-MS of three known controls ..... 91

5.13 Accuracy of the titration of a 0.4M $K_2CO_3$/0.2M $KHCO_3$ solution (figure 5.15) with the alkalinity method ..... 104

5.14 Accuracy of the titration of a 0.3M $K_2CO_3$/0.4 M $KHCO_3$ solution (figure 5.16) with the alkalinity method ..... 104

5.15 Accuracy of the titration of a 0.1M $K_2CO_3$/0.8 M $KHCO_3$ solution (figure 5.17) with the alkalinity method ..... 105

5.16 Accuracy of the titration of a 0.075M $K_2CO_3$/0.1 M $KHCO_3$ solution (figure 5.18) with the alkalinity method ..... 105

5.17 Accuracy of the titration of a 0.075M $K_2CO_3$/0.1 M $KHCO_3$ solution (figure 5.19) with the alkalinity method ..... 105

5.18 Accuracy of the titration of a 0M $K_2CO_3$/0.25 M $KHCO_3$ solution (figure 5.20) with the alkalinity method ..... 105

5.19 Accuracy of the titration of a 0.125M $K_2CO_3$/0 M $KHCO_3$ solution (figure 5.21) with the alkalinity method ..... 105

5.20 Accuracy of the titration of a 0.4M $K_2CO_3$/0.2 M KOH control solution (figure 5.22) with the alkalinity method ..... 107

5.21 Accuracy of the titration of a 0.3M $K_2CO_3$/0.4 M KOH control solution (figure 5.23) with the alkalinity method ..... 107

5.22 Accuracy of the titration of a 0.2M $K_2CO_3$/0.6 M KOH control solution (figure 5.24) with the alkalinity method ..... 107

5.23 Experiment conditions and results (bicarbonate-carbonate composition and conversion) from the titration curves. All the experiments have been cooled down by immersion in a bucket of cool water. The initial concentration of the bicarbonate of all experiments is 1M. The final solution of all experiments is colorless. Set of experiments #2. ..... 112

5.24 Experiment conditions and conversion calculated from conversion-pH equation and from titration curves. All the experiments have been cooled down by immersion in a bucket of cool water. The initial concentration of the bicarbonate of all experiments is 1M. The final solution of all experiments is colorless. Set of experiments #2. ..... 113

**CHAPTER 6. STUDY OF THE CARBONATE/BICARBONATE CHEMISTRY. THERMODYNAMIC PROPERTIES OF THE BICARBONATE DECOMPOSITION REACTION**

6.1 Experiment conditions, conversion and equilibrium constant ($K_{eq}$) calculated from conversion-pH equation and from titration curves, ionic strength (*I*), activity coefficients and equilibrium constant at zero ionic strength ($K_{eq}{}^{o}$). Set of experiments #2. ..... 118

6.2 Thermodynamic data at 25°C taken from Barner and Scheuerman. Data of the $CO_2$(aq) has been estimated ..... 120

6.3 Thermodynamic data at 25°C taken from Craig. Data of the cp° of carbonate and bicarbonate has been estimated ..... 120

6.4 Thermodynamic data at 300°C taken from Barner and Scheuerman [2]. Data of the $CO_2$ (aq) has been estimated ..... 120

6.5 Comparison of the thermodynamic data at 25°C of our Van't Hoff plot with Barner and Scheuerman . Barner and Scheuerman is calculated with the estimated value of $CO_2$(aq) ..... 123

6.6 Comparison of the thermodynamic data at 300°C of our Van't Hoff plot with Barner and Scheuerman . Barner and Scheuerman is calculated with the estimated value of $CO_2$(aq) ..... 123

6.7 Liquid and gas compositions for Hot-Carbonate Scrubbing system Data taken from Bureau of Mines in the Bulletin 597..... 128

6.8 Gas composition data. The numbers in brackets represent the position in the flow sheet for Hot-Carbonate Scrubbing system..... 129

6.9 Liquid composition data. The numbers into brackets represent the position in the flow sheet for Hot-Carbonate Scrubbing system ..... 129

6.10 Concentration equivalent of carbonate for runs 6A to 8B from Bureau of Mines ..... 137

6.11 Composition data in the spent and regenerated solutions and equilibrium constants of reactions $K_2CO_3 + CO_2 + H_2O \leftrightarrow 2KHCO_3$ and $2KHCO_3 \leftrightarrow K_2CO_3 + CO_2 + H_2O$ ..... 137

6.12 Temperature in *K*, natural logarithm of the equilibrium constants obtained from the Bureau of Mines data and Van't Hoff equation and Gibbs free energies calculated from both equilibrium constants ..... 138

6.13 Thermodynamic properties values of reaction $2HCO_3^- \leftrightarrow CO_3^{2-} + CO_2(aq) + H_2O$ estimated by SUPCRT92 code..... 140

# LIST OF FIGURES

**CHAPTER 2. LITERATURE REVIEW**

2.1 Schematic of tilted DCFC with a molten carbonate electrolyte (designed at Lawrence Livermore National Laboratory) ..... 7

2.2 Schematic of SARA's direct carbon fuel cell design ..... 10

2.3 Schematic of DCFC with a YSZ based solid electrolyte (designed at SRI) ..... 11

2.4 Effect of the temperature on the solubility of potassium carbonate plus potassium bicarbonate in aqueous solution ..... 18

**CHAPTER 3. FUEL CELLS DESIGNS**

3.1 Schematic diagram of the 1st design fuel cell apparatus ..... 22

3.2 Tubing diagram for 1st and 2nd design ..... 22

3.3 Schematic diagram of the 2nd design fuel cell apparatus ..... 25

3.4 Schematic diagram of the 3rd design fuel cell apparatus ..... 28

3.5 Schematic diagram of the 4th design fuel cell apparatus ..... 29

3.6 First fuel cell apparatus ..... 30

3.7 Second fuel cell apparatus ..... 30

3.8 Third fuel cell apparatus ..... 30

3.9 Forth fuel cell apparatus ..... 30

**CHAPTER 4. ELECTROLYTE**

4.1 Chemical and vapor-liquid equilibrium of the hydroxide system ..... 32

4.2 Chemical and vapor-liquid equilibrium of the carbonate system ..... 33

4.3 Mean activity coefficient ($\gamma_{\pm}$) of 1:1 and 1:2 electrolytes as a function of ionic strength (I) calculated with Davies equation ..... 36

4.4 Ion product of water ($pK_w$) as a function of ionic strength (I) at 25 and 50 °C calculated with Davies equation ..... 37

4.5 Henry's constant ($pK_H$) as a function of ionic strength (I) at 25 and 50°C ..... 38

4.6 First acidity constant ($pK_{a1}$) as a function of ionic strength (I) ..... 40

4.7 Second acidity constant ($pK_{a2}$) as a function of ionic strength (I) ..... 41

4.8 pH of Hydroxides of Group I and II vs. Concentration at standard conditions and at 220 °C and 700 psi. Lines pH vs. concentration when activity coefficients are assumed equal to one are indicated. Otherwise, activities are calculated using Davies equation. ..... 44

4.9 pH of a 0.1M and 8M Group I hydroxide vs. Temperature at 1 atm and 250 atm ..... 45

4.10 pH of Potassium Hydroxide vs. Concentration at 25 °C and 1 atm ..... 46
4.11 pH of 0.1 M solution of Potassium Hydroxide vs. temperature at 1 atm..... 47
4.12 pH vs. Concentration of potassium carbonate at 25, 100 and 200 °C ..... 53
4.13 Logarithmic concentration ratio diagram of the carbonate system at room temperature ..... 54
4.14 pH of Potassium Carbonate vs. Concentration from 0.2 to 5M at 22°C and 1 atm ..... 55
4.15 pH of Potassium Carbonate vs. Concentration from 0.2 to 1M at 22°C and 1 atm ..... 56
4.16 pH of 0.1 M solution of Potassium Carbonate vs. Temperature at 1 atm..... 57
4.17 pH of a 1M potassium carbonate solution vs. Temperature(°C) with a $CO_2$ atmosphere ..... 60
4.18 Logarithmic concentration diagram at room temperature and at a constant partial pressure of CO2 of 1 atm ..... 61
4.19 Boiling point of a Potassium Carbonate solution vs. molality ..... 63

**CHAPTER 5. STUDY OF THE CARBONATE/BICARBONATE CHEMISTRY. ANALYSIS OF THE FINAL EXPERIMENTAL SOLUTION**

5.1 Picture of crystal precipitates from the carbon fuel cell showing the presence of nickel carbonate by the greenish tint in the crystals ..... 64
5.2 TG, DTG and MS intensity (–○– water (m/z 18) and –▽– carbon dioxide (m/z 44)) of crystal precipitate from the carbon fuel cell run by the Hungarian Academy of Sciences ..... 65
5.3 Schematic diagram of the pressure vessel in the sand bath. TC is the thermocouple, TR is the temperature regulator, HSL is the low heater switch, HSM is the medium heater switch, HSH is the high heater switch, HSB is the boost heater switch, and AIR is the clean air supply ..... 67
5.4 pH of a 1M potassium bicarbonate solution vs. Temperature (°C)..... 70
5.5 Equilibrium concentrations of $H_2CO_3$, $HCO_3^-$, $CO_3^{2-}$ (M) for an initial 1M potassium bicarbonate solution vs. Temperature (°C)..... 71
5.6 Pressure results of selected pressure vessel experiments using KHCO3 electrolyte heated to 250°C ..... 72
5.7 Keq vs. Conversion of bicarbonate in reaction, $2HCO_3^- \leftrightarrow CO_3^{2-} + CO_2 + H_2O$ ..... 77
5.8 pH vs. conversion . Analytical results for an initial bicarbonate concentration of 1 M , 0.1 M and 0.01 M and experimental results for an initial bicarbonate concentration of 1 M and 0.1M..... 81
5.9 Schematic diagram of the titration apparatus..... 93
5.10 Titration curves to verify standard 0.1 M NaOH (Solution I). ..... 95

5.11 Titration curves to verify standard 0.1 M NaOH (Solution II) ..... 95
5.12 pH vs. Potassium Bucarbonate concentration. ..... 97
5.13 pH vs. Carbonic acid concentration. ..... 98
5.14 pH vs. Concentration Potassium Carbonate (M) ..... 100
5.15 Titration of a 0.4M $K_2CO_3$/0.2M $KHCO_3$ control solution ..... 102
5.16 Titration of a 0.3M $K_2CO_3$/0.4M $KHCO_3$ control solution ..... 102
5.17 Titration of a 0.1M $K_2CO_3$/0.8M $KHCO_3$ control solution ..... 102
5.18 Titration of a 0.075M $K_2CO_3$/0.1M $KHCO_3$ control solution. Concentration titrant [HCl]=0.122M ..... 102
5.19 Titration of a 0.075M $K_2CO_3$/0.1M $KHCO_3$ control solution. Concentration titrant [HCl]=0.096M ..... 103
5.20 Titration of a 0 M $K_2CO_3$/0.25M $KHCO_3$ control solution ..... 103
5.21 Titration of a 0.125M $K_2CO_3$/0 M $KHCO_3$ control solution ..... 103
5.22 Titration of a 0.4 M $K_2CO_3$/0.2 M KOH control solution ..... 106
5.23 Titration of a 0.3 M $K_2CO_3$/0.4 M KOH control solution ..... 106
5.24 Titration of a 0.2 M $K_2CO_3$/0.6 M KOH control solution ..... 106
5.25 Titration curve of experimental run #2 ..... 109
5.26 Titration curve of experimental run #3 ..... 110
5.27 Titration curve of experimental run #4 ..... 110
5.28 Titration curve of experimental run #5 ..... 110
5.29 Titration curve of experimental run #8 ..... 110
5.30 Titration curve of experimental run #10 ..... 111
5.31 Titration curve of experimental run #11 ..... 111

**CHAPTER 6. STUDY OF THE CARBONATE/BICARBONATE CHEMISTRY. THERMODYNAMIC PROPERTIES OF THE BICARBONATE DECOMPOSITION REACTION**

6.1 Van't Hoff plot for reaction 2 $HCO_3^-(aq) \leftrightarrow CO_3^{2-}(aq)+CO_2(aq)+H_2O$ ..... 119
6.2 Flow sheet for Hot-Carbonate Scrubbing system ..... 126

# NOMENCLATURE

| | |
|---|---|
| $a_i$ | Activity of component *i* |
| $c_p$ | Molar heat capacity |
| CAL | Calibration Standard |
| CCV | Continuing Calibration Verification Standard |
| CVS | Calibration Verification Standard |
| DCFC | Direct Carbon Fuel Cell |
| DI water | Deionized water |
| ΔG | Gibbs free energy change |
| $\Delta_f G^o$ | Gibbs free energy of formation |
| ΔH | Enthalpy change |
| $\Delta_f H^o$ | Enthalpy of formation |
| HDCFC | Hybrid Direct Carbon Fuel Cell |
| I | Ionic strength |
| [i] | Concentration of component *i* |
| $Kj^o$ | Equilibrium constant of reaction j (also called Extrapolated zero ionic strength constant of reaction j) |
| Kj | Equilibrium constant at finite ionic strength of reaction *j* |
| L | Enthalpy increase of the evaporation of 1 mol of water at temperature T |
| $L_B$ | Latent heat at the boiling point $T_B$ |
| MCFC | Molten Carbonate Fuel Cell |
| MVS | Method Verification Standard |
| $n_o$ | Initial moles |
| $n_f$ | Final moles |
| OCV | Open Circuit Voltage |

| | |
|---|---|
| P | Pressure or Phenolphtalein Alkalinity |
| pKj | Negative decimal logarithm of equilibrium constant of reaction *j* (-log $K_j$) |
| R | Gas constant (8.314 J/molK) |
| ΔS | Entropy change |
| SCC | Short Circuit Current |
| std.c.f | Standard(32 °F, 14.7 psi, dry gas) cubic feet per hour |
| T | Temperature or Total Alkalinity |
| $T_B$ | Boiling point |
| V | Volume or Voltage |
| YSZ | Yttria Stabilized Zirconia |
| $z_i$ | Charge of ion *i* |
| $\nu_{i,j}$ | Reaction stoichiometric coefficient of component i, |
| $\gamma_i$ | Activity coefficient of component *i* |
| $\gamma_{\pm}$ | Mean activity coefficient |

# CHAPTER 1. INTRODUCTION AND OBJECTIVE

## 1.1 Hydrogen Fuel Cells

World demand for energy is continuously increasing. The *World Energy Outlook* from the OECD's International Energy Agency (IEA) sets out the present situation and also predicts scenarios if the governments were to take no new initiatives bearing on the energy sector, beyond those already adopted by mid-2009 [1]. According to the *World Energy Outlook 2009* ,from 1980 to 2007 total world primary energy demand grew by 66%, and to 2030 the world demand for energy is projected to grow at a slightly lesser rate (40%, average 1.5% per year, from 503 EJ to 703 EJ). Electricity growth is almost double this, and is projected to grow 76% from 2007 to 2030 (growing at average 2.5% per year from 16,429 TWh to 28,930 TWh). Therefore, the need for developing new power generation technologies is increasing as well. One of these technologies is fuel cell (FC) technology.

In recent years, most fuel cells research programs have concentrated on fuel cells using hydrogen as a fuel. However, the hydrogen fuel cell presents problems pertaining to system sustainability and cannot be implemented on a global scale. The main problem of the global implementation of the hydrogen fuel cell is the insufficient reserves and resources. The present world production capacity for hydrogen can barely keep up with the demand by synthetic fertilizer production and petroleum hydrogenation[2]. Besides, there are also insufficient reserves and resources for both catalysts and corrosion resistant materials for the fuel cell [3].

The problem of insufficient reserves and resources arises again in the hydrogen production process. Hydrogen is mainly produced by methane reforming and water electrolysis. Hydrogen can also be produced from a reforming process of carbonaceous materials (coal, oil, natural gas, and biomass). On the one hand, this reforming process requires extensive gas cleanup as well as scarce catalyst materials. On the other hand, the process leads to a final gas product that is a mixture of hydrogen and carbon monoxide gases. 60 % of the energy content of the fuel is thrown away because most fuel cells cannot tolerate the CO component of the fuel. Besides the lack of resources, the hydrogen fuel cell also presents safety problems as the hydrogen has fire and explosion hazards.

Another type of fuel cell, which can use easily available and cheap fuel sources, should be considered. The direct carbon fuel cell (DCFC ), in which the chemical energy of carbon is directly converted into

electrical energy, without the reforming process, is one of the most promising alternative energy sources that doesn't give any of the previous problems regarding system sustainability [4].

## 1.2 Direct Carbon Fuel Cells

The overall reaction in a DCFC is the direct oxidation of carbon to $CO_2$:

$$C + O_2 \rightarrow CO_2$$

The thermodynamic efficiency of the electrochemical oxidation of the carbon even slightly exceeds 100% and is almost independent of temperature[5, 6]. This thermodynamic efficiency results from the positive change in entropy ($\Delta_r S^o$ =2.86 J/(K mol)). As a result, the standard Gibbs free energy change ($\Delta_r G^o$=-394.4kJ/mol at normal temperature and pressure (NTP 298.15 K, 0.1 MPa)) for the overall cell reaction is slightly larger than the standard reaction enthalpy change ($\Delta_r H^o$=-393.5kJ/mol), and the thermodynamic efficiency defined as $\eta_{th}$= $\Delta_r G^o$/ $\Delta_r H^o$ leads to a value slightly above 100%. In addition, the change in entropy is so small that this efficiency is not significantly affected by increasing the temperature[5, 6]. For example, at 600 °C, the Gibbs free energy is -395.5 kJ/mol and the standard enthalpy change is -394.0 kJ/mol.

As the theoretical standard potential [5] depends on the Gibbs free energy, by equation $E° = -\Delta_r G°/nF = -\Delta_f G°_{CO2}/nF$ with reactants and products in their standard states . This standard potential does not see a change if we go up to temperatures as high as 1100 K.

- At 298 K: $\Delta_f G°_{CO2}$=-394.4 kJ/mol, E° = 1.02 V
- At 1100 K:$\Delta_f G°_{CO2}$=-396.0 kJ/mol, E° = 1.02 V

Besides, the activities (chemical potentials) of both reactant carbon and the product carbon dioxide are fixed, and this results in a stable carbon anode potential during practical cell operation that is independent of position or extent of fuel conversion[7, 8]. In theory, this allows full conversion of the fuel in a single pass, in a well-designed cell with sufficient airflow.

### *1.2.1 Direct Carbon Fuel Cells with Coal as the Carbon Anode*

The DCFC uses solid carbon as fuel. It can use petroleum coke, coal coke, pyrolysed hydrocarbons, as well as biomass carbon (charcoal) for fuel. Most of the research done in DCFC uses coal as the carbon anode. The coal presents the advantage of being the most economic and most abundant fossil resource on the earth and particularly in North America. Presently, it is the world's leading fuel for electricity generation. The world coal consumption accounted for 27 % in 2006 and it is predicted to account for 28 % of the world's increase primary energy consumption by 2030, which means that coal will still be the main energy source in the near future[9]. However, most energy reserves of coal remain under-used , and copious amounts of greenhouse gasses are produced by conventional coal-fired plants. Improving efficiency in conversion and use of fuel is of chief importance in reducing expenses and pollution, and in prolonging resources.

A direct carbon fuel cell offers one of the most effective alternatives due to its significantly higher operating efficiency (more than double ) compared with conventional coal-fired power plants [10, 11]. Besides, the carbon fuel cell has low–$CO_2$ production rates emissions compared with conventional power plants. In principle, the off-gas can be pure carbon dioxide, which can be directly collected for industrial use[10] or sequestration leading to substantial cost reductions associated with $CO_2$ capture and storage.

Lots of research in DCFC using coal as an anode has been done and the carbon fuel cell is still being developed. However, this carbon fuel cell has to overcome corrosion problems (in Molten Electrolyte Fuel Cells) or efficiency problems (In Solid Oxide Fuel Cells) to be implemented on a global scale.

### *1.2.2 Direct Carbon Fuel Cells with Biocarbon as the Carbon Anode*

The latest idea in the direct carbon fuel cells is the Biocarbon fuel cell which is opening a new door in the DCFC research as biocarbon (carbonized charcoal) has shown better performance than coal in the carbon fuel cell due to its high reactivity and electrical conductivity- desired properties in the carbon fuel cell, it is inexpensive, it is easy to store and transport and its combustion does not contribute to climate change.

## 1.3 Objective

The research in this thesis was performed at the Hawaii Natural Energy Institute based at the University of Hawaii at Manoa; two principal foci were addressed: (1) to design and investigate the performance of an aqueous-alkaline biocarbon fuel cell that generates power at temperatures ~500 K, (2) to determine the electrolyte chemistry at conditions similar to those of the fuel cell.

Our Lab has been working in the first focus, the design of an aqueous-alkaline biocarbon fuel cell, since 2000. In 2007 T. Nunoura et al. [12] published the first paper in this topic. They studied the thermodynamics of the anode and cathode reactions and showed the experimental results of a first-generation, aqueous-alkaline biocarbon fuel cell built in the Lab. They showed that an aqueous-alkaline fuel cell operating at 518 K and 35.8 bar was able to realize an open-circuit voltage of 0.57 V, a short circuit current density of 43.6 $mA/cm^2$ and a maximum power of 19 mW, using a 6M KOH/ 1 M LiOH mixed electrolyte with a catalytic silver screen/platinum foil cathode and an anode composed of 0.5 g of compacted corncob charcoal previously carbonized at 950°C. A second paper published by M. Antal and G. Nihous [13] proved that the reactions of a moderate temperature aqueous-alkaline biocarbon fuel cell may be favored at temperatures as high as 300 °C and the carbonate electrolyte may be as effective as the hydroxide electrolyte.

Based on these promising findings, the work in the biocarbon fuel cell continued. Different fuel cells were designed and built to overcome the problems that arose. The fuel cell working with high concentrations of potassium carbonate solution as electrolyte showed the best performance. However, unexpected crystals determined by TG-MS as potassium bicarbonate appeared in this fuel cell that caused our research focus to take another direction: The study of the electrolyte. We decided to focus on the carbonate/bicarbonate chemistry and the understanding of the formation of these potassium bicarbonate crystals. To study the formation of the crystals, a “tubing bomb” that can stand pressures as high as 2000 psi and can be quickly heated in a sand bath was built. Previous literature [14] indicates the decomposition of dry bicarbonate into carbonate and $CO_2$. This research focuses on the thermodynamics of this decomposition reaction in solution at conditions close to the fuel cell conditions. By determining the equilibrium constant, the thermodynamic properties (enthalpy, entropy and Gibbs free energy) of the bicarbonate decomposition reaction and the temperature at which the potassium bicarbonate in solution will completely decompose, we can determine the allowable operation temperature for the fuel cell.

# CHAPTER 2. LITERATURE REVIEW

## 2.1 History of Direct Carbon Fuel Cells (DCFC)

In 1842, Grove developed the first fuel cell (which he called the *gas voltaic battery*), which produced electrical energy by combining hydrogen and oxygen [15]. In 1896, Dr. William W. Jacques built the first Direct Carbon Fuel Cell (DCFC) which gives high potentials. He obtained a current density as high as 100 mA/cm$^2$ using hydroxide melt as an electrolyte at temperatures between 400 °C and 500 °C [16]. However, the hydroxide turned to carbonate because of the absorption of the $CO_2$ by the hydroxide melt and the performance deteriorated with time.

For the next 40 years European researchers attempted to duplicate Dr. Jacques's results but without any success. In 1958, hydroxide-melt electrolytes were completely replaced by molten-carbonate electrolytes by Boers and Ketelaar [17, 18]. The molten carbonate cells gained interest against the molten hydroxide cells among the researchers and the use of a molten hydroxide electrolyte was ignored by DCFC researchers.

The next major find in DCFC came in 1979 during the oil crisis. Dr. Robert Weaver from Stanford Research Institute (SRI) was successful in proving that electrochemical oxidation of carbon is feasible. He found and confirmed that at temperatures near 700 °C, the electrochemical oxidation of carbon in their molten carbonate fuel cell proceeded completely to carbon dioxide, thus providing full release of the energy of the carbon [19]. Dr. Weaver and his research group tested different types of carbons in their molten carbonate DCFC. Their results demonstrated that a coal derived anode was much more electrochemically active than a graphite anode.

In 1987 Dr.Vutetakis [20] demonstrated a new approach towards electrochemical oxidation of coal at higher temperatures. The main difference with previous DCFC studies was that dispersed, granulated carbon was used as fuel with molten carbonate as electrolyte. His configuration did not yield higher current densities due to heavy chemical consumption of carbon by $CO_2$, which resulted in low carbon utilization efficiency. Funding for DCFC research was suspended temporarily until mid-1980s as the oil prices went down. In the recent years , different research institutions and companies are speeding up research and development into DCFCs. Different designs of DCFC are being researched at the Lawrence Livermore National laboratory (LLNL), Cell Tech Power LLC and SRI International simultaneously with SARA.

The recent molten carbonate carbon fuel cell of Cooper, Cherepy and coworkers from LLNL [21] showed the most promising results. Their cell worked at 800 °C and delivered current densities of 50-125 mA/cm$^2$. They used nine different carbons and realized that their highest discharge rates (100-125 mA/cm$^2$ at 0.8 V) were obtained with biocarbon anodes.

## 2.2 Electrolyte

According to the type of electrolyte used, the DCFC can be grouped into three broad categories.

**2.2.1 Molten Carbonate electrolyte** [18, 21-27]: The carbon is fed to a molten carbonate fuel cell (MCFC)

**2.2.2 Molten hydroxide electrolyte** [16, 28-30]: The carbon is used in the form of sacrificial anode in a molten hydroxide bath.

**2.2.3 YSZ-based Solid Electrolyte**[31-39]: DCFCs with The Yttria-Stabilized Zirconia (YSZ) design combines advances in the solid oxide and molten carbonate fuel cell technologies. The fuel cell is called "Hybrid Direct Fuel Cell". The solid carbon fuel is supplied to anode/ solid oxide electrolyte interface

The chemistry in the three groups- molten carbonate fuel cell, molten hydroxide fuel cell and Hybrid Direct Fuel Cell - and the chemistry in an our aqueous alkaline fuel cell are presented.

### *2.2.1 Molten Carbonate Fuel Cell (MCFC)*

Molten carbonate electrolytes are very good for DCFCs because of their high conductivity, their good stability when $CO_2$ is present, and the appropriate melting temperature for this application. Molten Carbonate Fuel Cells (MCFC) have widely used a eutectic molten carbonate electrolyte composed of a mixture of lithium carbonate ($Li_2CO_3$) and potassium carbonate ($K_2CO_3$) as electrolyte.
Electrochemical reactions involved with molten carbonate DCFC proposed recently by Cooper [21] are shown below.

Anode $C + 2CO_3^{2-} \rightarrow 3CO_2 + 4e^-$
Cathode $O_2 + 2\,CO_2 + 4e^- \rightarrow 2CO_3^{2-}$
Overall $C + O_2 \rightarrow CO_2$

Figure 2.1 shows a tilted molten carbonate fuel cell designed at Lawrence Livermore National Laboratory (LLNL) by Cooper et al.[10] The anode was composed of a paste of highly reactive carbon particulate fuel in a molten carbonate with a current collector of foam nickel. Cathode was a compressed foam nickel. Activation of the cathode catalyst was done by thermal treatment in air followed by lithiation to form a compact layer of nickel oxide (NiO). Anode and cathode were separated by several layers of Zirconia felt. The cell operates with carbon (anode side) and air/$CO_2$ mixture (cathode side). Oxygen in the air reacts with $CO_2$ to produce carbonate ions which oxidize the carbon particles at the anode. This tilted design allowed the excess electrolyte to drain from the cell, thus avoiding flooding of the cathode.

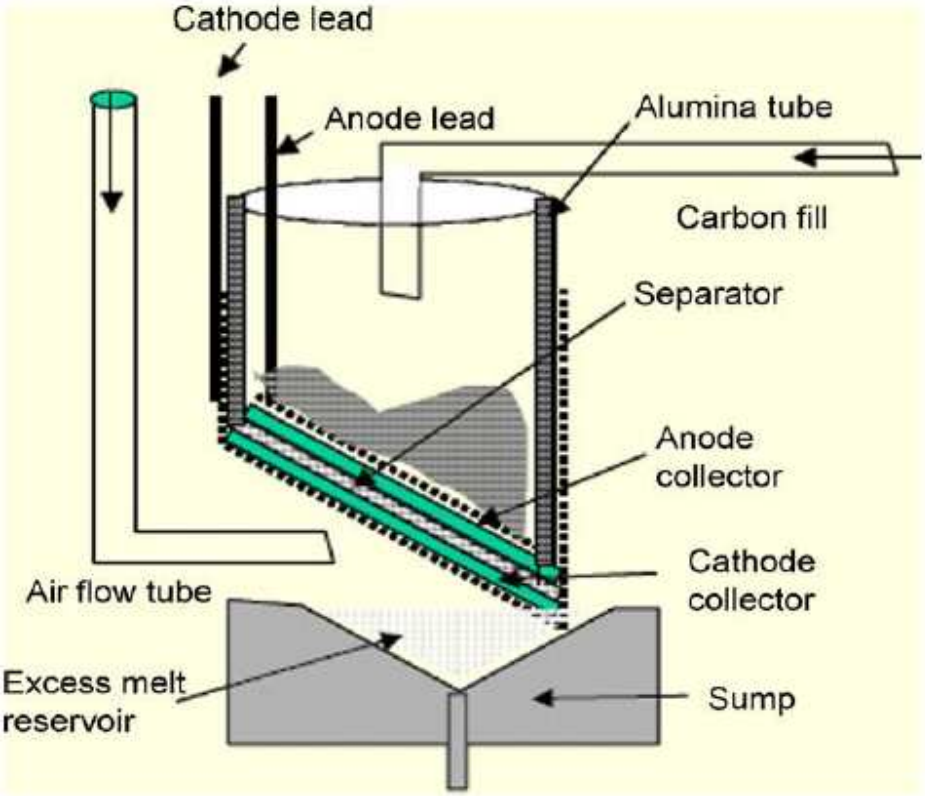


**Figure 2.1 Schematic of tilted DCFC with a molten carbonate electrolyte (designed at Lawrence Livermore National Laboratory)[10] [D.Cao et al.]**

This cell operates around 800˚C. It delivers current densities between 50 to 125 mA/cm$^2$ at a cell voltage of 0.8V [10, 21]. The main problems in the MCFC are the corrosive nature of the molten carbonates at the elevated temperatures used and durability and ash build-up in the electrolyte [10, 21]. The high temperatures cause degradation or failure of the fuel cell when it is run for a long period of time due to corrosion. Therefore, there are several design constraints, and expensive materials are required for the

electrodes and the housing. Another problem expected was the competition of the Boudouard reaction $C+CO_2 \rightarrow 2CO$ with the anodic reaction. Early researchers incorrectly assumed that the anodic reaction would be controlled by the equilibrium of the Boudouard reaction $C+CO_2 \rightarrow 2CO$. Although this equilibrium is expected at temperatures above 700 °C, it has been shown that molten carbonate oxidizes electrochemically in the 700-900 °C range to $CO_2$, yielding four electrons per carbon atom[5, 19, 20, 40]. However, if the carbon anode in the anode compartment is not polarized, for example, during standby or at point on the anode remote from current flow, then Boudouard equilibrium proceeds.

### *2.2.2 Molten Hydroxide Fuel Cell*

After Dr. William Jacques [16] successfully demonstrated the first DCFC, using molten hydroxide as the DCFC electrolyte , the molten hydroxide fuel cell has been discarded for a long time due to the carbonate formation as a byproduct. The molten hydroxide electrolyte present the advantages of higher ionic conductivity [41] and higher electrochemical activity of carbon i.e. higher anodic oxidation rates and lower overpotentials [42] compared to the molten carbonate electrolyte, therefore, the operating temperatures of the fuel cell can be lowered and consequently reduce the corrosion problem. Electrochemical reactions involved with the molten hydroxide DCFC are shown below.

Anode $C + 4OH^- \rightarrow CO_2 + 2H_2O + 4e^-$
Cathode $O_2 + 2H_2O + 4e^- \rightarrow 4OH^-$
Overall $C + O_2 \rightarrow CO_2$

In 2004, Zecevic et al. [28]brought up again the molten hydroxide electrolyte fuel cell again. Zecevic et al. described in their paper a patented medium-temperature molten hydroxide DCFC (around 600°C), which overcomes the historical carbonate formation due to the absorption of $CO_2$ by the hydroxide melt. Conversion of hydroxides into carbonates may be considered either as a chemical process represented by:

$2OH^- + CO_2 \rightleftharpoons CO_3^{2-} + H_2O$

Or as an electrochemical process taking place at the carbon anode and given by:

$C + 6OH^- \rightleftharpoons CO_3^{2-} + 3H_2O + 4e^-$

as proposed by Goret and Tremillon [42]. They investigated this process experimentally and proposed the mechanism in which the reaction $C+6OH^- \rightleftharpoons CO_3^{2-}+3H_2O+4e^-$ consists of two steps: a fast chemical step followed by a slow electrochemical step given by reactions:

$6OH^- \rightleftharpoons 3O^{2-} + 3H_2O$ (Fast)
$C + 3O^{2-} \rightleftharpoons CO_3^{2-} + 4e^-$ (Slow)

The rate of carbonate formation depends upon $O^{2-}$ and water concentration. The prevention or significantly reduction of carbonate formation was made by ensuring a high water content of the electrolyte which causes reactions $2OH^- + CO_2 \rightleftharpoons CO_3^{2-}+H_2O$ and $6OH^- \rightleftharpoons 3O^{2-} + 3H_2O$ to shift backward thus decreasing the carbonate formation. The high water content in the melt is simply achieved by maintaining a humid atmosphere above the melt (patent pending). Another means to prevent or reduce conversion of hydroxide melt into carbonate is based on the use of some oxide additives. A beneficial effect of MgO was already proved by Jacques [16] and could be explained via changes of acid-base properties of the hydroxide melt [42] .The effects of other oxides $SiO_2$, ZnO and MgO as well as oxyanions such as pyrophosphate and persulfate in preventing conversion of hydroxides into carbonates [28] is supposed to help but will need experimental verification.

Figure 2.2 depicts the Zecevic et al. [28]DCFC with a sodium hydroxide electrolyte designed at Scientific Applications and Research Associates (SARA). Zecevic et al. used a simple design in which the cell cylindrical container also serves as the air cathodes which was generally made of nickel foam lined steel or FeTi because of their good catalytic activity. A cylindrical graphite rod acts as the anode and the fuel, which was immersed into molten sodium hydroxide electrolyte contained in the cylindrical container. Humidified air was fed to cell from the bottom of the container in order to reduce the degradation of the electrolyte.

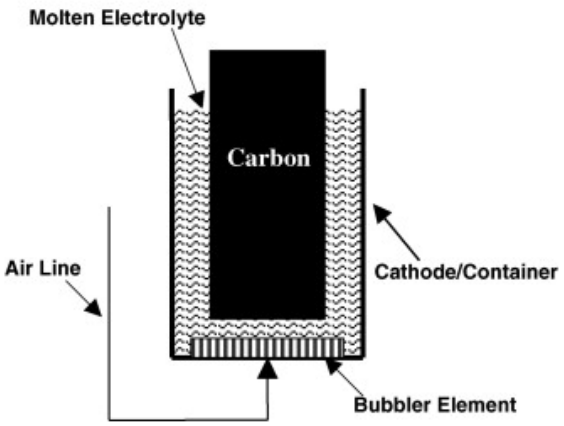


**Figure 2.2 Schematic of SARA's direct carbon fuel cell design [28][Zecevic *et al.* (2004)]**

Operation temperature of this DCFC was 630 °C. Maximum current density obtained exceeded 250mA/cm$^2$ at an operating voltage between 0.75 and 0.85V. The low temperature operation allows the use of less expensive materials for cell. All the merits mentioned above can be accomplished only if carbonate formation problem is overcome. However, the major drawbacks include eliminating the carbonate formation and finding suitable materials that survives the corrosive molten hydroxide electrolyte.

### *2.2.3 Hybrid Direct Fuel Cell (HDCFC)*

The hybrid direct carbon fuel cell (HDCFC) combines the molten carbonate fuel cell and solid oxide fuel cell technology. The cell consists of a solid Yttria Stabilized Zirconia (YSZ) electrolyte layer along with a liquid electrolyte which comprises a mixture of lithium carbonate ($Li_2CO_3$) and potassium carbonate ($K_2CO_3$)[10, 43]. One of the advantages of the HDCFC is the reduction of the possibility of the cathode corrosion in the carbonate because of the separation of the cathode and the anode in comparison with the molten carbonate fuel cell. The other advantage is that using air in the cathode chamber eliminates $CO_2$ circulation. The following mechanism was reported by Chuang (2006) [44]

Anode $C + 2O^{2-} \rightarrow CO_2 + 4e^-$
Cathode $O_2 + 4e^- \rightarrow 2O^{2-}$
Overall $C + O_2 \rightarrow CO_2$

Figure 2.3 shows the schematic of DCFC with a YSZ based solid electrolyte[10] patented by Balachov et al. at SRI International [45, 46].Its components include a U-tube consisting of a metal mesh cathode current collector, a cathode layer of Lanthanum Strontium Manganate (LSM), an electrolyte later, and a metal mesh anode current collector from inner to outer portion of the tube. This structure was immersed into a mixture of molten carbonate electrolyte and carbon particles. When this mixture is stirred causing a flow mode, the fuel cell operates better since there is an increase contact between the carbon particles and the anode current collector, which enhances mass transport.

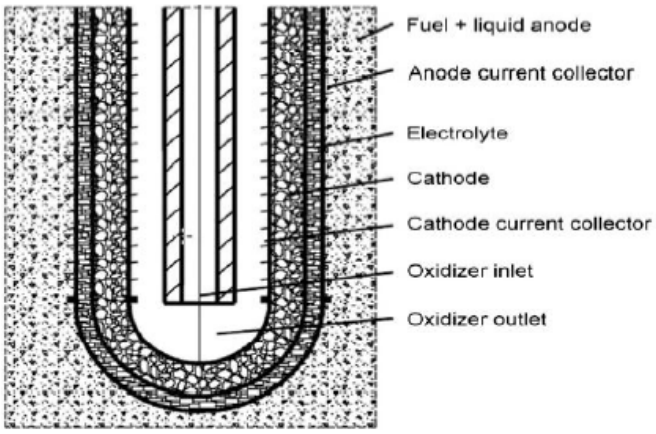


**Figure 2.3 Schematic of DCFC with a YSZ based solid electrolyte (designed at SRI) [10] [D.Cao *et al.* ]**

The cell generates an open circuit voltage (OCV) of 1.15- 1.23 V at 800 °C and a peak density of 50 $mW/cm^2$. This DCFC was intended to be used as a high energy density battery for military application [10]. The issues for DCFC using solid electrolyte include poor contact between the carbon anode and the electrolyte and the high operation temperature, which may lead to formation of CO due the reverse Boudouard reaction, $C+CO_2 \rightarrow 2CO$ [39]that lowered the DCFC efficiency.

In summary, the four fuel cells types present some advantages and disadvantages. The most encouraging results have been given by the molten carbonate fuel cells. Since DCFC technology is still at the beginning stage, serious efforts are required to address many challenges, both in the fundamental and the engineering aspects. The improvement of these cells hasn't just been made by changing the electrolyte but also other approaches have been made: like different designs and different carbons used as the electrode. The carbon used in the carbon fuel cell also plays an essential role. However, there are

few studies in the carbon performance in a carbon fuel cell; some of these findings are summarized in the next pages.

## 2.3 Carbon

The DCFC uses solid carbon fuel as the consumable anode in the DCFC. The carbon is an amazing element whose physical properties vary widely with the allotropic form. The three relatively well-known allotropes of carbon are amorphous carbon, graphite, and diamond.

Graphite, for example, is an electrical conductor but it is scarce, costly and inert while diamond, another allotrope, has a very low electrical conductivity, and it is also scarce, inert and costly. Coal, on the other hand, consists in amorphous carbon with various organic and some inorganic compounds. It is cheap and abundant but it is not a good electrical conductor and it has low reactivity. Vielstich explained that a high temperature was needed because of the low reactivity of coal [6]. This is the cause of the need of high temperatures on the carbon fuel cells, which lead to the problems described previously of the electrolyte. Bockris and Srinivasan [47] concluded that carbon fuel cells are impractical because of the low electrical conductivity of the coal and the cost and scarcity of the graphite. However, when biocarbon started to be tested as the consumable carbon anode of the carbon fuel cell, it showed higher reactivity and conductivity and Biocarbon fuel cells gained attention among the researchers.

### *2.3.1 Biocarbon*

The word Biocarbon refer to both charcoals and carbonized charcoals (Charcoals that have endured heat treatment temperatures (HTT) above 800 °C) . Charcoal is defined as a residue of solid nonagglomerated organic matter , of vegetable or animal origin, that results from carbonization by heat in the absence of air at a temperature above 300 °C [48]. Limited research has been done on Biocarbon fuel cells but they show encouraging results. Cooper et. al tested nine different carbons and realized that their highest discharge rates (100-125 $mA/cm^2$ at 0.8 V) were obtained with biocarbon anodes.

Mochidzuki et al. [49] showed the effects of the carbonization temperature on the properties of carbonized charcoal particles, including their electrical resistivity in a packed bed subject to compressive force, their chemical and physical composition. They proved that low electrical resistivities are manifest by many different charcoals after carbonization at a heat treatment temperature of 950 °C. They

visualize “carbonized charcoal to be a macromolecular, cross linked, three-dimensional, aromatic structure replete with conjugation and π bonds that facilitate the movement of electrons, as well as nanopores , and micromolecular cracks” [49]. They showed that a packed bed of carbonized charcoal particles subject to a compressive pressure (ca. 8MPa) can be a good electrical conductor ($\sigma$ <0.2 $\Omega$·cm) having an electrical resistivity comparable to that of a compact packed bed of graphite particles. In addition to this, a compact carbonized charcoal packed bed can have a very large surface area and is extremely reactive with a volumetric energy density comparable to conventional liquid fuels, and is competitive in prize with fossil fuels such as gasoline and natural gas.Therefore, Mochidzuki et al. concluded that compact packed beds of carbonized charcoal have promising applications as electrodes and consumable anodes in Biocarbon fuel cells and batteries.

In summary, in spite of the low electrical conductivity of the coal and the cost and scarcity of the graphite, a carbon fuel cell can be possible using carbonized charcoal as the carbon electrode as it has proved high reactivity to its high surface area [50-54] and high electrical conductivity[49] . As a fuel, charcoal offers many benefits. The charcoal can be produced from biomass in yields that approach the theoretical limit set by thermodynamics [50, 55-60], it is inexpensive to produce and easy to store and transport. An established infrastructure to deliver compacted charcoal beds with high-energy density is readily available to consumers worldwide[49]. When electrochemical combustion is performed, charcoal does not burden the atmosphere with $CO_2$ emissions, and does not contribute to climate change. In contrast with fossil fuels, charcoal has no mercury, almost no sulfur, low nitrogen, and produces very little ash[50, 57, 58, 60]. It has high electrical conductivity[49], a high surface area, and contains many bonds that enable it to be very reactive at relatively modest temperatures[50-54]. Compared to liquid fuels, charcoal has a high-energy density [49]. According to the protocol of the standard UN self-heating test [61], charcoal fines self-ignite at 140 °C. Carbonized charcoal particles burn steadily at 240 °C and higher in boiling water that contains dissolved oxygen. These findings suggest that biocarbons could suffer electrochemical combustion near 200 °C. For these reason we have a keen interest building an Aqueous- alkaline Biocarbon fuel cell that works at these temperatures.

## 2.4 Aqueous Alkaline Fuel Cell

As far as we know, no detailed mechanism of the anodic and cathodic reaction of the aqueous alkaline fuel cell is reported. Previous work in the Lab done by Nunoura et al. [12] and Antal and Nihous [13], however, studied the thermodynamics and reported a promising temperature range for the operation of

the aqueous alkaline fuel cell. Table 2.1 contains the independent reactions that can take place in the aqueous-alkaline biocarbon fuel cell and the thermodynamical data

**Table 2.1 Aqueous Alkaline Biocarbon Fuel-Cell Chemical Reactions and Thermodynamics at NTP.**

| Nº | Reaction | E° [V] | ΔG [kJ/mol] | ΔH [kJ/mol] | ΔS [J/K mol] |
|---|---|---|---|---|---|
| 1 | $C + 4OH^- \leftrightarrow CO_2 + 2H_2O + 4e^-$ | 0.621 | -240 | -45.2 | 391 |
| 2 | $O_2 + 2H_2O + 4e^- \leftrightarrow 4OH^-$ | 0.401 | -155 | -348 | -388 |
| 3 | $CO_2(g) + H_2O \leftrightarrow CO_2(aq) + H_2O$ | | 8.38 | -20.3 | -99.1 |
| 4 | $CO_2(aq) + OH^- \leftrightarrow HCO_3^-$<br>$HCO_3^- + OH^- \leftrightarrow H_2O + CO_3^{2-}$ | | -64.5 | -89.2 | -83.1 |
| 5 | $C + 2CO_3^{2-} \leftrightarrow 3CO_2(g) + 4e^-$ | 0.329 | -127 | 174 | |

Thus, the half reactions that can occur in the anode and cathode are:

**Cathode** $O_2 + 2H_2O + 4e^- \leftrightarrow 4OH^-$ (Reaction 2)

**Anode** $C + 4OH^- \leftrightarrow CO_2 + 2H_2O + 4e^-$ (Reaction 1)

$C + 2CO_3^{2-} \leftrightarrow 3CO_2 + 4e^-$ (Reaction 5)

Nunoura et al. [12] studied the temperature dependence of the anode and cathode reactions in the cell to determine the operation temperature. They concluded that while the anode half-reaction (Reaction 1) was favored at all temperatures of interest, the cathode reaction (Reaction 2) was only favored at temperatures below ~500 K (~230 °C), giving us a narrow temperature range to work, as the carbon need temperatures above 200°C for electrochemical combustion. Nunoura carried out experiments with 6 M aqueous potassium hydroxide and mixtures of aqueous potassium and lithium hydroxide 6MKOH/1 M LiOH as electrolytes at temperatures up to 245 °C and pressures around 30 atm. They obtained voltages over 0.4 V working with KOH and over 0.5 working with mixtures 6 M KOH/ 1 M LiOH.

Antal and Nihous in later work [13] concluded that the cathode reactions may indeed be favored at temperatures as high as 300 °C. Antal and Nihous took into account the temperature dependence of

$E^{o}_{SHE,298}$ - $E^{o}_{SHE,T}$ (Nunoura et al. assumed it to be 0). The experimental observations of Nunoura et al. support this. The best performance of their aqueous-alkaline fuel cell was when they increase the temperature to 240 $^{\circ}$C. When the electrolyte is exposed to $CO_2$, the $OH^-$ concentration decreases and carbonate ion is formed (reaction 4). However, the performance of the fuel cell will not be affected because ions, $OH^-$ and $CO_3^{2-}$, can be good oxidants at temperatures around 300 $^{\circ}$C. Indeed, the carbonate ion may increase the power density.

In Summary, the findings about the high reactivity and conductivity of the charcoals and the thermodynamics analysis of the Biocarbon fuel cell suggest that biocarbon can in fact undergo oxidation in an aqueous alkaline/carbonate fuel cell working at low to moderate temperatures. Experimentally, serious engineering challenges confront the development of a reliable carbon fuel cell. Our aqueous alkaline fuel cell showed the best performance with high concentrations of potassium carbonate solution as electrolyte but potassium bicarbonate crystals precipitated. The following section focuses on previous literature in the carbonate/bicarbonate chemistry.

## 2.5 Bicarbonate/Carbonate chemistry

Several researchers have focused their interest in the role of the carbonate/bicarbonate system in nature. The main reason of this interest is due to the fact that the carbonate system is the natural major source of buffering for water systems. Here, a variety of chemical species and reactions occur that are highly interactive. By far the most important species of this buffer system is carbon in the form of $CO_2$, $HCO_3^-$ and $CO_3^{2-}$[62-64]. The sources of the carbon is carbon dioxide from the atmosphere and carbonate containing minerals in the earth, limestone ($CaCO_3$) being the most common.

A great number of data on the carbonate chemistry of the oceans has been obtained over the last decades from programs such as GEOSECS (Geochemical Ocean Sections Study), TTO (Transient Tracers in the Oceans), and WOCE (World Ocean Circulation Experiment). Many of these data have been made available by CDIAC (Carbon Dioxide Information Analysis Center) [65].

As a result, the chemistry of ocean carbonate/bicarbonate chemistry in nature is very well understood. About $54x10^{14}$ moles per year of $CO_2$ is taken from the atmosphere by photosynthesis divided about equally between land and sea. Of this, all except 0.05% is returned by respiration (almost entirely due to

microorganisms); the remainder leaks into the slow, sedimentary part of the geochemical cycle. Since the beginning of large-scale industrialization around 1860, the oceans have taken up about 50% of the anthropogenic $CO_2$ produced by fossil fuel burning and cement-manufacturing (i.e. greenhouse gases). The carbon dioxide dissolves in seawater, produces hydrogen ions and neutralizes carbonate ions($CO_3^{2-}$):

$CO_2 + H_2O + CO_3^{2-} \rightarrow 2\ HCO_3^-$ (6)

A quantity known as the Revelle buffer factor (B)[66] is often used to express the way in which the partial pressure of $CO_2$ in the atmosphere P depends on the total dissolved carbonate $C_T$ in the ocean at constant alkalinity:

$$B = \frac{C_T}{P}\left(\frac{\partial P}{\partial C_T}\right)_{Alk} = \left(\frac{\partial log P}{\partial log C_T}\right)_{Alk}$$

Due to the buffer capacity of seawater, a change of 10 percent in the $CO_2$ content of the atmosphere will produce a 1 percent change in the concentration of total dissolved carbon in seawater. However, as the concentration of total dissolved carbon in seawater increases ,the absorptive capacity of the oceans increases. The real question, then, is to what extent is the world likely to be affected by effects on the global climate over a horizon of 50-500 years.

Although the chemistry of ocean acidification is very well understood, its impact on marine organisms and ecosystems remains poorly understood. The potentially dire consequences of ocean acidification have prompted the interest of scientists and students with a limited knowledge of the carbonate chemistry and its experimental manipulation. Another field of interest is the behavior of the carbonate/bicarbonate system at different conditions from atmospheric conditions.

Lehman et al. (1998)[14] listed the following number of reactions in a dry potassium carbonate/bicarbonate system favored at high temperatures

- $K_2CO_3 \leftrightarrow K_2O + CO_2$
- $K_2O + H_2O \leftrightarrow 2KOH$
- $K_2CO_3 + CO_2 + H_2O \leftrightarrow 2KHCO_3$
- $2KOH + CO_2 \leftrightarrow K_2CO_3 + H_2O$

The stability of $K_2CO_3$ (s) and the degree to which other compounds listed in the above reactions exist depend on the conditions and can be evaluated by the thermodynamic properties. The authors stated that $KHCO_3$, forms under certain conditions of $H_2O$ and $CO_2$ partial pressures, but dry $KHCO_3$ decomposes rapidly between 100 and 200°C into $K_2CO_3$ ,$CO_2$ and water. $K_2CO_3$ occurs in two forms, $\gamma$ and $\beta$. The $\gamma$

form transforms to the β form at 421° C and the β form is stable up to the melting point of 900° C where it decomposes into $K_2O$ and $CO_2$. The melting temperature is reduced to 891-896° C, when tested under air instead of $CO_2$ conditions.

Reaction $K_2CO_3 + CO_2 + H_2O \leftrightarrow 2KHCO_3$ has also been widely studied in solution. Carbonate-bicarbonate studies were performed back in the forties to sixties at temperatures up to 140 °C when there was keen interest in $CO_2$ removal by carbonate absorption. Solutions of sodium or potassium carbonate were among the earliest alkaline solutions used for $CO_2$ removal and were the principal agents in use until 1940. Later, these solutions were largely replaced by ethanolamines, especially when carbon dioxide is present in appreciable quantities. Several disadvantages of conventional carbonate scrubbing have made the process non-competitive with other methods. Because of the limited solubility of the bicarbonate, especially sodium, dilute solutions must be used to avoid precipitation. Consequently, the amount of carbon dioxide pickup is relatively low, about 1 to 2 cubic feet per gallon as compared to other alkaline solutions; and relatively high circulation rates are needed. Solubility studies showed a better performance of the potassium bicarbonate rather than the sodium bicarbonate.

Figure 2.4 shows the solubility limit of potassium carbonate-bicarbonate solutions with the temperature. The study was done by the Bureau of Mines[67]. Concentrations are expressed as percent equivalent concentration of potassium carbonate, which is defined as the concentration referring to a solution of zero conversion with only potassium carbonate and water present. Thus, a 40 % equivalent solution means a solution that would contain 40 grams of potassium carbonate and 60 grams of water if all the bicarbonate was converted back to the carbonate. Equivalent potassium carbonate concentrations of 40, 50 and 60 % were used with conversions to bicarbonate ranging from 97 to 15%.

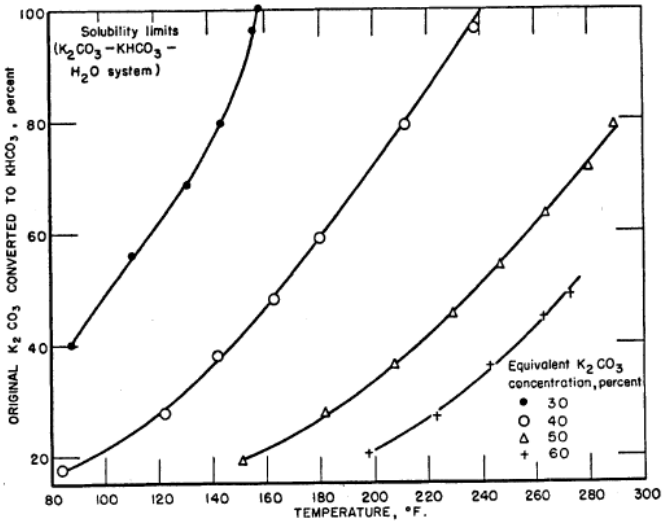


**Figure 2.4 Effect of the temperature on the solubility of potassium carbonate plus potassium bicarbonate in aqueous solution[4, 67]**

For each concentration the temperature of precipitation decreased with the percentage of bicarbonate, an expected result because the solubility of potassium bicarbonate is much less than that of the carbonate. For instance, a 60-percent equivalent solution precipitates at a bicarbonate conversion of only 25 % at 220°F (104.4°C) approx. and at a bicarbonate conversion of 50 % at 280°F(137.8 °C) approx.

Figure 2.4 also shows that at 220°F (104.4°C), for example, a 60-percent equivalent solution precipitates at a bicarbonate conversion of just 25 %, a 50-percent equivalent solution precipitates at a bicarbonate conversion of around 40 % and there is no danger of precipitation with a 30-percent solution.

When the temperature of the carbonate/bicarbonate solution increases, reaction $2KHCO_3 \leftrightarrow K_2CO_3 + CO_2 + H_2O$ proceeds. Butler [66] describes reaction $Na_2CO_3 + CO_2 + H_2O \leftrightarrow 2NaHCO_3$ (or $K_2CO_3 + CO_2 + H_2O \leftrightarrow 2KHCO_3$) as reversible within normally accessible temperature and pressure ranges. At lower temperatures and higher $CO_2$ partial pressures, the reaction proceeds to the right; at higher temperatures and lower pressures, it proceeds to the left. This behavior indicates that reaction of $CO_2$ absorption with carbonate is exothermic as it is favored at lower temperatures.

All these findings caused us to wonder if the fuel cell crystals, determined as potassium bicarbonate, could be avoided. On the one hand, the formation of potassium bicarbonate could diminish the performance of the fuel cell due to both the depletion of carbonate ions needed for the anode reaction and the crystal precipitation itself. On the other hand, Lehman showed that dry $KHCO_3$ decomposes rapidly between 100 and 200°C into $K_2CO_3$, $CO_2$ and water. Butler also confirmed that this reaction

occurs in solution but does not specify temperatures and pressures. Based on these findings, we decided to focus on the decomposition of the $KHCO_3$ in solution at the fuel cell operational temperatures (200-300 °C) and pressures (700-1000 psi) to see if the formation of these potassium bicarbonate crystals could be prevented.

# CHAPTER 3. FUEL CELLS DESIGNS

In these two years of research, serious engineering efforts have been required to confront the development of a reliable carbon fuel cell. In this chapter, four different fuel cell designs that have been tested in the Lab are presented.

## 3.1 First Design

The first design presented here started to be tested from January 2009 to January 2010 by Ms. Greer Tanner-Dempsey from the University of Waikato, NZ and Dr. Toshiaki Hanaoka from AIST, Japan. Figure 3.1 shows the schematic diagram of the fuel cell apparatus. To form the carbon anode, carbonized charcoal samples were poured into a Halsic-R porous ceramic tube (20.33 mm O.D. x 12.56 mm I.D. x 100.32 mm long, pore size of 24 μm , W. Handenwanger) and compressed by a nickel piston. The objective of this compression was to create an electrically conductive bed, as discussed in previous publication [49]. This carbon bed acted as an anode for the fuel cell, and electrical wires were attached to both the nickel piston and the base which enabled us to measure the carbon bed resistance. Metal foils were used to form the cathode. The cathode consisted in a cylinder of silver (20.35 mm Diameter x 44.50 mm long), covered by a silver screen cylinder. The Halsic-R cylindrical "ceramic" that contained the biocarbon was placed within the cathode cylinder. An electrical wire was attached to the cathode cylinder. The anode and cathode assembly was place in an Al-23 alumina tube (Alfa Aesar, 51.70 mm O.D. x 42.87 mm I.D. x 99.30 mm long). The ceramic was on top of the heating plate. The ceramic and the heating plate were sealed by a high temperature gasket (Kalrez® Spectrum) placed in between that prevented leaks. Four series high watt density Cartridge heaters (1/4'' Diameter x $1^{1/4}$'' long, 225 W ) were inserted in the heating plate. Two type-K thermocouples measured the temperature of the electrolyte and the heating plate respectively. To deliver air into the electrolyte, a sparger that was made of Nickel tubing was inserted below the foil/screen cathode. The circular bottom portion of the sparger had several holes, each 1 mm in diameter, and the stem portion was wrapped with Teflon tape, to prevent contact between the nickel tube and the fuel cells metals.

The apparatus was inserted in a pressure vessel (Figure 3.2). There were three lines of air delivery to the system: the first was used to pressurize the vessel, the second delivered air to the pneumatic cylinder to compress the charcoal bed, and the third was directed to the air sparger. A metering valve controlled the airflow to the sparger. Wires for measuring the resistance of the fuel cell, including the carbon bed

and for heating were connected to a hand-held milliohm meter (ISOTK M210) and a VariAC transformer via the connectors on the ceiling of fuel cell. Wires for measuring the open circuit voltage (OCV) were connected to a hand-held voltmeter (Fluke 87) via the same connectors. The compacting charcoal line, bulk air delivery line, vent line and drain line from sump were also connected to each corresponding line from the fuel cell.

After pressurizing and heating up the charcoal and stable conditions (stable OCV and resistance) were reached, the ohmmeter and voltmeter were disconnected and a Perkin-Elmer Model 362 potentiostat was connected to the anode and cathode. The counter and reference leads were connected to the anode, and the working and sense leads were connected to the cathode. The polarization curves were obtained with a scan speed of 0.5 mA/s. The potentiostat gives Voltage-Current values. The current and power densities were estimated as follows:

$$Current\ density\ \left[\frac{mA}{cm^2}\right] = \frac{Current\ [mA]}{Cross\ section\ of\ piston\ [cm^2](= 0.9957\ \ [cm^2])}$$

$$Power\ density\ \left[\frac{mW}{cm^2}\right] = Voltage[V]\ \cdot\ Current\ density\ \left[\frac{mA}{cm^2}\right]$$

Figure 3.6 shows the image of the actual first fuel cell apparatus.

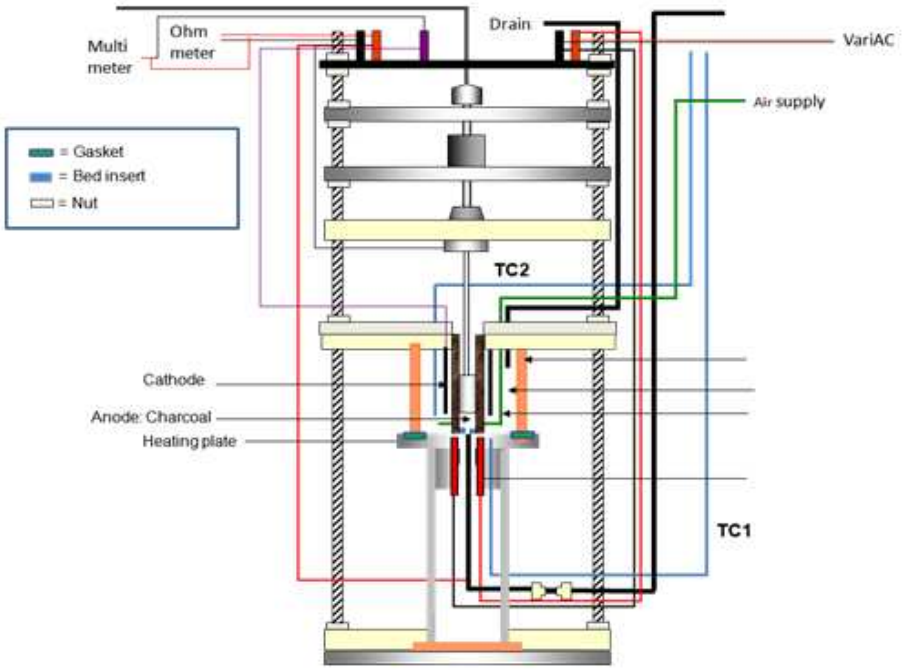


**Figure 3.1 Schematic diagram of the 1st design fuel cell apparatus**

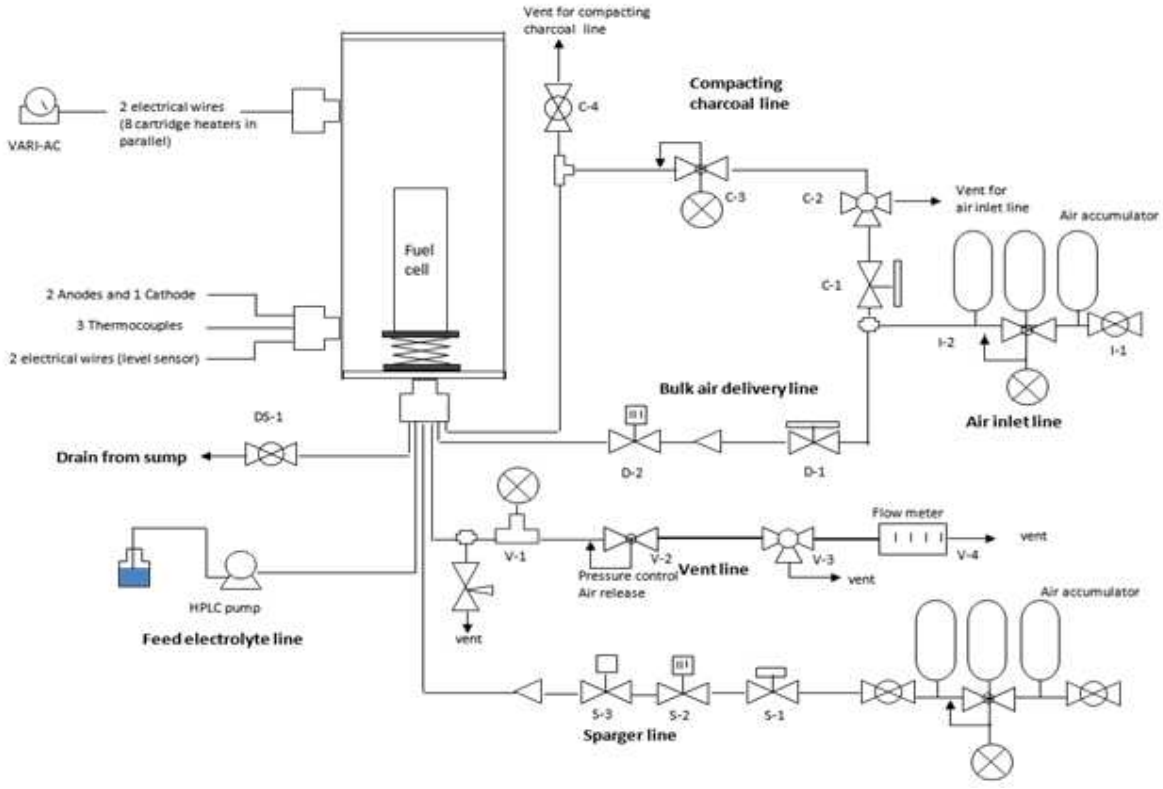


**Figure 3.2 Tubing diagram for 1st and 2nd design**

### *3.1.1 Results*

Two different heating plates were tried with this first design: Nickel and titanium .The Ni heating plate was tried by Ms. Tanner-Dempsey and Dr. Hanaoka. A summary of the conditions used and the results are shown in Table 3.1

**Table 3.1 Conditions and results of the biocarbon fuel cell using a Ni heating plate**

| Set #1 Run | Date | Electrolyte | Electrolyte flow rate ml/min | Electrolyte Temperature °C | $P_{vessel}$/ $P_{compaction}$ psi/psi | Gas to sparger | OCV V | SCC density $mA/cm^2$ | Max. Power density $mW/cm^2$ | Mass charcoal g |
|---|---|---|---|---|---|---|---|---|---|---|
| 1 | 09/28/2009 | 8M K2CO3 | 0.18 | 152 | 700/802 | Air/CO2= 1250psi/ 500psi | 0.83 | 235.4 | 43.6 | 0.4 |
| 2 | 10/06/2009 | 3M K2CO3 | 0.27 | 169 | 700/800 | Air | 0.106 | 6.5 | 0.16 | 0 |
| 3 | 10/09/2009 | 3M K2CO3 | 0.27 | 190 | 700/800 | Air | 0.368 | 77.7 | 6.4 | 0.4 |
| 4 | 10/21/2009 | 3M K2CO3 | 0.27 | 187 | 700/801 | Air/CO2= 1650psi/ 100psi | 0.404 | 135.6 | 12.3 | 0.4 |
| 5 | 10/30/2009 | 3M KHCO3 | 0.27<br>0.27<br>0 | 195<br>195<br>195 | 700/800 | Air | 0.21<br>0.22<br>0.22 | 39.2<br>45.5<br>67.3 | 1.8<br>1.5<br>3.2 | 0.4 |
| 6 | 11/04/2009 | 3M KHCO3 | 0.27<br>0.27<br>0 | 188<br>188<br>188 | 700/800 | Air/CO2= 1650psi/ 100psi | 0.13<br>0.13<br>0.13 | 22<br>22<br>22 | 0.5<br>0.65<br>0.8 | 0.4 |

For the first time, Ms. Tanner-Dempsey and Dr. Hanaoka discovered, in 28th September of 2009, that a low-temperature carbon fuel cell generated power at efficiencies exceeding 80%. At an anode temperature of 234 °C and electrolyte temperature of 152°C the Ni/ceramic cell offered an open-circuit voltage (OCV) as high as 0.83 V and a SCC of 235 $mA/cm^2$ with a maximum power density of 43.6 $mW/cm^2$. An empty Ni cell test on 10/6/09 (Run #6) delivered 0.1 V OCV with a SCC of 6.5 $mA/cm^2$ and a maximum power density of only 0.17 $mW/cm^2$ under similar conditions, indicating that the power measurements of Run #5 experiment were due to carbon oxidation and not corrosion of the Ni cell heating plate. Similar results were obtained from the cell by Ms. Tanner-Dempsey and Dr. Hanaoka a couple weeks later using a stainless steel (SS) cell, but afterwards they were unable to reproduce their work. This distressing situation evoked many hypotheses concerning the underlying explanation for the carbon fuel cell's promising performance.

In January 2010 , Ana Pascual from Universidad de Zaragoza and I continued the project with this first biocarbon fuel cell design. We carried out experiments from January 2010 until June 2010 changing the heating plate to titanium. Eventually we discovered that the biocarbon is susceptible to low-temperature electrochemical oxidation in the cell only after it has soaked in the electrolyte (i.e. an 'incubation' or 'seasoning' period) of several days. We succeeded in reproducing the results of Ms. Tanner-Dempsey and Dr. Hanaoka using a Ti/ceramic cell. Table 3.2 contains the data of the conditions and results of this Ti/ceramic cell

**Table 3.2 Conditions and results of the biocarbon fuel cell using a Ti heating plate**

| Set #2 Run | Date | Electrolyte | Electrolyte flow rate ml/min | Electrolyte Temperature °C | $P_{vessel}$/ $P_{compaction}$ psi/psi | Gas to sparger psi/psi | OCV V | SCC density $mA/cm^2$ | Max. Power density $mW/cm^2$ | Mass charcoal g |
|---|---|---|---|---|---|---|---|---|---|---|
| 1 | 05/28/2010 | 7.5 molal $K_2CO_3$ | 2 | 112 | 750/0 | Air/$CO_2$= 1000/200 | 0.837 | 235 | 45.19 | 0.4 |
| 2 | 06/01/2010 | 7.5 molal $K_2CO_3$ | 2 | 112 | 750/0 | Air/$CO_2$= 1000i/200 | 0.849 | 92.4 | 19.795 | 0.4 |
| 3 | 06/05/2010 | 7.5 molal $K_2CO_3$ | 2 | 100 | 750/0 | Air/$CO_2$= 1000/200 | 0.936 | 82 | 15.86 | 0 |
| 4 | 06/15/2010 | 7.5 molal $K_2CO_3$ | 2 | 109 | 750/0 | Air/$CO_2$= 1000/200 | 0.934 | 165 | 36.23 | 0 |

At an anode temperature of 235° C and an electrolyte temperature of 112 °C , the cell offered an open-circuit voltage (OCV) as high as 0.80 V and a SCC of 235 $mA/cm^2$ with a maximum power density of 45.2 $mW/cm^2$. We also observed that no compaction was needed to get these OCV, SCC and maximum power density. However, a subsequent empty Ti/ceramic cell test manifested 0.934 V OCV with a SCC of 165 $mA/cm^2$ and a maximum power density of 36.2 $mW/cm^2$. This power delivery from the Ti heating plate anode was not reproducible. However, there were indications that Ti may suffer serious corrosion in the presence of $K_2CO_3$ and $CO_2$ at elevated pressures and temperatures. The fact that a high OCV and high SCC were given by both an empty cell and a cell with charcoal indicated that the high values obtained in the OCV could be due to the corrosion of Ti rather than the electrochemical oxidation of charcoal. This was a surprise since Ti is regarded to be relatively inert. A related test with a Ni electrode delivered negligible power, corroborating our earlier findings. We tested alternative candidate electrode materials, including Ni, SS, Ti. All high temperature, molten carbonate carbon fuel cell researchers have employed SS cells. We decided to test the SS fuel cell.

M. Antal and G.Nihous show that the fuel cell reactions are favored at temperatures as high as 300°C [13]. To reach our goal of high temperatures, we had to try another design as the high temperature gasket could not survive temperatures above 250 °C. We designed and had fabricated a solid stainless steel cell (2nd design) that employed no gaskets or other seals.

## 3.2 Second design

Figure 3.3 shows the schematic diagram of the second design of the fuel cell. Basically, we substituted the gasket and heating plate by a solid stainless steel container. Eight series high watt density Cartridge heaters (1/4'' Diameter x $1^{1/4}$'' long, 225 W) were used (4 inside the wall and 4 on the bottom) and insulation (a layer of kaowool stayed in the middle of two vermiculite coated fiberglass strips) surrounded the SS cell. Three thermocouples were used this time that measured the temperatures of the SS cell wall, SS cell bottom and electrolyte. We also controlled the electrolyte level. To keep it constant, the apparatus was equipped with a level sensor. When evaporation of water caused a decrease in the level of the electrolyte, additional eater was delivered from a Waters 510 HPLC pump into the cell. The ceramic sleeve was placed inside the Stainless Steel wall so that the cell was able to electrically isolate the anode and the cathode from the wall and contain the electrolyte. Both the 1st and 2nd design use the same tubing diagram (Figure 3.2). Figure 3.7 shows an image of the actual fuel cell apparatus.

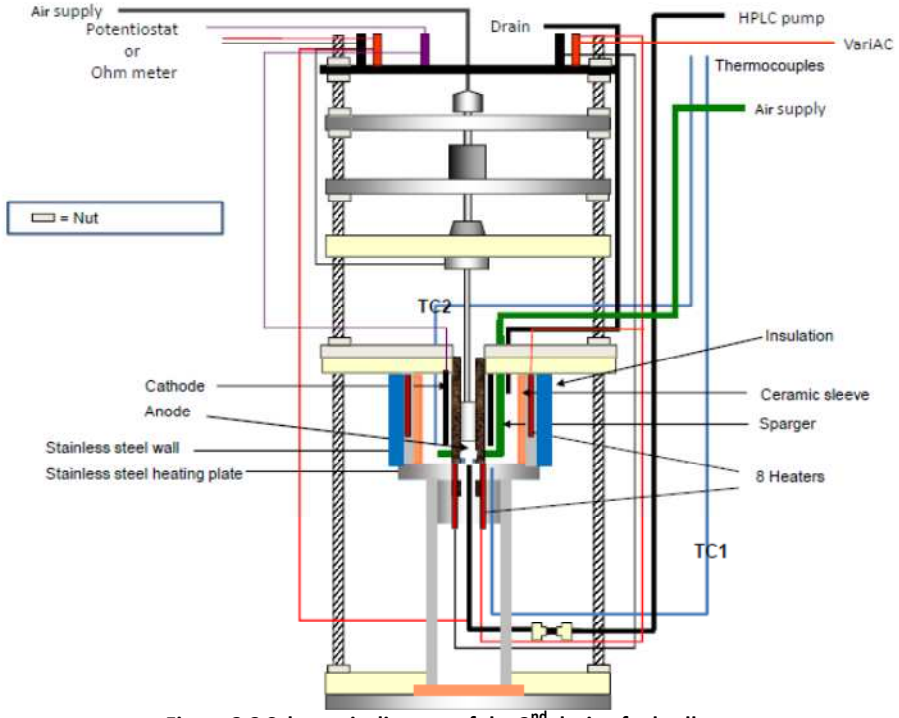


**Figure 3.3 Schematic diagram of the 2nd design fuel cell apparatus.**

### *3.2.1 Results*

This design was tested from 09 July 2010 to 21 March 2011.The results are shown in table 3.3

**Table 3.3 Conditions and results of the SS biocarbon fuel cell**

| Set #3 Run | Dates | Electrolyte | Electrolyte flow rate ml/min | Electrolyte Temperature/ Heaters bottom Temperature °C | $P_{vessel}$/ $P_{compaction}$ psi/psi | Gas to sparger | OCV V | SCC density $mA/cm^2$ | Max. Power density $mW/cm^2$ | Mass Charcoal (g) |
|---|---|---|---|---|---|---|---|---|---|---|
| 1 | 08/16/2010 | 7.5molal K2CO3 | 2 | 230/287 | 750/0 | Air | 0.771 | | | 0.4 |
| 2 | 08/27/2010 | 7.5molal K2CO3 | 2 | 217/230 | 750/0 | Air | 0.608 | | | 0.4 |
| 3 | 11/08/2010 | 6M KOH/ 1M LiOH | 2 | 177.1/213.5 | 700/0 | Air | 0.46 | | | 0.4 |
| 4 | 12/15/2010 | 6M KOH/ 1M LiOH | 2 | 220/260 | 700/0 | Air | 0.497 | 410 | 48.14 | 0.4 |
| 5 | 01/21/2011 | 6M KOH/ 1M LiOH | 2 | 223.7/267 | 700/0 | Air | 0.514 | 258 | 37.41 | 0.4 |
| 6 | 03/07/2011 | 6M KOH/ 1M LiOH | 2 | 183/221 | 730/0 | Air | 0.05 | | | 0 |
| 7 | 03/14/2011 | 6M KOH/ 1M LiOH | 2 | 289/350 | 730/0 | Air | 0.75 | 436 | 121.4 | 0.4 |
| 8 | 03/21/2011 | 6M KOH/ 1M LiOH | 2 | 126.5/157 | 700/0 | Air | 0.747 (not stable) | | | 0.4 |
| 9 | 03/30/2011 | 6M KOH/1M LiOH | 2 | 109/141 | 700/0 | Air | 0.614 (not stable) | | | 0.4 |

Although this cell delivered some promising results, we encountered insurmountable problems with its operation. At high temperatures (and pressures) moisture from evaporation of the aqueous electrolyte condensed everywhere in the pressure vessel. Condensation on the electrical connections, which delivered power to the heaters, caused short circuits and heater burnout and we had to stop the experiments. Therefore, we could not connect the Fuel Cell to the potentiostat in most of the cases and get the value of the SCC and maximum power density. The loss of one or more heaters on nearly every run was too big an expense to bear. Also, after the cell cooled and the pressure vessel was opened, the cell was filled with crystals. It was nearly impossible to remove the electrodes from the cell as they were encased in crystals.

Ashley Blitz, an undergraduate student in Global Environmental Science at UH worked in our laboratory writing the "Experimental Analysis of an Undesirable Crystal Precipitate in a Developmental Carbon Fuel Cell" as her undergraduate thesis. In her research, Ashley determines the chemical composition and formula of the carbon fuel cell crystal precipitate and she researches the way to prevent them from forming in the fuel cell during operation. Crystals taken from the fuel cell were analyzed using

temperature programmed desorption analysis (TGA-MS) by the Hungarian Academy of Sciences Central Research Institute for Chemistry. These analyses have been key to our understanding of the high temperature chemistry occurring within the electrolyte. The crystals were determined as potassium bicarbonate. We learned from Ashley's work that the formation of $KHCO_3$ is not favored at temperatures above 200 °C; the troublesome crystals observed in our early work formed at high pressure while the large pressure vessel cooled. A carbon fuel cell operating at 250 °C and above should experience no problems with the formation of $KHCO_3$, providing the cell is quickly cooled and pressure is quickly released.

Her project was the beginning of the second part of this thesis: determination of the electrolyte chemistry at the fuel cell conditions. The role of the electrolyte and the thermodynamic properties of the decomposition reaction of bicarbonate into carbonate and $CO_2$ are studied and presented in the next chapters. Experiments to study the decomposition reaction of bicarbonate were carried out in a new built "tubing bomb" that was suitable for use at pressures of 2000 psi and temperatures of 300 °C. Moreover, it could be quickly heated and cooled in a fluidized sand bath. These findings caused us to assemble a carbon fuel cell based on the concept of a tubing bomb. Figure 3.4 shows the schematic diagram of this third design.

## 3.3 Third and fourth design

In the third design, carbonized charcoal samples were poured into a cylindrical basket (16.4 mm diameter x 50 mm long) to form the carbon anode,. This charcoal is not compressed as previous results did not see any effect. The cathode consisted in a cylindrical basket of the same size as the anode. We tested Ni and SS metals for the electrodes but used the same metals for the cathode and anode. When we tested the SS electrodes, we inserted small pieces of Ni in the SS cathode to catalyze the reactions.

The walls of the cell are the tubing bomb and the Swagelok fittings accommodate Connax electrical connections that permit the entry of electrodes and gas flow into the tubing bomb. The electrode tubes were made of SS. This cell is easily and quickly heated to 300 °C in the fluidized sand bath. Two type-K thermocouples measured the temperature of the electrolyte and the sand bath respectively. The apparatus was inserted in a pressure vessel (Figure 4.4). There were two lines of air delivery to the system: the first delivered air through the SS cathode. It was first used to pressurize the vessel and once the cell is pressurized, it was used to deliver air to the cathode. A metering valve controlled the airflow

to the sparger. The second air line was used to fluidize the sand bath. The resistance and OCV of the fuel cell were measured by connecting the SS electrode tubes to a hand-held voltmeter (Fluke 87).

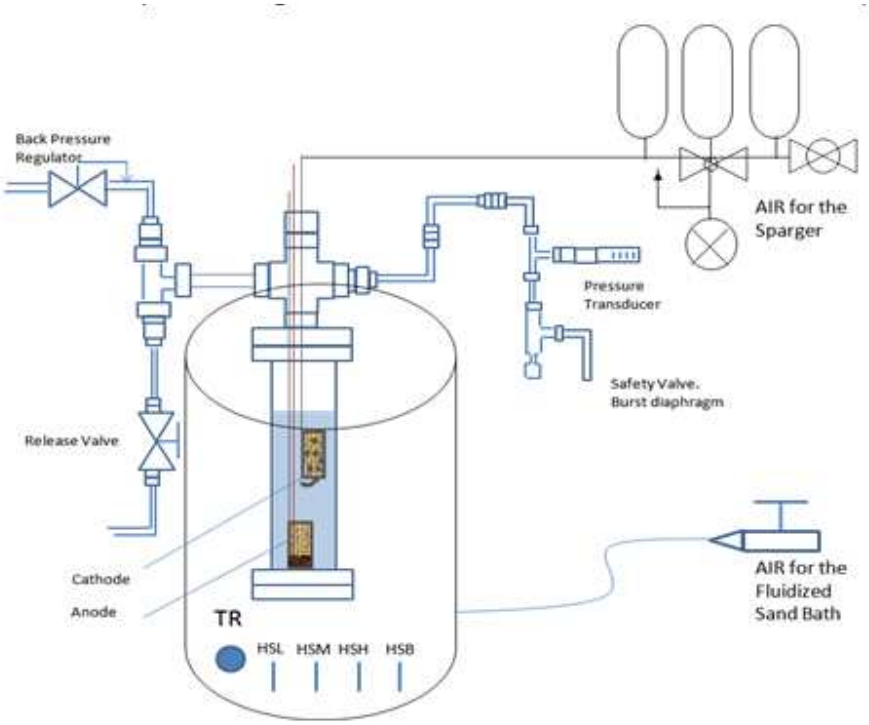


**Figure 3.4 Schematic diagram of the 3rd design fuel cell apparatus.**

This cell was tested from 18 April 2011 to 11 Oct 2011. The cell showed short-circuiting problems: There was little space for the electrodes inside the cell, its internal diameter was 2 inches. The electrodes were bent every time we inserted and took them apart because the 0.80 inches entrance was too narrow. When they bent, they were likely to touch the wall and produced a short-circuit. To fix this problem, a new cell was designed based on this last design. A wider entrance of 2.22 inches through a cross was implemented (4th design) .The electrode baskets and tubes metals were changed to copper. Unlike all our previous cells, this cell appears to have no significant mechanical or electrical problems at temperatures approaching 320 °C and pressures somewhat above 2000 psi. This cell is being tested right now. Figure 3.5 shows the schematic diagram of the fuel cell apparatus. Figure 3.8 and 3.9 show the actual images of the third and forth fuel cell apparatus

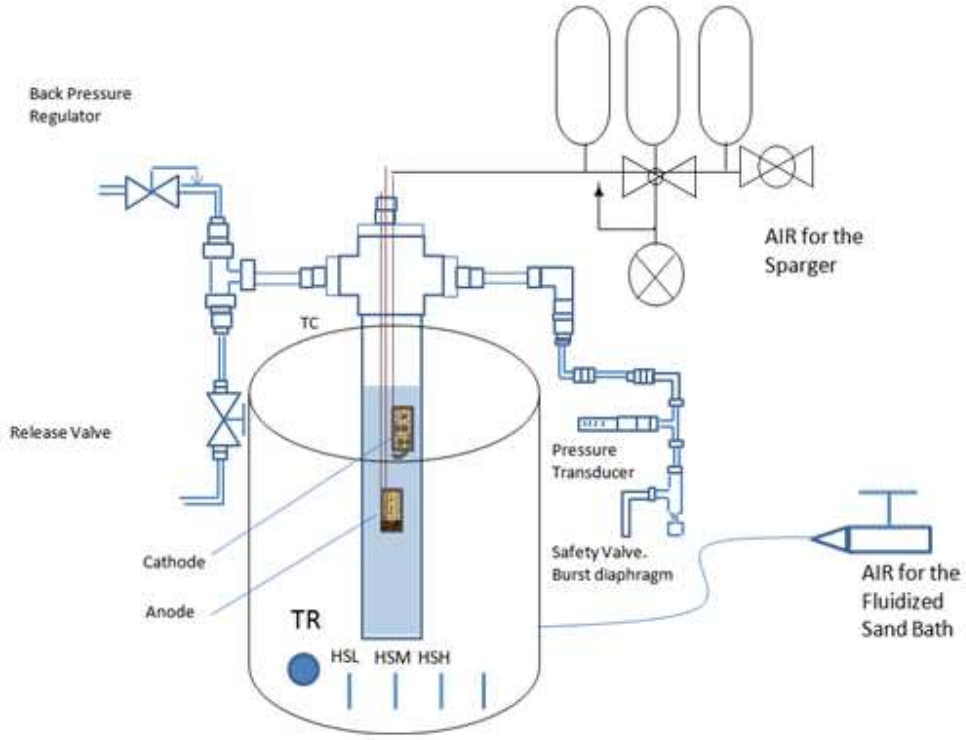


**Figure 3.5 Schematic diagram of the 4th design fuel cell apparatus.**

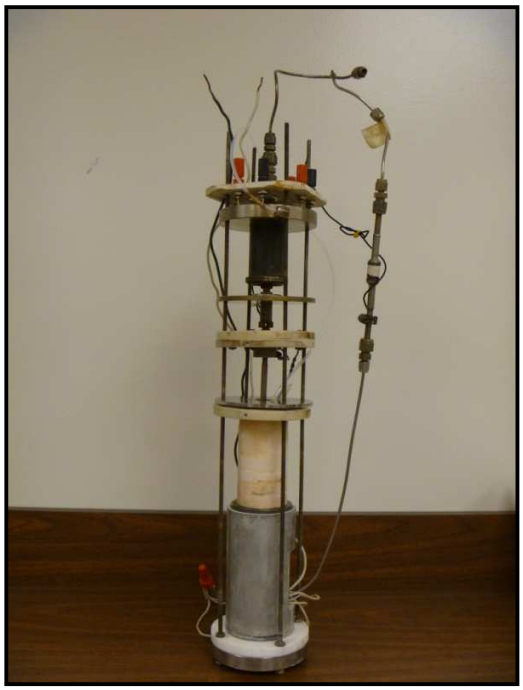

**Figure 3.6 First fuel cell apparatus**

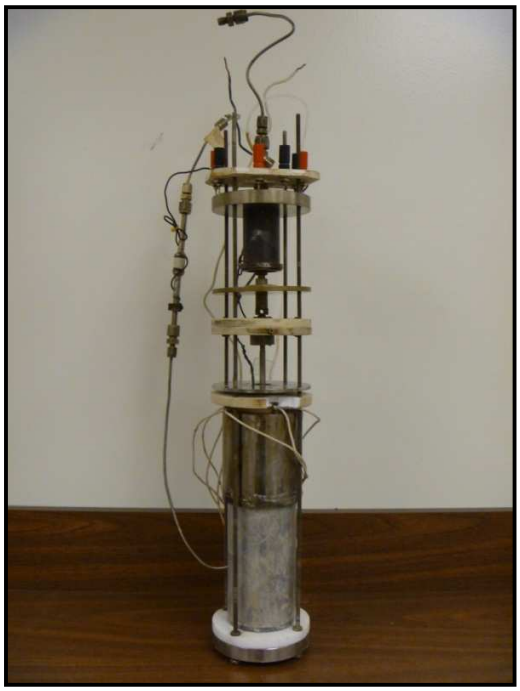

**Figure 3.7 Second fuel cell apparatus**

**Figure 3.8 Third fuel cell apparatus**

**Figure 3.9 Forth fuel cell apparatus**

In summary, our results indicate that biocarbon can indeed oxidize vigorously in an aqueous alkaline/carbonate environment at low to moderate temperatures and thereby generate power in a fuel cell at efficiencies exceeding 80%. But we have been facing serious engineering challenges in the development of a reliable carbon fuel cell. One of the major challenges we faced was the understanding of the high temperature chemistry occurring within the electrolyte. The next chapters focus on the role of the electrolyte and the chemistry going on in the fuel cell.

# CHAPTER 4. ELECTROLYTE

The key role of the electrolyte in the DCFC is to create a medium through which carbonate or hydroxide ions can travel from the cathode to the anode. Electrolytes can also act as a kind of filter, preventing undesirable ions or electrons from disrupting the desired chemical reactions. In the aqueous alkaline fuel cell, the electrolyte consists in a liquid mixture that presents a good ionic conductivity.

In this chapter, we have focused on the electrolytes: hydroxide, bicarbonate and carbonate. We have analyzed the dependence of the pH with temperature and pressure, the dependence of solubility in water with the temperature and the boiling point at different pressures. Figure 4.1 and figure 4.2 illustrates the aqueous potassium hydroxide and the aqueous carbonate system respectively

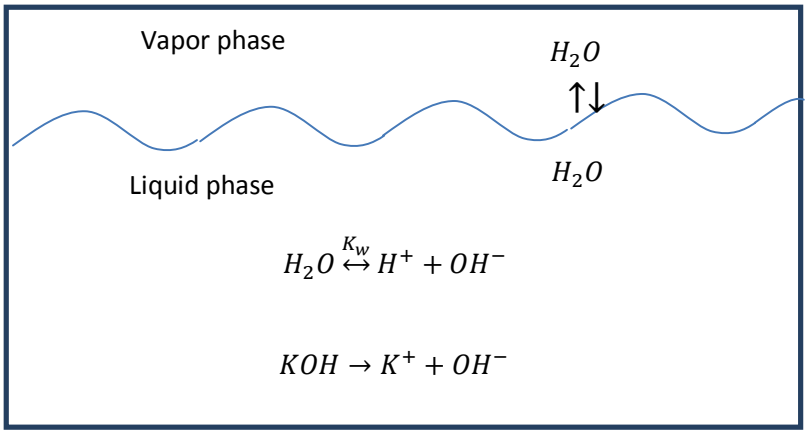


**Figure 4.1 Chemical and vapor-liquid equilibrium of the hydroxide system**

Reaction $KOH \rightarrow K^+ + OH^-$ describes the complete dissociation of dissolved KOH; reaction $H_2O \overset{K_w}{\leftrightarrow} H^+ + OH^-$describes the ionization of water to hydronium ($H^+$), and hydroxide ($OH^-$) ions, where $Kw$ is the dissociation constant of water and is expressed as $Kw = [H^+][OH^-]$.

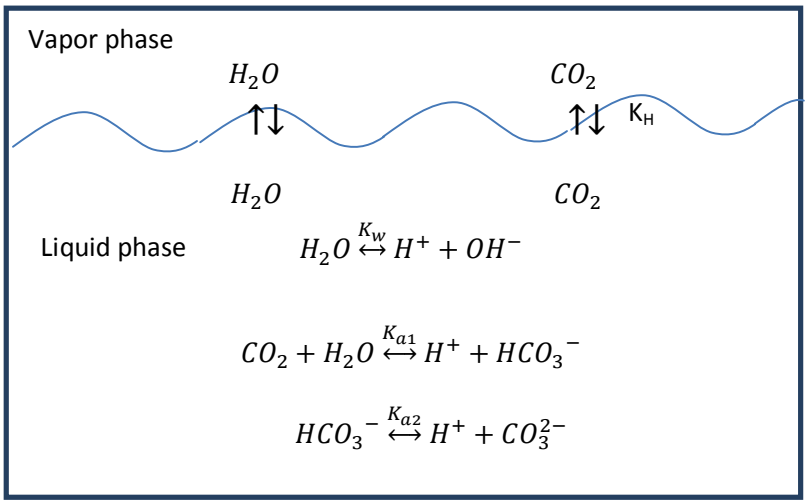


**Figure 4.2 Chemical and vapor-liquid equilibrium of the carbonate system**

Reaction $H_2O \overset{K_w}{\leftrightarrow} H^+ + OH^-$ describes the ionization of water to hydronium ($H^+$) and hydroxide ($OH^-$) ions; reaction $CO_2 + H_2O \overset{K_{a1}}{\leftrightarrow} H^+ + HCO_3^-$ describes the hydrolysis and ionization of dissolved $CO_2$ to $H^+$ and bicarbonate $HCO_3^-$ ions; reaction $HCO_3^- \overset{K_{a2}}{\leftrightarrow} H^+ + CO_3^{2-}$ describes the dissociation of $HCO_3^-$ to $H^+$ and carbonate, $CO_3^{2-}$ ions and reaction $CO_2(g) \overset{K_H}{\leftrightarrow} CO_2(aq)$ describes the equilibrium between the $CO_2$ in the gas phase and the $CO_2$ in solution . Once $CO_2$ is dissolved, a small proportion of the $CO_2$ reacts with water to form carbonic acid ($H_2CO_3$), at equilibrium $[H_2CO_3]$ is only about $10^{-3}$ as large as $[CO_2]$ and has no special significance in the acid-base equilibria, since both are uncharged. Hence, $[H_2CO_3]+[CO_2]$ is written simply as $[CO_2]$ .

The chemical equilibrium constant for the above j reactions are expressed in terms of the activity of component i as given by the following relationship:

$$K_j{}^o = \prod_i a_i{}^{\nu_{i,j}} \qquad \text{Equation 4.1}$$

Where $K_j{}^o$ is the chemical equilibrium constant (Butler called it the extrapolated zero ionic strength constant) and depends on the temperature and pressure. Table 4.1 shows the dependence of the $pK^o$ at (defined as $-\log K^o$) of the above reactions with the temperature

**Table 4.1 Equilibrium constants (extrapolated to zero ionic strength)**

| Temperature (°C) | $pK_H^o$ (mole/L·atm) | $pKa_1^o$ (mole/L) | $pKa_2^o$ (mole/L) | $pKw^o$ |
|---|---|---|---|---|
| 0 | 1.11 | 6.579 | 10.625 | 14.955 |
| 5 | 1.19 | 6.517 | 10.557 | 14.734 |
| 10 | 1.27 | 6.464 | 10.490 | 14.534 |
| 15 | 1.33 | 6.419 | 10.430 | 14.337 |
| 20 | 1.41 | 6.381 | 10.377 | 14.161 |
| 25 | 1.47 | 6.352 | 10.329 | 13.999 |
| 30 | 1.53 | 6.327 | 10.290 | 13.833 |
| 35 | 1.59 | 6.309 | 10.250 | 13.676 |
| 40 | 1.64 | 6.298 | 10.220 | 13.533 |
| 45 | 1.68 | 6.290 | 10.195 | 13.394 |
| 50 | 1.72 | 6.285 | 10.172 | 13.263 |
| 100 | 1.99 | 6.45 | 10.16 | 12.27 |
| 150 | 2.07 | 6.73 | 10.33 | 11.64 |
| 200 | 2.05 | 7.08 | 10.71 | 11.28 |

*$pK_H^0$, $pK_{a1}^0$, $pK_{a2}^0$ were selected by Stumm,W. and Morgan, J.J.1981. Aquatic Chemistry 2d ed. New York: Wiley, pp.206-206. $pK_w^0$ values are found in Sillen, L.G. and Martell, A.E. Stability Constant. Special publ. no.17 (1964) and 25 (1971). London: The Chemical Society.*

$\nu_{i,j}$ is the reaction stoichiometric coefficient of component i, $a_i$ is the activity of component *i.* In order to calculate the activity of an ion in a solution, one must know the concentration and the activity coefficient, $\gamma_i$. The activity of an ion species, i , is equal to the concentration of i, [i] multiplied by the activity coefficient of i, $\gamma_i$.

$$a_i = \gamma_i[i] \qquad \text{Equation 4.2}$$

When each activity in equation 4.1 is replaced by the product of a concentration and an activity coefficient, the equilibrium constant is defined as

$$K_j{}^o = \prod_i [i]^{\nu_{i,j}} \gamma_i{}^{\nu_{i,j}} \qquad \text{Equation 4.3}$$

One important simplification that Butler does is defining a new equilibrium constant at finite ionic strength ($K_j$) by combining the activity coefficients ($\gamma_i{}^{\nu_{i,j}}$) with the extrapolated zero ionic strength constant ($K_j{}^o$). This new constant, therefore, is just a function of temperature, pressure and ionic medium. For example, the first ionization constant of $CO_2$ at finite ionic strength would be

$$K_{a1} = \frac{[H^+][HCO_3^-]}{[CO_2]} = K_{a1}^o \frac{\gamma_o}{\gamma_+ \gamma_-}$$

Where $\gamma_o$ , $\gamma_+$ and $\gamma_-$ are the activity coefficients of the $CO_2$, $H^+$ and $HCO_3^-$ respectively. The zero ionic strength constant ($K_j{}^o$) can be employed if the major ionic components do not change very much as the reactions proceed to equilibrium and the ionic constant is therefore nearly constant.

Activity coefficients may be calculated theoretically, using the Debye-Hückel equation or extensions such as Davies equation, Pitzer equations or TCPC model. The Debye-Hückel limiting law enables us to determine the activity coefficient of an ion in a dilute solution of known ionic strength. The ionic strength (I) of a solution is a function of the concentration of all ions present in that solution

$$I = \frac{1}{2}\sum_i [i] z_i^2 \qquad \text{Equation 4.4}$$

Where [i] is the concentration of an ion with charge $z_i$. The Davies equation is an empirical extension of Debye–Hückel theory which can be used to calculate activity coefficients of electrolyte solutions at relatively high concentrations. The equation, originally published in 1938 [68] ,was refined by fitting to experimental data. The final form of the equation gives the activity coefficient for an ion with charge *z* and the mean activity coefficient of an electrolyte which dissociates into ions having charges $z_+$ and $z_-$ as a function of ionic strength, *I*. Notice that this equation of activity coefficients does not depend on density or dielectric constant as in Debye- Hückel

$$\log \gamma = -0.5 z^2 f(I) \text{ (For an ion of charge z)}$$

$$\log \gamma_\pm = -0.5 z_+ z_- f(I) \text{ (For a compound which dissociates into ions of charges } z_+ \text{ and } z_-\text{)}$$

$$f(I) = \left( \frac{I^{\frac{1}{2}}}{1 + I^{\frac{1}{2}}} - 0.2I \right) \left( \frac{298}{t + 273} \right)^{\frac{2}{3}} \qquad \text{Equation 4.5}$$

Where t is the temperature in degrees centigrade, and the function applies only to the temperature range 0-50 °C. $\gamma_\pm$ is defined as the mean activity coefficient and can also be given by equations 4.6 and 4.7.

For 1-1 electrolytes, such as KCl $\gamma_\pm = (\gamma_+ \gamma_-)^{1/2}$ Equation 4.6

For 1-2 electrolytes, such as $K_2CO_3$ $\gamma_\pm = (\gamma_+^2 \gamma_=)^{1/3}$ Equation 4.7

$\gamma_+$, $\gamma_-$ and $\gamma_=$are the activity coefficients for an ion of charge +1,-1 and -2. And can also be calculated as previous expression $\log\gamma = -0.5z^2 f(I)$.Notice that equation 4.5 agrees mathematically with 4.6 and 4.7. We can verify this agreement by applying logarithms to both sides of equations 4.6 and 4.7 and substituting $\log\gamma_\pm = -0.5z_+z_-f(I)$ and apply $\log\gamma = -0.5z^2 f(I)$ for $\gamma_+$, $\gamma_-$ and $\gamma_=$ , i.e $\log\ \gamma_+ = \log\ \gamma_- = -\ 0.5f(I)$ and $\log\ \gamma_= = -0.5 \cdot 4f(I) = -2f(I)$

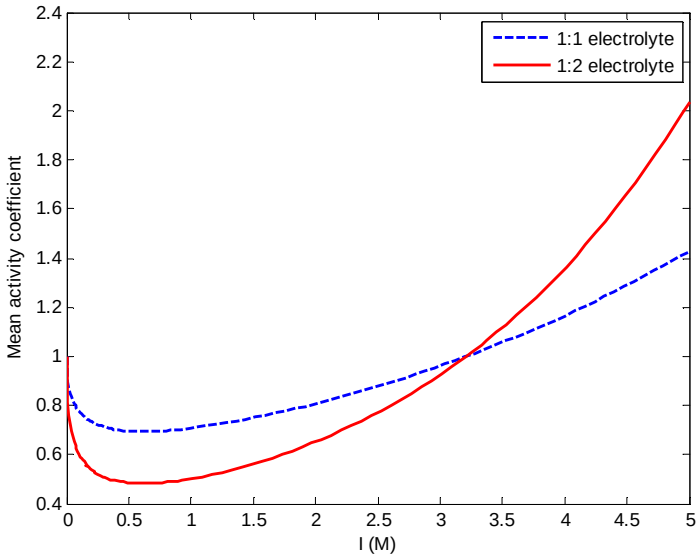


**Figure 4.3 Mean activity coefficient ($\gamma_\pm$) of 1:1 and 1:2 electrolytes as a function of ionic strength (I) calculated with Davies equation**

Experimentally, the activity of a single ionic species cannot be directly measured without some empirical assumption, but the mean activity coefficient can be measured with rigorous thermodynamics measurements. Butler[66] compares activity coefficients calculated from Davies equation to experimental values of the activity coefficients for three 1-1 salts and two 1-2 salts in his figure 2.5. At ionic strength above 0.5 M, the experimental activity coefficients are significantly different from those given by Davies equation.

### Effect of ionic strength on ion product of water, $K_w$

The activities of hydroxide ions in water is related to the concentration of hydrogen ions by the dissociation constant of water, ${K_w}^o$

$$ {K_w}^o = a_{H^+} a_{OH^-} $$

Or

$$K_w = \frac{K_w^o}{\gamma_+\gamma_-} = [H^+][OH^-] \qquad \text{Equation 4.8}$$

Notice that $K_w = K_w^o$ in the absence of electrolyte (i.e. pure water).With the approximation that the activity coefficients of $H^+$ ($\gamma_+$) and $OH^-$ ($\gamma_-$) are equal to $\gamma_\pm$and $\log\gamma_\pm = -0.5 z_+ z_- f(I) = -0.5 f(I)$ and taking logarithms

$$pK_w = pK_w^o - 1.0\ f(I) \qquad \text{Equation 4.9}$$

Figure 4.4 illustrates the ion product of water ($pK_w$) vs. the ionic strength (I) calculated from equation 4.9 at 25 and 50 °C. $pK_w^o$ =13.999 at 25 °C and $pK_w^o$ =13.263 at 50 °C [69].

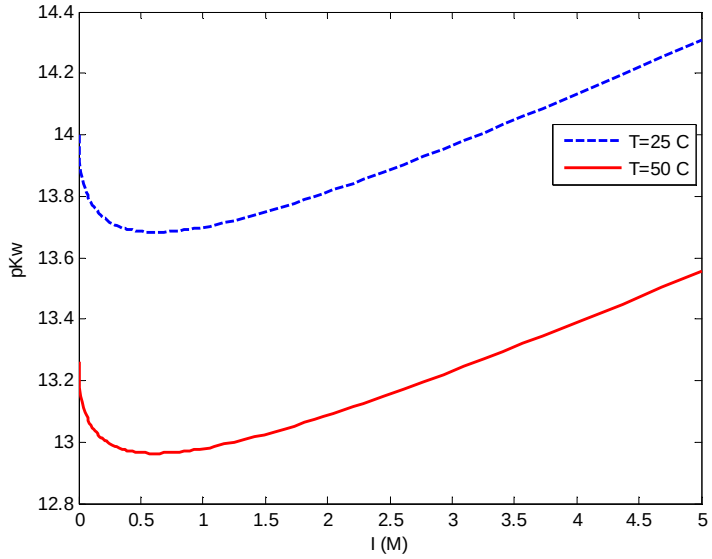


**Figure 4.4 Ion product of water ($pK_w$) as a function of ionic strength (I) at 25 and 50 °C calculated with Davies equation**

### Effect of ionic strength on $K_H$

Equation 4.10 describes the change of Henry's constant with the activity coefficient [66] as:

$$K_H^o = \frac{[CO_2]\gamma_o}{P} = K_H\gamma_o \qquad \text{Equation 4.10}$$

For uncharged species as $CO_2$, the activity coefficient $\gamma_0$ mostly follows a "salting-out" model:

$$log\ (\gamma_o)\ =\ bI \qquad \text{Equation 4.11}$$

This simple model predicts activities of many species (dissolved undissociated gases such as $CO_2$, $H_2S$, $NH_3$, undissociated acids and bases) to high ionic strengths (up to 5 mol/kg). The value of the constant b for $CO_2$ depends on the solution and temperature. Ellis and Golding (1963) [70] and Malinin (1959)[71] give values of this constant for $CO_2$ in NaCl solutions. A typical value of constant b at 25 and 50 °C is 0.10.

Taking logarithms on both sides of equation 4.10

$$\log\left(K_H^o\right) = \log(K_H) + \log\left(\gamma_o\right) \qquad \text{Equation 4.12}$$

Or

$$\mathrm{p}K_H = \mathrm{p}K_H^o + \mathrm{bI} \qquad \text{Equation 4.13}$$

Figure 4.5 illustrates the Henry's constant ($pK_H$) vs. the ionic strength (I) calculated from equation 4.13 at 25 and 50 °C. $pK_H^o$ [64]=1.47 at 25 °C and $pK_H^o$[64] =1.72 at 50 °C with a b constant of 0.10.

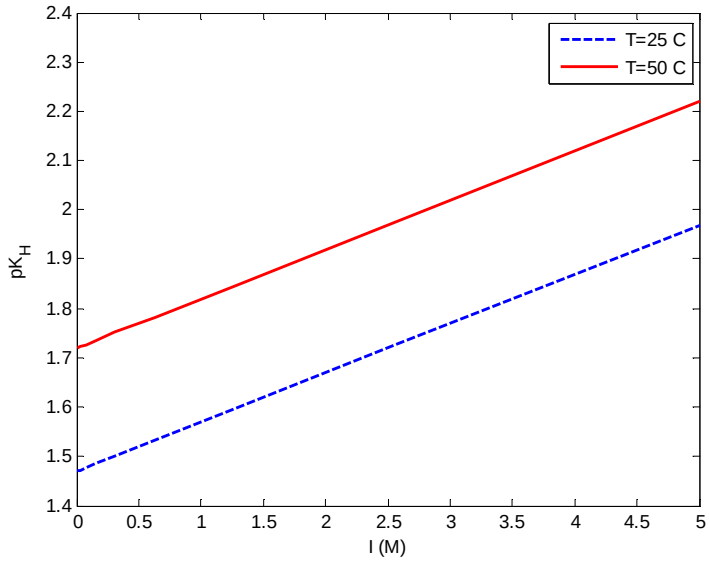


**Figure 4.5 Henry's constant ($pK_H$) as a function of ionic strength (I) at 25 and 50°C**

Figure 4.5 shows a linear increase of the $pK_H$ with the ionic strength (I) , as well as an increase of the $pK_H$ from 25 to 50 °C, i.e. the $K_H$ decreases with both the ionic strength and the temperature (from 25 to 50 °C). The decrease in the $K_H$ , defined as $[\boldsymbol{CO_2}]/\boldsymbol{P}$ (see equation 4.12), indicates that the solubility of $CO_2$ decreases with increasing temperature from 25 to 50 °C and with the ionic effect. A change in the $pK_H$ at 25 °C from 1.47 at zero ionic strength to 1.96 at ionic strength 5M, and a change in the $pK_H$ at zero ionic

strength from 1.47 at 25°C to 1.72 at 50°C indicates a significant change in the Henry's constant ($\boldsymbol{K_H = 10^{-pK_H}}$) with temperature and pressure. Both lines are parallel which shows that the decrease in the Henry's constant with temperature will be the same regardless the ionic strength.

The decrease in solubility of permanent gases with increasing temperature at around the room temperature, and consequently the increase in partial pressure at a given gas concentration has been described by previous researchers. Takahashi et al. (2002)[72] explains that this can be verified when heating water in a pot: small bubbles evolve and rise, long before the water reaches boiling temperature. Similarly, carbon dioxide from a carbonated drink escapes much faster when the drink is not cooled because the required partial pressure of $CO_2$ to achieve the same solubility increases in higher temperatures. Partial pressure of $CO_2$ in the gas phase in equilibrium with seawater doubles with every 16 K increase in temperature.[5]

However, P. Cohen explains that the solubility of gases does not always decrease with increasing temperature. For aqueous solutions, the Henry-law constant usually goes through a maximum (i.e., the solubility goes through a minimum). For most permanent gases, the minimum is below 120 °C. It is often observed that the smaller the gas molecule (and the lower the gas solubility in water), then the lower the temperature of the maximum of the Henry-law constant. Thus, the maximum is about 30 °C for helium, 92 to 93 °C for argon, nitrogen and oxygen, and 114 °C for xenon [73].

**Effect of ionic strength on first acidity constant, $K_{a1}$**

The first acidity constant is the equilibrium constant for reaction $CO_2 + H_2O \overset{K_{a1}}{\longleftrightarrow} H^+ + HCO_3^-$ , which describes the hydrolysis and ionization of dissolved $CO_2$ to $H^+$ and bicarbonate $HCO_3^-$ ions. And it is given by

$$K_{a1} = \frac{[H^+][HCO_3^-]}{[CO_2]} = K_{a1}^o \frac{\gamma_o}{\gamma_- \gamma_+} \qquad \text{Equation 4.14}$$

Where $\gamma_o$ , $\gamma_+$ and $\gamma_-$ are the activity coefficients of the $CO_2$, $H^+$ and $HCO_3^-$ respectively. With the approximation that the activity coefficients of $H^+$ ($\gamma_+$) and $HCO_3^-$ ($\gamma_-$) are equal to $\gamma_\pm$ and $\log \gamma_\pm = -0.5 z_+ z_- f(I) = -0.5 f(I)$ , the activity coefficient of $CO_2$ ($\gamma_o$) is given by equation 4.11, $log\ (\gamma_o) = bI$ and taking logarithms, equation 4.14 leads to

$$pK_{a1} = pK_{a1}^o - 1.0\ f(I) - bI \qquad \text{Equation 4.15}$$

Figure 4.6 illustrates the first acidity constant ($pK_{a1}$) vs. the ionic strength (I) calculated from equation 3.15 at 25 and 50 °C. $pK_{a1}^{o}$[64] =6.352 at 25 °C and $pK_{a1}^{o}$ [64]=6.285 at 50 °C with a b constant of 0.10.

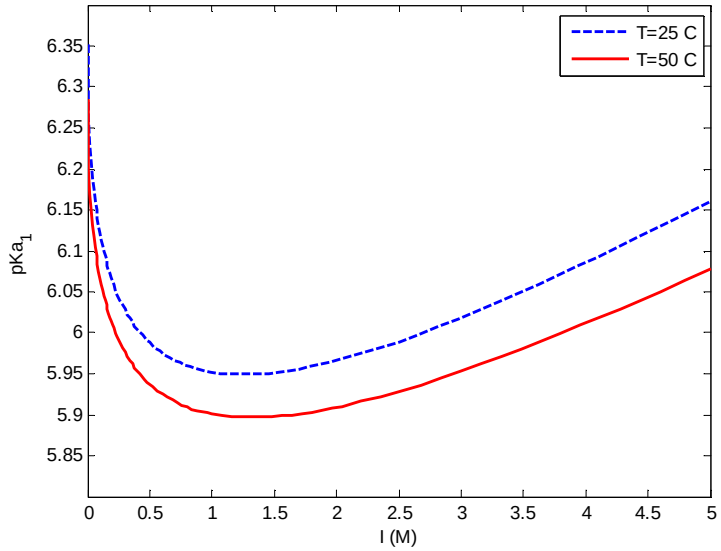


**Figure 4.6 First acidity constant ($pK_{a1}$) as a function of ionic strength (I)**

**Effect of ionic strength on second acidity constant, $K_{a2}$**

The second acidity constant is the equilibrium constant for reaction $HCO_3^- \overset{K_{a2}}{\longleftrightarrow} H^+ + CO_3^{2-}$, which describes the dissociation of $HCO_3^-$ to $H_3O^+$ and carbonate, $CO_3^{2-}$ ions.

$$K_{a2} = \frac{[H^+][CO_3^{2-}]}{[HCO_3^-]} = K_{a2}^o \frac{\gamma_-}{\gamma_= \gamma_+} \qquad \text{Equation 4.16}$$

Where $\gamma_=$ , $\gamma_+$ and $\gamma_-$ are the activity coefficients of the $CO_3^{2-}$, $H^+$ and $HCO_3^-$ respectively. With the approximation that the activity coefficients of $H^+$ ($\gamma_+$) and $HCO_3^-$ ($\gamma_-$) are equal, both terms cancel in equation 4.14. And the activity coefficients of $CO_3^{2-}$ ($\gamma_=$) is given by equation 4.7, $\log \gamma = -0.5 z^2 f(I) = -2 f(I)$ . And taking logarithms, equation 4.16 leads to

$$pK_{a2} = pK_{a2}^o - 2.0\, f(I) \qquad \text{Equation 4.17}$$

Figure 4.7 illustrates the second acidity constant ($pK_{a2}$) vs. the ionic strength (I) calculated from equation 3.15 at 25 and 50 °C. $pK_{a2}^{o}$[64] =10.329 at 25 °C and $pK_{a2}^{o}$[64] =10.171 at 50 °C

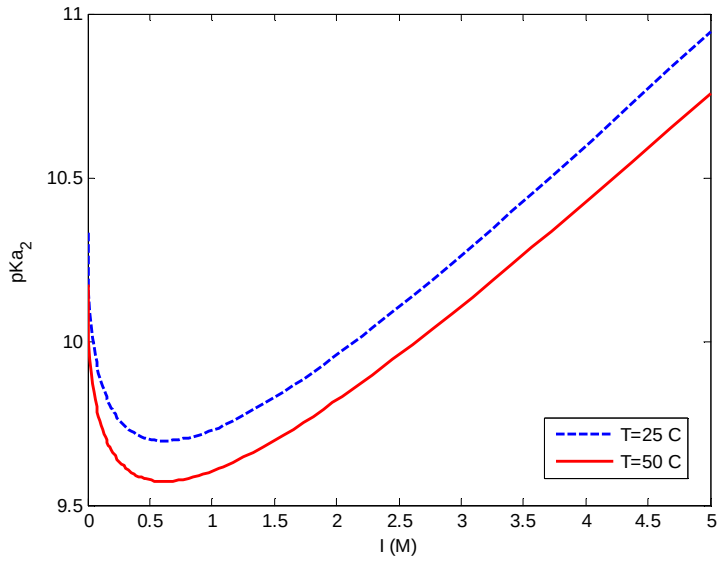


**Figure 4.7 Second acidity constant ($pK_{a2}$) as a function of ionic strength (I)**

## 4.1 pH and Solubility of the $H_2O$-Hydroxide system

### *4.1.1 Solubility*

The hydroxides are strong bases that completely dissociate in solution as figure 4.1 shows. However, when the hydroxide concentration reaches their saturation concentration, the concentration does not increase more and the hydroxide precipitates. The solubility of a substance fundamentally depends on the solvent as well as on temperature and pressure. Table 4.2 shows the solubility of hydroxides in water with the temperature, under 1 atm pressure, units in g/ 100g $H_2O$.

**Table 4.2 Solubility in water with the temperature, under 1 atm pressure, units in g/100 g $H_2O$ [74]**

| | | 0°C | 10°C | 20°C | 30°C | 40°C | 50°C | 60°C | 70°C | 80°C | 90°C | 100°C |
|---|---|---|---|---|---|---|---|---|---|---|---|---|
| Group I | **LiOH** | 11.9 | 12.1 | 12.3 | | 12.7 | | 13.1 | 14.6 | 16.6 | 17.8 | 19.1 |
| | **NaOH** | | 98 | 109 | 119 | 129 | | 174 | | | | |
| | **KOH** | 95.7 | 103 | 112 | 126 | 134 | 154 | 127 | | | | 178 |
| | **CsOH** | | | | 300 | | | | | | | |
| Group II | **$Mg(OH)_2$** | | | 0.0009628 | | | | | | | | |
| | **$Ca(OH)_2$** | 0.189 | 0.182 | 0.173 | 0.16 | 0.141 | | 0.121 | | 0.086 | 0.076 | |
| | **$Sr(OH)_2$** | 0.91 | 1.25 | 1.77 | 2.64 | 3.95 | | 8.42 | | 20.2 | 44.5 | 91.2 |
| | **$Ba(OH)_2$** | 1.67 | 2.48 | 3.89 | 5.59 | 8.22 | 11.7 | 20.9 | | 101 | | |

At 20 °C and 1 atm, the solubility in mol/$L_{H2O}$ (molal) is

**Table 4.3 Solubility in mol /$L_{H2O}$ at 20 °C . The solubility of CsOH is given at 30 °C**

| Group I | C (molal) | Group II | C (molal) |
|---|---|---|---|
| **LiOH** | 5.136 | **$Mg(OH)_2$** | ≈0 |
| **NaOH** | 27.252 | **$Ca(OH)_2$** | 0.023 |
| **KOH** | 19.962 | **$Sr(OH)_2$** | 0.146 |
| **CsOH** | 20.011 | **$Ba(OH)_2$** | 0.227 |

The table gives an idea about the solubility of the hydroxides at room conditions. In Group I hydroxides, NaOH, KOH and CsOH are good candidates for the fuel cell because the molalities at which they become saturated are very high. Previous literature shows that CsOH is a catalyst in many molten carbonate fuel cells. The LiOH, however, can present problems of precipitation. The solubility of these compounds increase with the temperature, however the LiOH increase in solubility with the temperature is not significant. In Group II, the saturation concentrations at 20 °C are low. However, the $Ba(OH)_2$ and the $Sr(OH)_2$ solubility increase a lot with the temperature, so they might be good candidates for the fuel cell.

### *4.1.2 pH*

The hydroxides of the Group I and Group II metals usually are considered to be strong bases. They completely dissociate in water into the cation and the hydroxide ion ($OH^-$).

Hydroxide from Group I:$BOH \rightarrow B^+ + OH^-$

Hydroxide from Group II:$B(OH)_2 \rightarrow B^{2+} + 2OH^-$

If the hydroxide concentration is $C_{BOH}$ , the $OH^-$ concentration can be determined as

$$[OH^-] = C_{BOH} \quad \text{(Group I)}$$

$$[OH^-] = 2C_{BOH} \quad \text{(Group II) Equation 4.19}$$

pH and pOH are defined as a negative decimal logarithm of the hydrogen ($H^+$) and hydroxide ion ($OH^-$) activities in a solution.

$$pH = -log_{10}(a_{H^+})$$

$$pOH = -log_{10}(a_{OH^-}) \quad \text{Equation 4.20}$$

where $a_{H^+}$ and $a_{OH^-}$ are the activities of hydrogen and hydroxide ions. As $a_{OH^-} = \gamma_-[OH^-]$

$$pOH = -log_{10}(\gamma_-[OH^-]) = -log\gamma_- - log[OH^-] \quad \text{Equation 4.21}$$

Where the activity coefficient ($\gamma_-$) is given by the Davies equation (Equation 4.5).

Taking logarithms of equation 4.8 ($Kw^o = a_{H^+}a_{OH^-}$) we obtain a relationship between pH and pOH

$$pH = -\log Kw^o - pOH = pKw^o - pOH \quad \text{Equation 4.22}$$

To get the activity coefficient in equation 4.21, the ionic strength is needed (Equation 4.4, $I = \frac{1}{2}\sum_i [i] z_i^2$) for solving the Davies equation (Equation 4.5)

$$I = \frac{1}{2}\left([OH^-] \cdot 1^2 + [B^+] \cdot 1^2\right) = \frac{1}{2}\left(C_{BOH} \cdot 1^2 + C_{BOH} \cdot 1^2\right) = C_{BOH} \quad \text{(Group I)}$$

$$I = \frac{1}{2}\left([OH^-] \cdot 1^2 + [B^{2+}] \cdot 2^2\right) = \frac{1}{2}\left(2C_{BOH} \cdot 1^2 + C_{BOH} \cdot 2^2\right) = 3C_{BOH} \text{(Group II)}$$

$pKw^o$ changes with the temperature and the pressure and the data are taken from *The Ionization Constant of Water over Wide Ranges of Temperature and Density* by Bandura and Lvov (2005)[75].

Therefore, the pH depends on the temperature and the pressure. Equations 4.20, 4.21 and 4.22 are solved using MatLab and the pH vs. the concentration of hydroxide $C_{BOH}$ of the Group I and Group II at standard conditions( 1atm and 25°C) and at the fuel cell operation conditions ( 700 psi and 220 °C approx.) is plotted in figure 4.8. Beware that the reliability of Davies equations at high temperatures and high concentrations is very poor. Butler, in his figure 4.5, compares experimental activity coefficients with the ones calculated from Davies equations for three 1-1 salts (HCl, NaCl and $NaClO_4$) and two 1-2 salts ($MgCl_2$ and $NaClO_4$) and observes that at ionic strength above 0.5 M, the experimental activity coefficients are significantly different from those given by Davies equation. In addition, the dependence of temperature in Davies equation applies only to the temperature range 0-50 °C. Figure 4.8 also illustrates the pH vs. Concentration (M) assuming $\gamma = 1$ for all concentrations to see the effect of $\gamma$ whose values are uncertain. The effect should be small at low concentrations because $\gamma \to 1$ as $[OH^-] \to 0$ . Figure 4.8 indicates the lines pH vs. concentration when activity coefficients are assumed equal to one. The activity coefficients are not assumed equal to one unless indicated and are calculated with Davies equation.

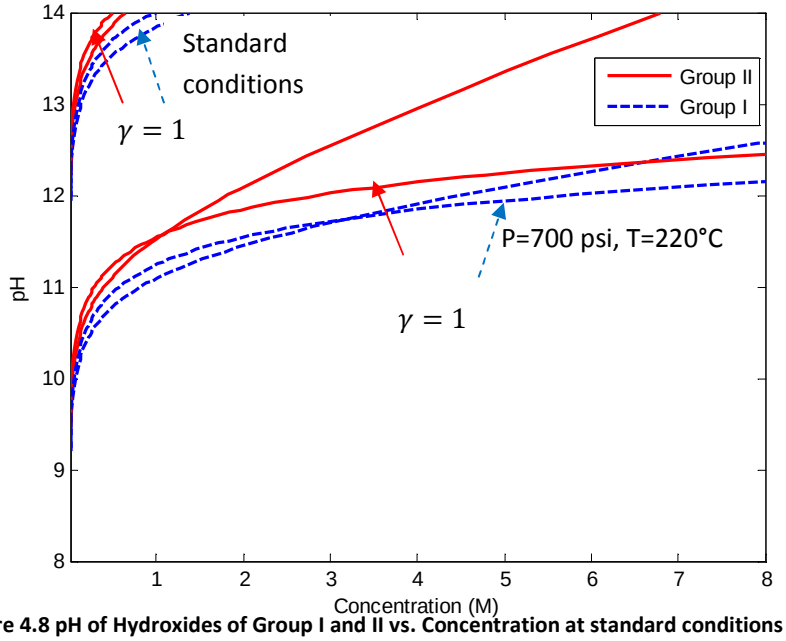


**Figure 4.8 pH of Hydroxides of Group I and II vs. Concentration at standard conditions and at 220 °C and 700 psi. Lines pH vs. concentration when activity coefficients are assumed equal to one are indicated. Otherwise, activities are calculated using Davies equation.**

The pH at the fuel cell operation conditions (high temperature and pressure) is significantly lower from the pH at standard conditions, so a higher concentration is needed to get a high pH in the fuel cell. Observe that, as expected, the effect of the activity coefficients is negligible at low concentrations, the

lines of activity coefficient equal to one ($\gamma = 1$) converge with their respective lines when activity coefficients were considered. Observe that the effect is much greater in the group II hydroxides as the ionic strength is three times higher. Figure 4.9 shows the variation of the pH of a Group I hydroxide with the temperature for two different pressures and two different concentrations.

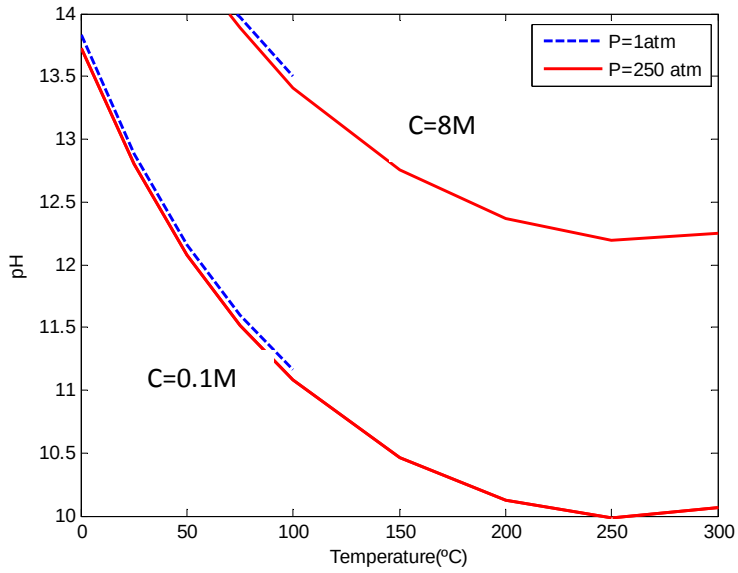


**Figure 4.9 pH of a 0.1M and 8M Group I hydroxide vs. Temperature at 1 atm and 250 atm**

In this range of pressure, the variation of the pH with the pressure is negligible. The pH change is due mainly because of the temperature difference and the concentration of the hydroxide.

### *4.1.3 Validation of the pH model*

- **pH vs. Concentration**

Different solutions of potassium hydroxide have been prepared to see if the experimental and theoretical results agree. The theoretical results have been obtained from equations 4.20 to 4.22 considering activity coefficients and assuming activity coefficients equal to one. A 6 M solution of potassium hydroxide has been prepared (39.19 g of Potassium Hydroxide 85.9% pure from *FisherChemicals* have been dissolved in 0.1 L). This solution has been diluted several times. The pH of all these solutions has been measured, plotted into figure 4.10 and compared to the theoretical solutions. The pH meter used is Mettler Toledo 'Seven easy'. Its relative pH and temperature accuracy is ±0.01 and ±0.05 in respectively. The buffers used to calibrate have pHs of 7, 10 and 12.45.

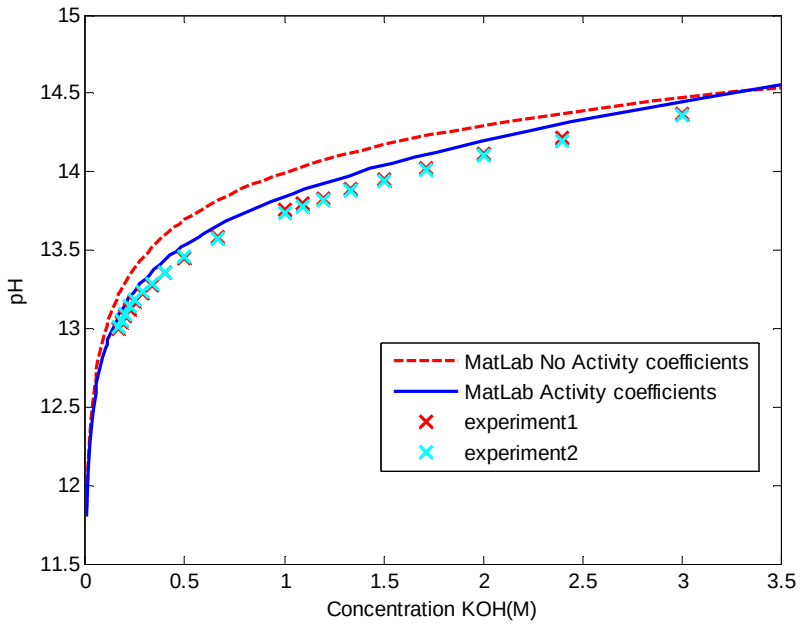


**Figure 4.10 pH of Potassium Hydroxide vs. Concentration at 25 °C and 1 atm**

The experimental values are lower than expected. The difference between the theoretical and experimental pH varies from 0.081 to 0.10 considering activity coefficients and from 0.10 to 0.24 not considering activity coefficients. Observe that the introduction of the activity coefficients values in the pH calculation reduces the pH difference, the pH-concentration accuracy improves in all the range of concentrations we experimented (from 0.17 M to 3 M), and the calculated curve follows the same tendency as the experimental curve.

In page 41, it is stated that Davies model of activity coefficients was checked by Butler[66]. Butler compares activity coefficients calculated from Davies equation to experimental values of the activity coefficients for three 1-1 salts and two 1-2 salts in his figure 2.5. For the electrolytes used in Butler, at ionic strength above 0.5 M, the experimental activity coefficients are significantly different from those given by Davies equation. However, our experimental observations indicate that for KOH, the model seems to be applicable to concentrations as high as 3M. Higher concentrations could not be tested at room temperature because of the extremely high pH reading, out of the pH-meter measurement range. The reproducibility of the pH in the experiments carried out is very good. The pH difference between experiment 1 and 2 fluctuates from 0 to 0.02.

- **pH vs. Temperature**

A 0.1 M solution of potassium hydroxide has been prepared (0.65 g of Potassium Hydroxide 85.9% pure from *FisherChemicals* have been dissolved in 0.1 L). This solution has been heated. The pH of the solution at the different temperatures from room temperature (23°C) to almost 100 °C have been measured, plotted into figure 4.11 and compared to the pH-temperature values calculated in MatLab both considering activity coefficients calculated with Davies equation and assuming activity coefficients equal to one.

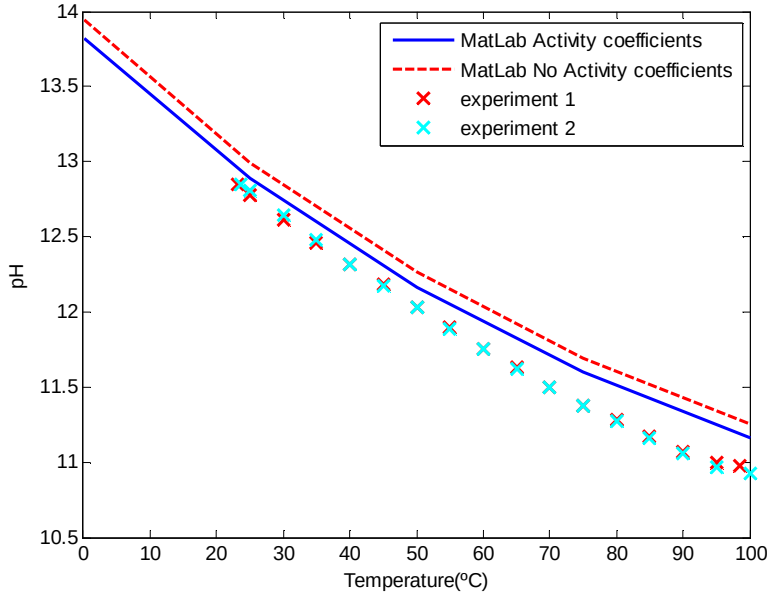


**Figure 4.11 pH of 0.1 M solution of Potassium Hydroxide vs. temperature at 1 atm**

The pH obtained experimentally follows the same tendency than the theoretical pH. The experimental values are lower than expected, the difference between the calculated pH is lowered when activity coefficient are introduced in the pH calculation. The pH difference between the calculated values using activity coefficients and the experimental values varies from 0.10 to 0.24. The reproducibility is good. The pH difference between both experiments goes from 0 to 0.03.

The discrepancy shown in both figures 4.10 and 4.11 could be due to the fact that the pH -meter is designed to read $H^+$ concentration, the pH-meter can miss accuracy in very basic solutions where the $H^+$

concentration is very low. Besides, the potassium hydroxide solution is not pure (85.9 %), which can alter the expected value. The pH of the 1M KOH solution 85.9% pure used in the experiments was compared to the pH of a 1M standard NaOH solution to check the reliability of our model. The pH of the 1M NaOH standard solution was 13.9 as opposed to 13.76 given by the KOH solution. The pH of this standard is over the curve. The difference in the pH between this standard NaOH and the MatLab pH considering activity coefficients is 0.06. The experimental pHs obtained with the KOH solution, slightly lower than expected, could be due to the impurity of this KOH solution. Moreover, the pHs measured are above the buffers pH (7, 10 and 12.45) so these values are extrapolated by the pH-meter. In figure 4.10, the deviation is higher at higher concentrations, the equation used (Davies equation, equation 4.5) misses accuracy at high concentration (Concentrations above 0.5 M). However, the accuracy seems pretty good up to concentrations of KOH of 3M. In figure 4.11, the deviation is higher at higher temperatures, Davies equation also misses accuracy at temperatures over 50 °C but the accuracy seems acceptable until temperatures of 100 °C.

## 4.2 pH and Solubility of the $H_2O$-Carbonate system

### *4.2.1 Solubility*

The carbonates completely dissociate in solution, $B_2CO_3 \leftrightarrow 2B^+ + CO_3^{2-}$. The carbonate ion ($CO_3^{2-}$) is a weak, polyprotic base which in solution is in equilibrium the bicarbonate and $CO_2$ as shown in figure 4.2. However, when the carbonate concentration reaches their saturation concentration, it precipitates. The solubility depends on the solvent, temperature and pressure.

| | | 0°C | 10°C | 15°C | 20°C | 30°C | 40°C | 50°C | 60°C | 70°C | 80°C | 90°C | 100°C |
|---|---|---|---|---|---|---|---|---|---|---|---|---|---|
| **Group I** | **Li2CO3** | 1.54 | 1.43 | | 1.33 | 1.26 | 1.17 | | 1.01 | | 0.85 | | 0.72 |
| | **Na2CO3** | 7 | 12.5 | | 21.5 | 39.7 | 49 | | 46 | | 43.9 | 43.9 | |
| | **K2CO3** | 105 | 109 | | 111 | 114 | 117 | 121.2 | 127 | | 140 | 148 | 156 |
| | **Cs2CO3** | | | 260.5 | | | | | | | | | |
| **Group II** | **BeCO3** | | | | 0.218 | | | | | | | | |
| | **MgCO3** | | | | 0.039 | | | | | | | | |
| | **CaCO3** | | | | 0.000617 | | | | | | | | |
| | **BaCO3** | | | | 0.001409 | | | | | | | | |

Table 4.4 shows the solubility in water with the temperature of different carbonates, under 1 atm of pressure, the units are given in g/ 100g $H_2O$.

**Table 4.4 Solubility of carbonates in water with the temperature, under 1 atm pressure, units in g/100 g $H_2O$[74]**

| | | 0°C | 10°C | 15°C | 20°C | 30°C | 40°C | 50°C | 60°C | 70°C | 80°C | 90°C | 100°C |
|---|---|---|---|---|---|---|---|---|---|---|---|---|---|
| Group I | $Li_2CO_3$ | 1.54 | 1.43 | | 1.33 | 1.26 | 1.17 | | 1.01 | | 0.85 | | 0.72 |
| | $Na_2CO_3$ | 7 | 12.5 | | 21.5 | 39.7 | 49 | | 46 | | 43.9 | 43.9 | |
| | $K_2CO_3$ | 105 | 109 | | 111 | 114 | 117 | 121.2 | 127 | | 140 | 148 | 156 |
| | $Cs_2CO_3$ | | | 260.5 | | | | | | | | | |
| Group II | $BeCO_3$ | | | | 0.218 | | | | | | | | |
| | $MgCO_3$ | | | | 0.039 | | | | | | | | |
| | $CaCO_3$ | | | | 0.000617 | | | | | | | | |
| | $BaCO_3$ | | | | 0.001409 | | | | | | | | |

At 20 °C and 1 atm, the solubility in mol/$L_{H2O}$ is

**Table 4.5 Solubility of carbonates in water in mol /$L_{H2O}$ at 20 °C**

| Group I | C (molal) | Group II | C (molal) |
|---|---|---|---|
| $Li_2CO_3$ | 0.17 | $Be\ CO_3$ | 0.032 |
| $Na_2CO_3$ | 2.88 | $Mg\ CO_3$ | 0.005 |
| $K_2CO_3$ | 8.14 | $Ca\ CO_3$ | $6.1x10^{-5}$ |
| $Cs_2CO_3$(15°C) | 7.99 | $BaCO_3$ | ≈0 |

The candidates for the fuel cell are the potassium and cesium carbonate that present the higher solubility. However, as figure 4.2 shows, the solution contains the carbon dioxide and bicarbonate along with the carbonate. At very high pH, the carbonate is the main component in the solution but as the pH decreases, the carbonate concentration decreases and the bicarbonate concentration increases. Table 4.6 contains the data of the bicarbonates solubility.

**Table 4.6 Solubility of bicarbonates in water with the temperature, under 1 atm pressure, units in g/100 g $H_2O$**

| | | 0°C | 10°C | 20°C | 30°C | 40°C | 50°C | 60°C |
|---|---|---|---|---|---|---|---|---|
| Group I | $LiHCO_3$ | | | 5.74 | | | | |
| | $NaHCO_3$ | 7 | 8.1 | 9.6 | 11.1 | 12.7 | | 16 |
| | $KHCO_3$ | 22.5 | 27.4 | 33.7 | 39.9 | 47.5 | | 65.6 |
| Group II | $CaHCO_3$ | | | 16.6 | | | | |

At 20 °C and 1 atm, the solubility in mol/$L_{H2O}$ is

**Table 4.7 Solubility of bicarbonates in water in mol /$L_{H2O}$ at 20 °C**

| Group I | C (molal) | Group II | C (molal) |
|---|---|---|---|
| **$LiHCO_3$** | 0.845 | **$Ca(HCO_3)_2$** | 1.642 |
| **$NaHCO_3$** | 1.143 | | |
| **$KHCO_3$** | 3.366 | | |

The sodium and potassium bicarbonate solubilities are lower than their respective carbonates. This can cause problems of precipitation.

### *4.2.2 pH*

When a carbonate is dissolved in water, it dissociates completely in solution

Carbonate from Group I: $B_2CO_3 \leftrightarrow 2B^+ + CO_3^{2-}$

Carbonate from Group II: $BCO_3 \leftrightarrow B^{2+} + CO_3^{2-}$

The basic equations of the carbonate system consist of the equilibria, a charge balance and mass balances on carbonate and the cation[66].

Equilibria

$$K_{a1} = \frac{[H^+][HCO_3^-]}{[CO_2\ ]} \qquad \text{Equation 4.23}$$

Equation 4.23 would be written properly as $K_{a1} = \frac{[H^+][HCO_3^-]}{[H_2CO_3\ ]}$, however, the carbonic acid ($H_2CO_3$) is in equilibrium with $CO_2$ dissolved ($CO_{2,\,aq}$) and water, at equilibrium [$H_2CO_3$] is only about $10^{-3}$ as large as [$CO_2$] and has no special significance in the acid-base equilibria, since both are uncharged. Hence, [$H_2CO_3$] + [$CO_2$] is written simply as [$CO_2$].

$$K_{a2} = \frac{[H^+][CO_3^{2-}]}{[HCO_3^-\ ]} \qquad \text{Equation 4.24}$$

Mass balance on carbon and cation

$$C_{CO_3} = [CO_2\,] + [HCO_3^-\,] + [CO_3^{2-}] \qquad \text{Equation 4.25}$$

$$[B^+] = 2C_{CO_3} \text{ (Group I)}$$

$$[B^{2+}] = C_{CO_3} \text{(Group II)} \qquad \text{Equation 4.26}$$

Where $C_{CO_3}$ is the molar concentration of the carbonate solution.

Charge balance

$$[B^+] + [H^+] = [HCO_3^-\,] + 2[CO_3^{2-}] + [OH^-] \text{ (Group I)}$$

$$2[B^{2+}] + [H^+] = [HCO_3^-\,] + 2[CO_3^{2-}] + [OH^-] \text{ (Group II)} \qquad \text{Equation 4.27}$$

Expressing the carbonate and bicarbonate concentrations in terms of $H^+$ and $CO_2$, equations 4.23 and 4.24 become

$$[HCO_3^-\,] = K_{a1}\frac{[CO_2\,]}{[H^+]} \qquad \text{Equation 4.28}$$

$$[CO_3^{2-}] = K_{a1}K_{a2}\frac{[CO_2\,]}{[H^+]^2} \qquad \text{Equation 4.29}$$

Substituting these equations in equation 4.25

$$C_{CO_3} = [CO_2\,] + K_{a1}\frac{[CO_2\,]}{[H^+]} + K_{a1}K_{a2}\frac{[CO_2\,]}{[H^+]^2} \qquad \text{Equation 4.30}$$

Working out $[CO_2]$

$$[CO_2\,] = \frac{C_{CO_3}[H^+]^2}{[H^+]^2 + K_{a1}[H^+] + K_{a1}K_{a2}} \qquad \text{Equation 4.31}$$

And if this expression is substituted in equations 3.28 and 3.29, we obtain

$$[HCO_3^-] = \frac{K_{a1} C_{CO_3} [H^+]}{[H^+]^2 + K_{a1}[H^+] + K_{a1}K_{a2}} \quad \text{Equation 4.32}$$

$$[CO_3^{2-}] = \frac{K_{a1} K_{a2} C_{CO_3}}{[H^+]^2 + K_{a1}[H^+] + K_{a1}K_{a2}} \quad \text{Equation 4.33}$$

The concentration of $OH^-$ is related to the concentration of $H^+$ by the dissociation constant of water by equation 4.8 ( $[OH^-] = Kw/[H^+]$). If all these terms are substitute in the charge balance, we find the same equation for carbonates from both Groups I and II

$$2C_{CO_3} + [H^+] = \frac{K_{a1} C_{CO_3} [H^+] + 2K_{a1}K_{a2}C_{CO_3}}{[H^+]^2 + K_{a1}[H^+] + K_{a1}K_{a2}} + \frac{Kw}{[H^+]} \quad \text{Equation 4.34}$$

Where the equilibrium constants, $K_{a1}$ and $K_{a2}$, and the dissociation constant of water, $Kw$, depend mainly on the temperature and ionic medium and are calculated with equations 4.8, 4.14 and 4.16. Solution of equation 4.34 is different for carbonates from group I and II as the ionic effect is different. The ionic strength for carbonates of groups I and II is calculated with equation 4.4($I = \frac{1}{2}\sum_i [i] z_i^2$).

$$I = \frac{1}{2}\left([CO_3^{2-}] \cdot 2^2 + [B^+] \cdot 1^2\right) = \frac{1}{2}\left(C_{CO_3} \cdot 4 + 2 \cdot C_{CO_3} \cdot 1\right) = 3C_{CO_3} \quad \text{(Group I)}$$

$$I = \frac{1}{2}\left([CO_3^{2-}] \cdot 2^2 + [B^{2+}] \cdot 2^2\right) = \frac{1}{2}\left(C_{CO_3} \cdot 4 + C_{CO_3} \cdot 4\right) = 4C_{CO_3} \quad \text{(Group II)}$$

Setting the value of the carbonate concentration, $C_{CO_3}$, and the temperature, eq. 4.34 can be solved in Matlab, so that we can obtain the $[H^+]$ and therefore the pH of a solution at a certain temperature. Figure 4.12 shows the pH of a Group I carbonate versus the concentration (M) at 25, 100 and 200°C considering ionic effect and assuming activity coefficients equal to one. Activity coefficients are calculated with Davies equation unless indicated. When activity coefficients are assumed equal to one, it is indicated

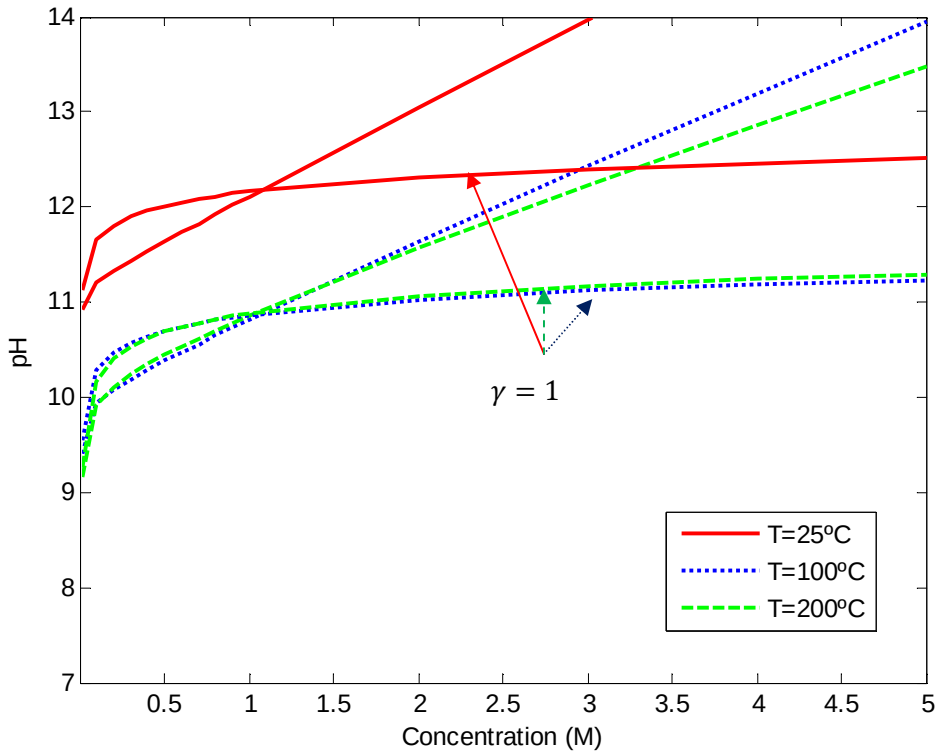


**Figure 4.12 pH vs. Concentration of potassium carbonate at 25, 100 and 200 °C**

According to figure 4.12, the temperature has a big effect in the pH from 25 to 100 °C, but from 100 to 200°C, the pH almost does not change. Observe the effect of the ionic effect in the lines, the tendency is totally different. Keep in mind that the equations assuming ionic effect are reliable until 0.5 M. In the next section, 'validation of the pH model', we prove that the model is good for potassium carbonate concentrations as high as 1M. Therefore, the graph shape in figure 4.12 from 1M to 5M should not be considered. Also, the fact that the pH does not change from 100 to 200°C could not be tested experimentally as the pH electrode is able to read pHs at temperatures as high as 100 °C.

Also, if we know the value of the pH and the temperature, it is possible to know the concentrations of all the species using equations 4.31 to 4.33 assuming that there is no ionic effect, i.e. activity coefficients equal to one ($\gamma = 1$). Solving for the logarithmic concentration ratios at different pH and plotting the solution, we get figure 4.13.

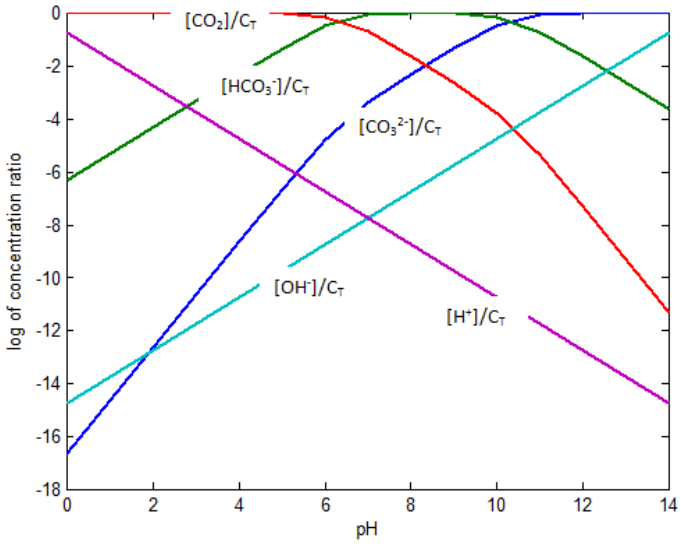


**Figure 4.13 Logarithmic concentration ratio diagram of the carbonate system at room temperature**

$C_T$ is the sum of bicarbonate, carbonate and $CO_2$ concentrations. The results agree with Butler's results (Figure 4.2 in Butler[66])

### *4.2.3 Validation of the pH model*

- **pH vs. Concentration**

Different solutions of potassium carbonate have been prepared to see if the experimental and theoretical results agree. A 5 M (mol/L) solution of potassium carbonate has been prepared (69.105 g of Potassium Carbonate anhydrous from *FisherChemicals* have been dissolved in 0.1 L). This solution has been diluted. The pH of all these solutions have been measured, plotted into figure 4.14 and compared to the theoretical solutions calculated from equation 4.14. The equation has been calculated using activity coefficients or without using them and both solutions are plotted. The pH meter used is Mettler Toledo 'Seven easy'. Its relative pH and temperature accuracy is ±0.01 and ±0.05 in respectively. The buffers used to calibrate have pHs of 7, 10 and 12.45.

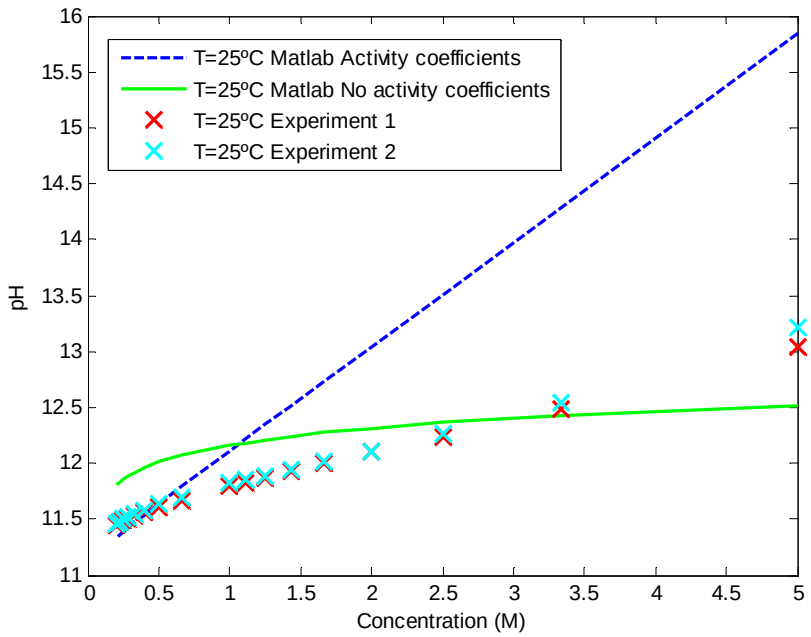


**Figure 4.14 pH of Potassium Carbonate vs. Concentration from 0.2 to 5M at 22°C and 1 atm**

The reproducibility of the pH in the experiments carried out is good. The pH difference between experiments varies from 0 to 0.18. The experimental pH at concentrations over 1M differs a lot from both pHs obtained by equation 4.34, considering activity coefficients or without considering them, especially when we consider activity coefficients. Observe that a simple linear correction would give the pH curve the correct shape in the whole range of concentrations. Remind that the equation used to calculate the activity coefficients (Davies equation, equation 4.5) misses accuracy at high concentration (Concentrations above 0.5 M for the species tested in Butler). Observe that the accuracy for $K_2CO_3$ is good for concentrations al low concentrations. At concentrations of 1M, the pH difference starts to be significant; the pH difference at 1M is 0.32. At low concentrations ([$K_2CO_3$] <1M) equation 4.34 solution including the activity coefficients fits the data very well, figure 4.15 shows the experimental data and equation 4.34 solution for the concentrations lower than 1M. The difference between the theoretical and experimental pH is less than 0.12 in all the cases. Also observe that the pH –concentration seems to follow a linear relationship.

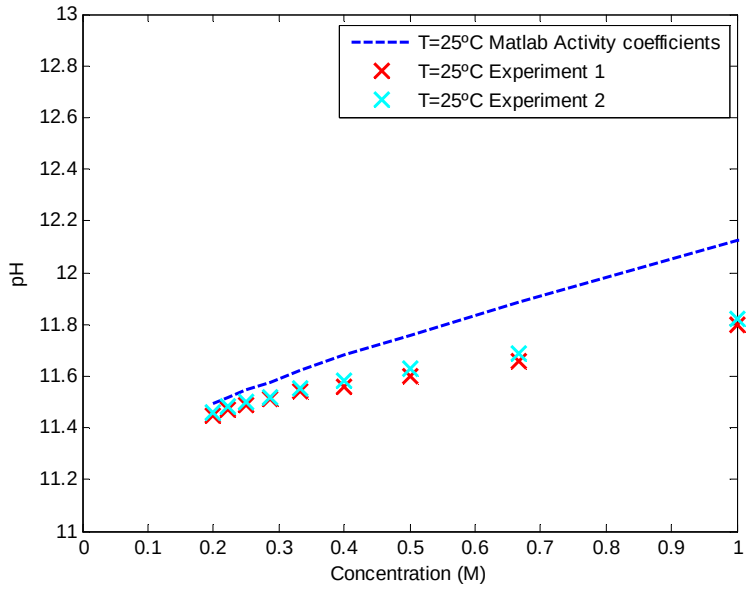


**Figure 4.15 pH of Potassium Carbonate vs. Concentration from 0.2 to 1M at 22°C and 1 atm**

- **pH vs. Temperature**

A 0.1 M solution of potassium carbonate has been prepared (1.382 g of Potassium Carbonate from *FisherChemicals* have been dissolved in 0.1 L). This solution has been heated. The pH of the solution at the different temperatures from room temperature (23°C) to 100 °C have been measured, plotted into figure 4.16 and compared to the theoretical solutions. Two solutions have been obtained, one considering activity coefficient and another one without considering them.

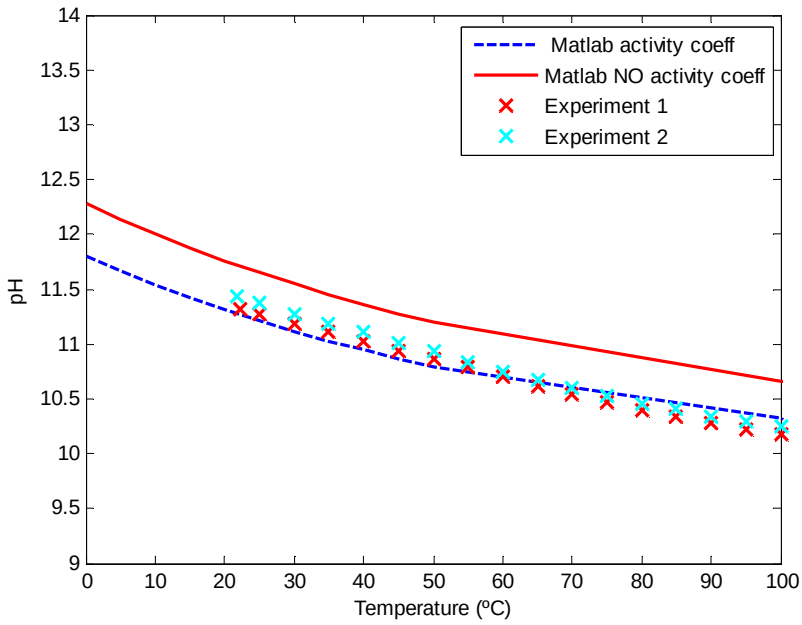


**Figure 4.16 pH of 0.1 M solution of Potassium Carbonate vs. Temperature at 1 atm**

The pHs obtained experimentally seem to follow a more linear tendency than the theoretical results. Figure 4.16 shows a good agreement between the experimental data and the solution considering activity coefficients. Observe that this validation was performed only for 0.1 M solution of $K_2CO_3$, which is a value that Davies equation can be used. From figure 4.15, we can conclude that the model cannot be applied to concentration over 1M because the pH difference is significant. The accuracy of the solution improves when activity coefficients are considered. The decrease in the pH with the temperature indicates the increase in the bicarbonate concentration (Figure 4.13). The potassium bicarbonate solubility is lower than the carbonate (Table 4.4 and Table 4.6) and the temperature increase can cause problems of precipitation. Indeed, lots of potassium bicarbonate crystals appear in the fuel cell working with high concentrations solutions of potassium carbonate.

### *4.2.4 Carbonate with a $CO_2$ atmosphere*

Figure 4.2 illustrates the proposed system. In a solution in equilibrium with a constant partial pressure of carbon dioxide, the gaseous $CO_2$ is in equilibrium with the $CO_2$ dissolved in the electrolyte. This equilibrium is governed by Henry's law

$$[CO_2] = K_H P_{CO_2}$$ Equation 4.35

Carbon dioxide is slightly soluble in pure water; as with all gases, the solubility decreases with temperature but it increases with the pressure. Wiebe et al. (1940) [76] give data of $CO_2$ solubility at temperatures from 12 to 40 °C and high pressures in cc/g $H_2O$.

**Table 4.8 Solubility of carbon dioxide in water at cc S.T.P/g $H_2O$ with pressure from 12 to 40°C**

SOLUBILITY OF CARBON DIOXIDE IN WATER
(CC. S. T. P. PER G. OF $H_2O$)

| Total pressure in atm. | Temperatures, °C. | | | | | |
|---|---|---|---|---|---|---|
| | 12 | 18 | 25 | 31.04 | 35 | 40 |
| 25 | | 19.51 | | 14.18 | 12.95 | 11.62 |
| 50 | 35.54 | 32.03 | 27.23 | 24.15 | 22.21 | 20.35 |
| 75 | 36.33 | 33.85 | 31.17 | 29.33 | 27.84 | 25.81 |
| 100 | 36.77 | 33.98 | 31.75 | 30.17 | 29.13 | 27.81 |
| 125 | | | | | | 28.71 |
| 150 | 38.39 | 35.75 | | 31.59 | 30.52 | 29.39 |
| 200 | 39.77 | 37.17 | | 32.78 | 31.83 | 31.74 |
| 300 | 41.07 | 39.31 | | | | |
| 400 | | | 38.62 | 36.78 | 35.73 | 34.87 |
| 500 | | | | 38.67 | 37.99 | 36.73 |

Considering a potassium carbonate solution with a $CO_2$ atmosphere in equilibrium, the equations of the system consist of the equilibria, a charge balance and mass balance on potassium.

Equilibria

$$K_{a1} = \frac{[H^+][HCO_3^-]}{[CO_2]}$$ Equation 4.36

$$K_{a2} = \frac{[H^+][CO_3^{2-}]}{[HCO_3^-]}$$ Equation 4.37

Mass balance on potassium

$$[K^+] = 2C_{CO_3}$$ Equation 4.38

Where $C_{CO_3}$ is the molar concentration of the solution of potassium carbonate

Charge balance

$$[K^+] + [H^+] = [HCO_3^-] + 2[CO_3^{2-}] + [OH^-] \qquad \text{Equation 4.39}$$

Expressing the concentrations in terms of $H^+$ and $P_{CO_2}$, eq.4.36 and 4.37 become

$$[HCO_3^-] = K_{a1}\frac{[CO_2]}{[H^+]} = K_{a1}K_H\frac{P_{CO_2}}{[H^+]} \qquad \text{Equation 4.40}$$

$$[CO_3^{2-}] = K_{a1}K_{a2}K_H\frac{P_{CO_2}}{[H^+]^2} \qquad \text{Equation 4.41}$$

The concentration of $OH^-$ is related to the concentration of $H^+$ by the dissociation constant of water, $[OH^-] = Kw/[H^+]$.Substituting equations 4.38, 4.40 and 4.41 in 4.39

$$2C_{CO_3} + [H^+] = K_{a1}K_H\frac{P_{CO_2}}{[H^+]} + 2K_{a1}K_{a2}K_H\frac{P_{CO_2}}{[H^+]^2} + \frac{K_w}{[H^+]} \qquad \text{Equation 4.42}$$

Or reorganizing

$$[H^+]^3 + 2C_{CO_3}[H^+]^2 - \left(K_{a1}K_HP_{CO_2} + K_w\right)[H^+] - 2K_{a1}K_{a2}K_HP_{CO_2} = 0 \qquad \text{Equation 4.43}$$

Where the equilibrium constants, $K_{a1}$ and $K_{a2}$, the dissociation constant of the water, $K_w$, and Henry´s constant, $K_H$, depend mainly on the temperature and ionic medium and are calculate using equations 4.8, 4.14 and 4.16. The ionic strength has been calculating using equation 4.4 for a group I carbonate ( $I = \frac{1}{2}\left([CO_3^{2-}]\cdot 2^2 + [B^+]\cdot 1^2\right) = \frac{1}{2}\left(C_{CO_3}\cdot 4 + 2\cdot C_{CO_3}\cdot 1\right) = 3C_{CO_3}$ ). Setting the value of the potassium carbonate concentration, $C_{CO_3}$, the partial pressure of $CO_2$ , $P_{CO_2}$ , and the temperature, equation 4.43 has been solved in MatLab, so that we can get the $[H^+]$ and therefore the pH of a solution at a certain temperature. Figure 4.17 shows the pH of a 1 M Potassium Carbonate solution with different constant partial pressure of $CO_2$ at different temperatures

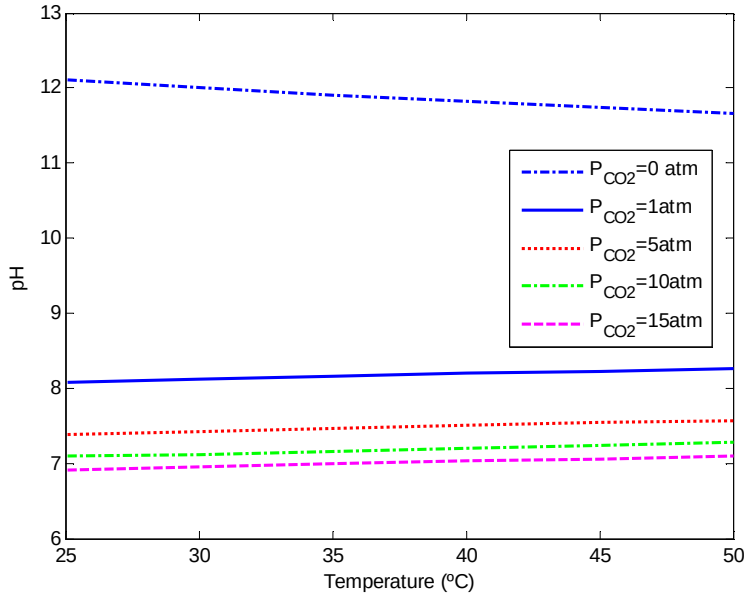


**Figure 4.17 pH of a 1M potassium carbonate solution vs. Temperature(°C) with a $CO_2$ atmosphere**

The presence of a partial pressure of $CO_2$ changes completely the behavior of the pH of the carbonate solution with the temperature. The pH of the solution without $CO_2$ decreases with the temperature. pKa1 and pKa2 decrease with the temperature (Table 4.1), so the respective equilibrium constants(defined as –log(pK)), Ka1 and Ka2, increase with the temperature, which means that the equilibrium reactions are shifted to the formation of $H^+$ and the solution become more acid, therefore, the pH decrease with the temperature. The pH of the solution with $CO_2$ increases with the temperature. Table 4.1 shows that, as opposed to pKa, pKh increase with the temperature, so that, Kh (defined as –log(pKh))decreases. On the one hand, a decrease in Henry´s constant causes a decrease in the concentration of the $CO_2$ in solution and consequently, an increase in the basicity. On the other hand, an increase in the equilibrium constants cause a shift of the reactions to the formation of $H^+$ causing an increase of the acidity. From figure 4.17, we can determine that at a certain partial pressure of $CO_2$, the effect of the Henry´s constant is more important than the effect of the equilibrium constants as the pH of a solution increases with the temperature. At the same temperature, as the constant pressure of $CO_2$ increases, the solution is more acid as the $H_2CO_3$ concentration increases.

Setting the value of the temperature (T=25 °C) and the partial pressure of $CO_2$ (P=1atm), all the species concentrations cal also be calculated from equations 4.35, 4.40 and 4.41 as a function of pH and represented in figure 4.18. The ionic effect is considered zero, i.e. activity coefficients equal to one ($\gamma = 1$).

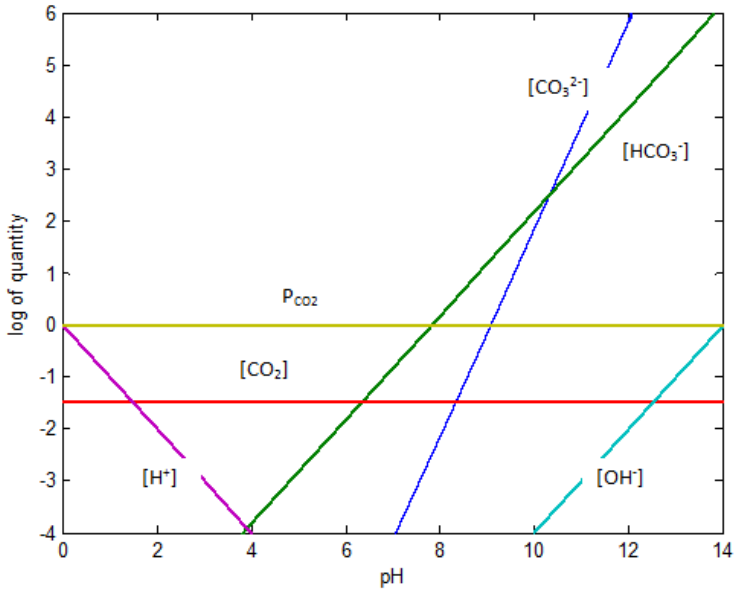


**Figure 4.18 Logarithmic concentration diagram at room temperature and at a constant partial pressure of CO2 of 1 atm**

These results agree with figure 2.1 in Butler [66]

## 4.3 Boiling point

In the carbon fuel cell, the electrolyte –an aqueous solution of $K_2CO_3$- is heated to more than 100 ˚C under pressure. The boiling points at different pressures are estimated, so that we can assure that the temperature in the carbon fuel cell is below the boiling point and therefore assure that the electrolyte is in its liquid state.

Equation 4.44 [77] relates the boiling point T with the mole fraction of water x

$$\left.\frac{\partial lnx}{\partial T}\right|_P = -\frac{L}{RT^2} \qquad \text{Equation 4.44}$$

Where *L* is the enthalpy increase of the evaporation of 1 mol of the water at temperature *T* and *R* is the gas constant (8.314 J/molK). This equation applies strictly under conditions of constant total pressure, as when the solution is under the pressure of the atmosphere. Under the same conditions the temperature coefficient of $L_i$ is given by

$$\left.\frac{\partial L_i}{\partial T}\right|_P = \left.\frac{\partial h^v}{\partial T}\right|_P - \left.\frac{\partial H_i}{\partial T}\right|_P = c_{pi}^v - c_{pi} \equiv \Delta c_p \qquad \text{Equation 4.45}$$

Where $\Delta c_P$ is the molar heat capacity of the solvent as a vapor less the molar heat capacity of the solvent as a liquid.Over the small ranges of temperature which are usually encountered in the measurement of boiling point elevation, $\Delta c_p$ may usually be assumed constant. Therefore the differential equation can be integrated as: $L_i: L_B \rightarrow L$, $T: T_B \rightarrow T$

$$L - L_B = \Delta c_p\ (T - T_B) \qquad \text{Equation 4.46}$$

Where $L_B$ corresponds to the latent heat at the boiling point $T_B$of water. Substituting this equation in 4.44

$$\left.\frac{\partial lnx}{\partial T}\right|_P = -\frac{L_B + \Delta c_p\ (T - T_B)}{RT^2} \qquad \text{Equation 4.47}$$

This differential equation is integrated: $x: 1 \rightarrow x$, $T: T_B \rightarrow T$

$$ln\frac{1}{x} = \frac{L_B \Delta c_p T_B}{R}\left(\frac{1}{T_B} - \frac{1}{T}\right) + \frac{\Delta c_p}{R} ln\frac{T}{T_B} \qquad \text{Equation 4.48}$$

So, the boiling point at different molalities can be obtained. Data of the $L_B$, $\Delta c_p$, and $T_B$ are selected from Steam Tables in SI-Units [78]. Figure 4.19 depicts the boiling point temperature versus the molality of a potassium carbonate solution at two pressures (580 and 750 psi).

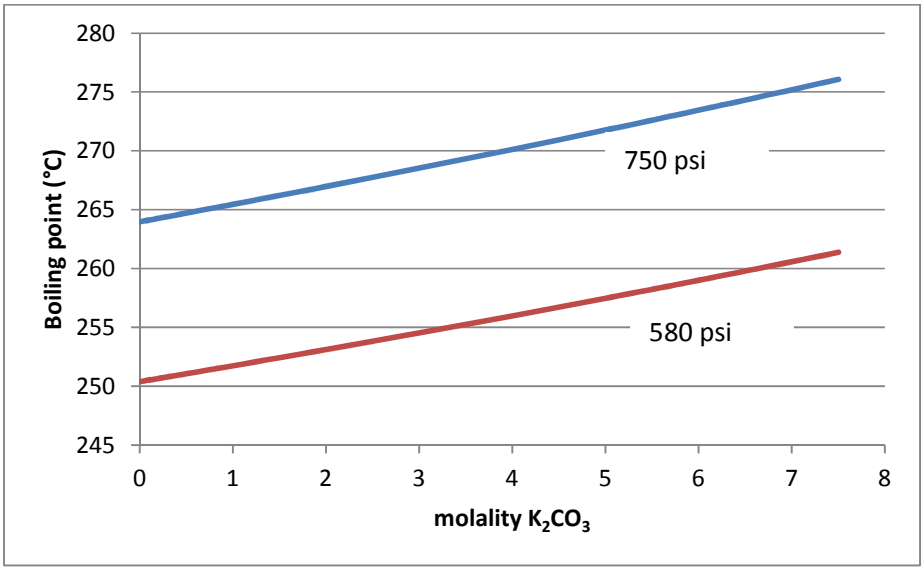


**Figure 4.19 Boiling point of a Potassium Carbonate solution vs. molality**

The graph gives us an idea of the upper limit temperature of the fuel cell. The pressure the fuel cell is working is around 700 psi. According to the graph, the temperature that can be reached to a 5 M $K_2CO_3$ electrolyte in its liquid phase is between 257 and 272 °C.

# CHAPTER 5. STUDY OF THE CARBONATE/BICARBONATE CHEMISTRY. ANALYSIS OF THE FINAL EXPERIMENTAL SOLUTION

As mentioned earlier, this study started with Ashley Blitz when she did "Experimental Analysis of an Undesirable Crystal Precipitate in a Developmental Carbon Fuel Cell" as her undergraduate thesis. In her research, Ashley determined the chemical composition and formula of the crystal precipitate being produced from the carbon fuel cell (Figure 5.1) and she researched the way to prevent them from forming in the fuel cell during operation. The crystals were determined as potassium bicarbonate. Her work is summarized in the following section.


**Figure 5.1 Picture of crystal precipitates from the carbon fuel cell showing the presence of nickel carbonate by the greenish tint in the crystals**

The research continued in the Laboratory. We studied the thermodynamic properties of these crystals as well as the reactions favored at the fuel cell conditions. The work is presented in the two following chapters.

## 5.1 Summary of previous work in the Lab

### *5.1.1 Determination of the crystals*

In Ashley's work, the crystals in the fuel cell were sent to the Hungarian Academy of Science in Hungary and they were identified as mainly $KHCO_3$ by Thermogravimetry-Mass Spectrometry (TG-MS) (Figure 5.2).

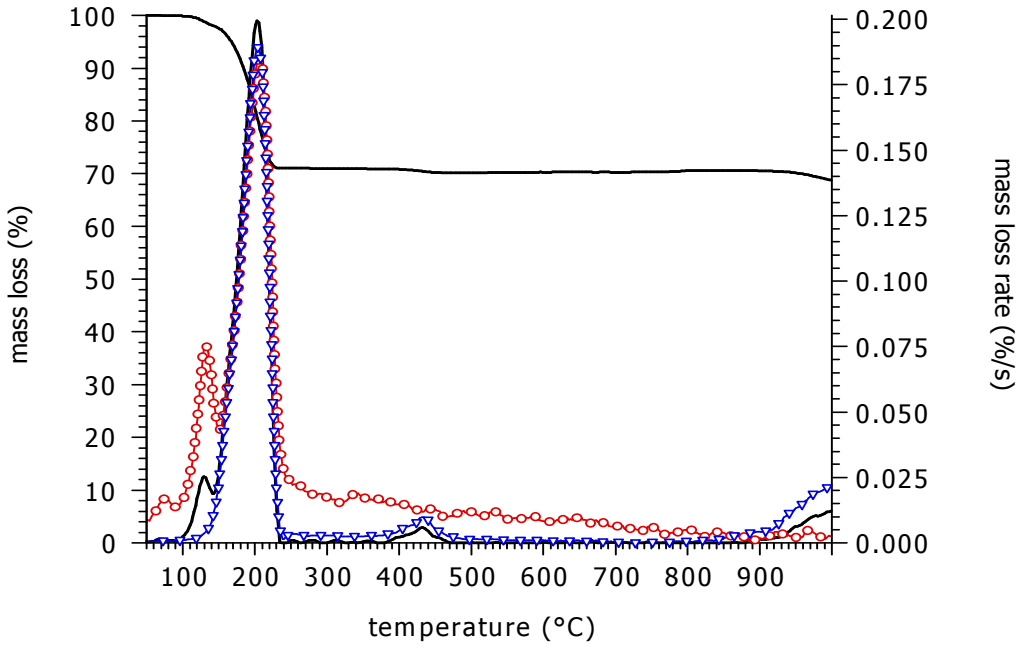


**Figure 5.2 TG, DTG and MS intensity (–○– water (m/z 18) and –∇– carbon dioxide (m/z 44)) of crystal precipitate from the carbon fuel cell run by the Hungarian Academy of Sciences**

The TG-MS revealed that the crystals consisted of a mixture of mainly potassium bicarbonate (~88 %) and potassium carbonate (~12 %). The rapid decomposition of the crystals between 150-240° C according to the DTG is consistent with the decomposition of potassium bicarbonate into potassium carbonate, $CO_2$ and water as described by Lehman et al. **[14]**

$$2KHCO_3 \leftrightarrow K_2CO_3 + CO_2 + H_2O \qquad \text{Reaction 5.1}$$

The decomposition peak beginning at 900 °C indicates the decomposition of $K_2CO_3$ into $K_2O$ and $CO_2$.

$$K_2CO_3 \leftrightarrow K_2O + CO_2 \qquad \text{Reaction 5.2}$$

The DTG peak around 430 °C indicates the presence of nickel carbonate, which explains the greenish tint of the electrolyte crystals. The decomposition of the potassium bicarbonate crystals between 150-240 °C caused us to wonder if it also occurred in solution; consequently, we decided to study the temperature where the potassium bicarbonate decomposes in solution.

### *5.1.2 Temperature to prevent the formation of the crystals*

To improve the understanding of $KHCO_3/K_2CO_3$ equilibria, we built a "tubing bomb" (figure 5.3) that was suitable for use at pressures of 2000 psi and temperatures of 300 °C. Moreover, it could be quickly heated and cooled in a fluidized sand bath. We learned that the decomposition of bicarbonate also occurs in solution by reaction

$$2HCO_3^- \leftrightarrow CO_3^{2-} + CO_2 + H_2O \qquad \text{Reaction 5.3}$$

The decomposition of bicarbonate is described in Butler [79] as reversible within normally accessible temperature and pressure ranges. At lower temperatures and higher $CO_2$ partial pressures, the reaction proceeds to the left; at higher temperatures and lower pressures, it proceeds to the right.

We observed the decomposition of bicarbonate in the whole range of temperatures we worked (from 150 to 320°C) and at the respective saturation pressure with different extents of the reaction depending on the temperature. We observed high conversion of the bicarbonate over 200 °C. This means that the troublesome crystals of potassium bicarbonate observed in our early work were formed at high pressure while the large pressure vessel cooled. A carbon fuel cell operating at 200 °C and above should experience no problems with the formation of KHCO3, providing the cell is quickly cooled and pressure is quickly released. Recognizing the importance of reaction 5.3, I gave emphasis to determining the equilibrium constant and thermodynamic properties (enthalpy, entropy and Gibbs free energy) for the reaction of decomposition of bicarbonate in aqueous solution. The work was presented in the 2011 AiChE Annual Conference in Minneapolis.

## 5.2 Determination of the equilibrium constant of the potassium bicarbonate decomposition reaction

### *5.2.1 Apparatus*

Figure 5.3 is the schematic diagram of the equipment employed to study the thermodynamic decomposition of potassium bicarbonate. The apparatus consisted in a 1" cylindrical stainless steel tube rated to 3100 psi at 25° C, a thermocouple to measure the temperature , a pressure transducer to measure the pressure, a pressure release valve to depressurize the vessel, a safety burst diaphragm which prevents the pressure from exceeding the pressure limit of the vessel. The vessel was submerged in a Techne Fluidized Sand Bath Model SBL-2D. The small thermal capacity of the sand gives the bath a

rapid heat up from room temperature and it has the desirable characteristics of accessibility, uniformity of temperature, and good heat transference.

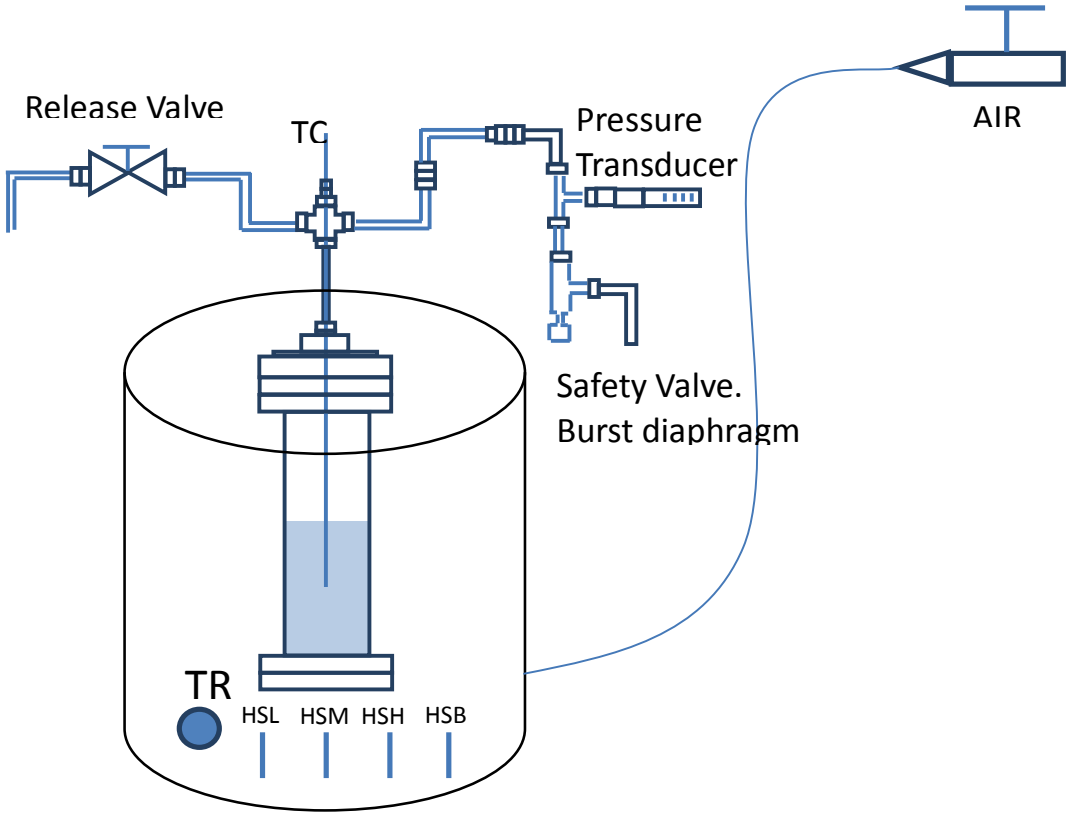


**Figure 5.3 Schematic diagram of the pressure vessel in the sand bath. TC is the thermocouple, TR is the temperature regulator, HSL is the low heater switch, HSM is the medium heater switch, HSH is the high heater switch, HSB is the boost heater switch, and AIR is the clean air supply.**

### *5.2.2 Procedure*

In a typical experiment, the potassium bicarbonate solution (1 or 0.1 M (mol/L)) was placed inside the canister. To begin the experiment, the air was supplied to the sand bath until the sand appeared to be boiling or fluidized. Once fluidization occurred, the four heaters were switched on and the sand bath was heated at a rate of 6° C/min. The pressure was recorded at increments of 10°C from 150°C on until the desired temperature was obtained (150,200,250, 300 or 320°C). The temperature was held for 1, 2,

4 or 8 hours and then the pressure vessel was removed from the fluidized sand bath and cooled to room temperature. The effect of cooling was also studied. After the experiment, while the vessel was cooled down, the $CO_2$ can back react to form bicarbonate. The $CO_2$ that hadn't backreacted escaped when the vessel was depressurized. We studied three different methods of cooling: (1) Cooling the vessel naturally, which means taking the vessel out of the sand bath and letting it cool down at room temperature which takes around 1 hour, (2) cooling it down using a fan until it reaches room temperature, which takes around 5 to 10 minutes and (3) submerging the vessel in a bucket of cool water, which takes around 30 seconds. The remaining electrolyte was extracted, measured the volume, measured the pH and the sample was analyzed.

### *5.2.3 Reactions and Assumptions*

The final liquid solution consisted of carbonate, bicarbonate and $CO_2$ (aq). The first aspect we noticed is that there are two processes that contributed to the carbonate, bicarbonate and $CO_2$ (aq) concentrations: the acid-base equilibrium and the decomposition of the bicarbonate. At lower temperatures, the decomposition of the bicarbonate is not spontaneous, so the acid-base equilibrium is the only process that governs the carbonate, bicarbonate and $CO_2$ (aq) concentrations. However, at higher temperatures, the decomposition of bicarbonate becomes important and the carbonate and $CO_2$ concentrations are mainly due to this process.

**Effect of the acid-base equilibrium in the bicarbonate , carbonate and $CO_2$ (aq) concentrations**

When potassium bicarbonate is dissolved in water, the potassium bicarbonate dissociates completely in solution

$$KHCO_3 \leftrightarrow K^+ + HCO_3^- \qquad \text{Reaction 5.4}$$

In solution, the bicarbonate, carbonate and $CO_2$ (aq) are in equilibrium and the concentrations can be determined by the $CO_3^{2-}$- $HCO_3$-$CO_2$ (aq) equilibrium equations, the mass balance on carbon and potassium and a charge balance

**Equations**

Equilibria

$$H_2O + CO_2(aq) \leftrightarrow H^+ + HCO_3^- \qquad \text{Reaction 5.5}$$

$$HCO_3^- \leftrightarrow H^+ + CO_3^{2-} \qquad \text{Reaction 5.6}$$

$$K_{a1} = \frac{[H^+][HCO_3^-]}{[H_2CO_3\,]} \qquad \text{Equation 5.1}$$

$$K_{a2} = \frac{[H^+][CO_3^{2-}]}{[HCO_3^-\,]} \qquad \text{Equation 5.2}$$

Mass balance on carbon and potassium

$$[KHCO_3]_o = [H_2CO_3\,] + [HCO_3^-\,] + [CO_3^{2-}] \qquad \text{Equation 5.3}$$

$$[K^+] = Ca \qquad \text{Equation 5.4}$$

Where $Ca$ is the molar concentration of the bicarbonate solution

Charge balance

$$[K^+] + [H^+] = [HCO_3^-\,] + 2[CO_3^{2-}] + [OH^-] \qquad \text{Equation 5.5}$$

The concentration of $OH^-$ is related to the concentration of $H^+$ by the dissociation constant of water, $Kw$

$$[OH^-] = \frac{Kw}{[H^+]} \qquad \text{Equation 5.6}$$

Manipulating these six equations (5.1-5.6), we can solve for the pH if we know the bicarbonate concentration and the temperature.

$$Ca + [H^+] = Ca\frac{K_{a1}[H^+] + 2K_{a1}K_{a2}}{[H^+]^2 + K_{a1}[H^+] + K_{a1}K_{a2}} + \frac{Kw}{[H^+]} \qquad \text{Equation 5.7}$$

Where the equilibrium constants, $K_{a1}$ and $K_{a2}$, and the dissociation constant of water, $Kw$, depend mainly on the temperature and the ionic medium, and are calculated with equations in chapter 3 (3.9, 3.15 and 3.16).

$$pK_w = pK_w^o - 1.0\,f(I) \qquad (3.9)$$

$$pK_{a1} = pK_{a1}^o - 1.0\,f(I) - bI \qquad (3.15)$$

$$pK_{a2} = pK_{a2}^o - 2.0\,f(I) \qquad (3.17)$$

*f(I)* is determined by Davies equation (Chapter 3, equation 3.5), *b* is a constant ( a typical value of 0.10 is used [71, 80]), *I* is the ionic strength and is calculated from all the ions in the solution as follows:

$$I = \frac{1}{2}([K^+]1^2 + [HCO_3{}^-]1^2) = \frac{1}{2}(Ca + Ca) = Ca$$

And $pK_w^o$, $pK_{a1}^o$ and $pK_{a2}^o$ are the equilibrium constants at ionic strength zero. $pK_{a1}^o$ and $pK_{a2}^o$ and $pK_w^o$ are taken from Stumm,W. and Morgan (1981) [64](See chapter 3,table 3.1). $pK_w^o$ agrees with data from Bandura and Lvov (2005) [75, 79]. The initial potassium bicarbonate concentration ($Ca$) is known (1M) and the only unknown in equation 5.7 is the $H^+$ concentration ($[H^+]$). Solving for the $H^+$ concentration in MatLab, the pH is directly determined by equation 5.8

$$pH = -log\ a_{H^+} = -\log(\gamma_+) - \log[H^+] \qquad \text{Equation 5.8}$$

$\log(\gamma_+)$ is calculated with Davies equation(Chapter 3), $\log\gamma = -0.5z^2 f(I)$.For $H^+$(z=1) $\log(\gamma_+) = -0.5f(I)$. The pH of a 1M (mol /L $_{solution}$) potassium bicarbonate solution is solved in MatLab for different temperatures with equations 5.7 and 5.8 and plotted in figure 5.4:

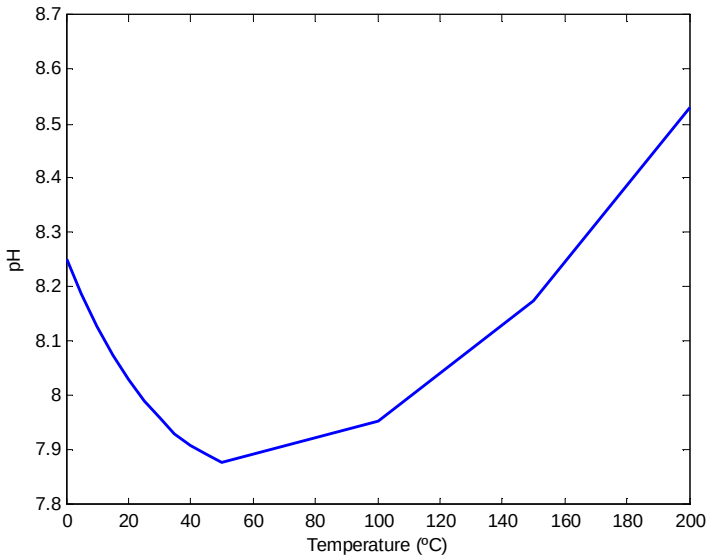


**Figure 5.4 pH of a 1M potassium bicarbonate solution vs. Temperature (°C)**

Once the $H^+$ concentration is known, the rest of the species concentrations can be determined from equations 5.1 to 5.3. Figure 5.5 shows the species concentrations (M) vs. temperature (°C)

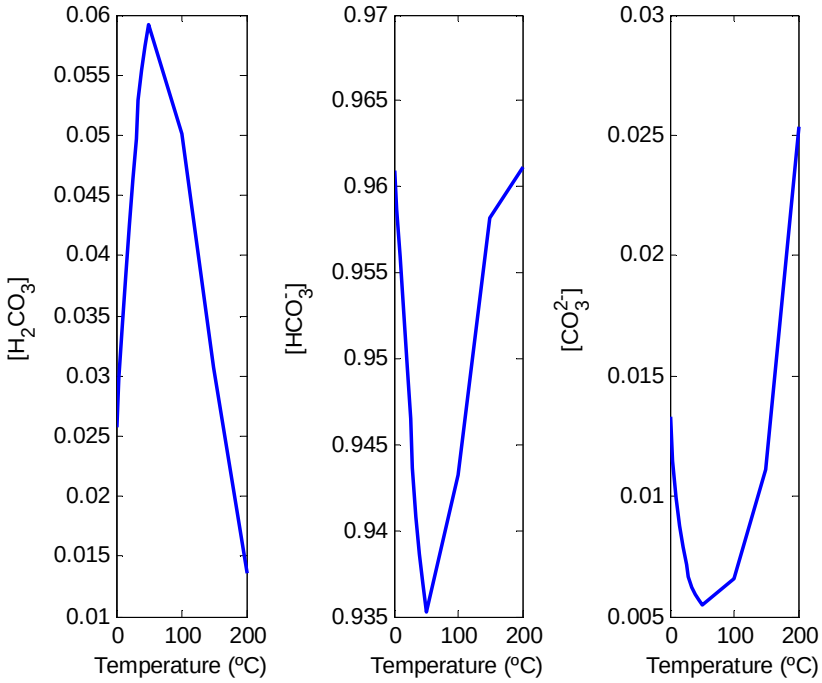


**Figure 5.5 Equilibrium concentrations of $H_2CO_3$, $HCO_3^-$, $CO_3^{2-}$ (M) for an initial 1M potassium bicarbonate solution vs. Temperature (°C)**

According to this acid-base equilibrium model, in the range of temperature from 0 to 200 °C, the bicarbonate is the main component in the solution (from $\sim 93.5\%$ to $\sim 96\%$) and the pH doesn't go over 9. These values are consistent with the experimental observations at low temperatures but don't agree with our experimental observations at high temperatures. Experimentally, we observed the decomposition reaction of bicarbonate ( $2HCO_3^- \leftrightarrow CO_3^{2-} + CO_2 + H_2O$ ) in the whole range of temperatures we worked (from 150 to 320 °C). So, the presence of carbonate is not only dependent on acid - base equilibria but also on the decomposition reaction.

**Effect of the decomposition of bicarbonate in the bicarbonate , carbonate and $CO_2$ (aq) concentrations**

As it has been stated before, the decomposition of bicarbonate is given by reaction 5.3, $2HCO_3^-(aq) \leftrightarrow CO_3^{2-}(aq) + CO_2(aq) + H_2O$. According to figure 5.5 and the experimental results, we consider that the concentration of the carbonate and the bicarbonate in the solution is due to the reaction of decomposition and not the acid-base equilibria because its effect on the species concentrations is minor. When the reaction of decomposition takes place, the $CO_3^{2-}$ and $CO_2$ concentration will start to increase. As we didn't observe a rise in the pressure, we assumed that the $CO_2$ was dissolved in the solution. Figure 5.6 shows the pressure versus temperature of 1M $K_2CO_3$ solutions from 150 to 200° C

(data taken from Ashley's Undergraduate Thesis [81]). Experimental data of three experiments are shown as well as the steam pressure and the theoretical total pressure, which corresponds to the steam pressure plus the $CO_2$(g) pressure if all the bicarbonate is decomposed and the $CO_2$ is released. These first 1M $KHCO_3$ experiments displayed the same results as the 0.1M $KHCO_3$ experiments. From these experiments it was suspected that the $CO_2$ formed as a result of the decomposition of the $KHCO_3$ was not being released as gaseous $CO_2$ but rather as aqueous $CO_2$.

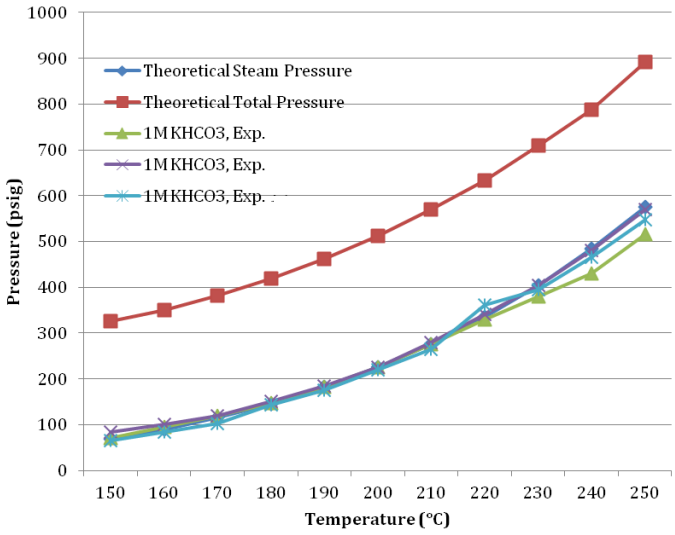


**Figure 5.6 Pressure results of selected pressure vessel experiments using KHCO3 electrolyte heated to 250°C [81]**

After the experiment, while the vessel cools down, the $CO_2$ (aq) can back react to form bicarbonate. The $CO_2$ that hadn't back reacted escaped when the vessel was depressurized after cooling down. So we decided to analyze three cases: (1) Assume that there is no back reaction and all the $CO_2$ is released and escapes when the vessel is open, (2) Assume the maximum conversion of the $KHCO_3$ (all the $KHCO_3$ reacts) and the bicarbonate observed is due to the $CO_2$ that back reacts, (3) Assume part of the conversion of the $KHCO_3$ and some of the $CO_2$ back reacts and the rest escapes. The bicarbonate observed is due to the $CO_2$ that back reacted and the bicarbonate that didn't reacted.

In these three cases, a table is presented. This table tabulates the data of the *initial moles* , in all the cases we start with $n_o$ moles of bicarbonate; *the final moles before opening the vessel*, these final moles represent the moles in equilibrium at the experimental temperature; the *final moles after back rxn but before release of $CO_2$* for cases 2 and 3, these moles represent the moles after cooling down the vessel at the temperature of depressurization, i.e. when we are cooling the vessel the reaction tends to reach its equilibrium at lower temperatures ; and finally the *final moles after release of $CO_2$* which are the

moles when the $CO_2$ left escapes. The equilibrium constant at the experimental temperature is calculated with *the final moles before opening the vessel* because these final moles represent the moles in equilibrium at the experimental temperature.

**Case #1: Assume that there is no back reaction and all the $CO_2$ is released and escapes when the vessel is open**

If we start with an initial solution of potassium bicarbonate of $n_o$ moles and we assumed that *x* is the moles of $CO_2$ produced, we can write all the final moles in terms of *x*. The following chart contains the moles of the species before and after the reaction

**Table 5.1 Moles of the species before and after the bicarbonate decomposition for case #1**

| $2HCO_3^-(aq) \leftrightarrow CO_3^{2-}(aq) + CO_2(aq) + H_2O$ | | | |
|---|---|---|---|
| | **$HCO_3^-$** | **$CO_3^{2-}$** | **$CO_2$** |
| **Initial moles** | $n_o$ | 0 | 0 |
| **Final moles before opening the vessel** | $n_o$ -2x | x | x |
| **Final moles after $CO_2$ escapes** | $n_o$ -2x | x | 0 |

The composition of the final solution will be

- moles $HCO_3^-$= $n_o$ -2x
- moles $CO_3^{2-}$= x

The x is determined by this final composition and the equilibrium constant is determined as:

$$K_{eq}{}^{o} = \frac{a_{CO_3{}^{2-}} a_{CO_2}}{a^2_{HCO_3{}^-}} = \frac{\gamma_{CO_2}\gamma_{CO_3{}^{2-}}}{\left(\gamma_{HCO_3{}^-}\right)^2}\frac{\left[CO_3{}^{2-}\right][CO_2]}{[HCO_3{}^-]^2}$$

Where $K_{eq}{}^{o}$ depends on the temperature. Regrouping the extrapolated zero ionic strength equilibrium constant ($K_{eq}{}^{o}$) and the activity coefficients ($\gamma_{CO_2}, \gamma_{CO_3{}^{2-}}$ and $\gamma_{HCO_3{}^-}$) into the equilibrium constant ($K_{eq}$)

$$K_{eq} = K_{eq}{}^{o}\frac{\left(\gamma_{HCO_3{}^-}\right)^2}{\gamma_{CO_2}\gamma_{CO_3{}^{2-}}} = \frac{\left[CO_3{}^{2-}\right][CO_2]}{[HCO_3{}^-]^2} \qquad \text{Equation 5.9}$$

$K_{eq}$ depends on the temperature and ionic medium. The concentrations are calculated when equilibrium is reached from the final moles before opening the vessel (Table 5.1), so

$$K_{eq} = \frac{(x/V)^2}{((\mathrm{n_o} - 2\mathrm{x})/\mathrm{V})^2} = \frac{x^2}{(\mathrm{n_o} - 2\mathrm{x})^2} \qquad \text{Equation 5.10}$$

**Case #2: Assume the maximum conversion of the $KHCO_3$ (all the $KHCO_3$ reacts).**

Consider that the bicarbonate conversion is maximum (all bicarbonate reacts) and *y* moles of $CO_2$ back react before they are released and escape.

**Table 5.2 Moles of the species before and after the bicarbonate decomposition for case #2**

| $2HCO_3^-(aq) \leftrightarrow CO_3^{2-}(aq) + CO_2(aq) + H_2O$ | | | |
|---|---|---|---|
| | **$HCO_3^-$** | **$CO_3^{2-}$** | **$CO_2$** |
| **Initial moles** | $n_o$ | 0 | 0 |
| **Final moles before opening the vessel** | 0 | $n_o/2$ | $n_o/2$ |
| **Final moles after back rxn but before release of $CO_2$** | 2y | $n_o/2$-y | $n_o/2$-y |
| **Final moles after release of $CO_2$** | 2y | $n_o/2$-y | 0 |

The composition of the final solution can give us the y, moles of $CO_2$ trapped

- moles $HCO_3^-$= 2y
- moles $CO_3^{2-}$= $n_o/2$-y

In this case, the true equilibrium constant is infinity as we have total conversion of bicarbonate before the back reaction occurs:

$$K_{eq} = \frac{(\mathrm{n_o}/2)^2}{0} = \infty \qquad \text{Equation 5.11}$$

Our experiments do not support the total conversion of bicarbonate, at least, not in all the cases. Experimentally, we observed different conversions with the temperature. If all the bicarbonate had dissociated, when the reaction was quenched, we would have expected similar conversion of bicarbonate as similar amounts of $CO_2$ would be trapped. The moles of bicarbonate after disassembly would be 2y.

**Case #3: Assume that part of the $KHCO_3$ reacts and part of the $CO_2$ does not escape**

**Table 5.3 Moles of the species before and after the bicarbonate decomposition for case #3**

| $2HCO_3^-(aq) \leftrightarrow CO_3^{2-}(aq) + CO_2(aq) + H_2O$ | | | |
|---|---|---|---|
| | **$KHCO_3$** | **$K_2CO_3$** | **$CO_2$** |
| **Initial moles** | $n_o$ | 0 | 0 |
| **Final moles before opening the vessel** | $n_o$ -2x | x | x |
| **Final moles after back rxn but before release of $CO_2$** | $n_o$ -2x+2y | x-y | x-y |
| **Final moles after release of $CO_2$** | $n_o$ -2x+2y | x-y | 0 |

The composition of the final solution will be

- moles $HCO_3^-$= $n_o$ -2x+2y= $n_o$ -2(x-y)
- moles $CO_3^{2-}$= x-y

The unknown x and y cannot be determined separately with just the final composition data. The parameter we can obtain from the final composition analysis is the (x-y). As the equilibrium constant is determined as:

$$K_{eq} = \frac{x^2}{(\mathrm{n_o} - 2\mathrm{x})^2} \qquad \text{Equation 5.12}$$

Where $K_{eq}$ depends on the temperature and ionic medium and is defined as $K_{eq} = {K_{eq}}^o \frac{\left(\gamma_{HCO_3^-}\right)^2}{\gamma_{CO_2}\gamma_{CO_3^{2-}}}$. We need another parameter that relates x , moles of $CO_2$ produced, and y, moles of $CO_2$ trapped in the solution, to get the equilibrium constant. This parameter can be calculated in the case where we get total conversion of bicarbonate. In this particular case, x would be $n_o/2$ and the final solution analysis, give us the x-y parameter. Therefore, this case can give us the x/y relation.

Note that when x= $n_o/2$ , table 5.3 is reduced to table 5.2, which means that case #3 is reduced to the more simplified case #2. Similarly, when y= 0, table 5.3 is reduced to table 5.1, i.e. case #3 is reduced to case #1.

Experimentally, we assumed that there is no back reaction of the $CO_2$ and all the $CO_2$ is released and escapes when the vessel is open (Case #1). Two reasons support this assumption; first, we are being conservative. When the final composition is calculated, the first case considers that there is no back

reaction; therefore the concentration of bicarbonate in equilibrium is less than if a back reaction is considered. And second, we discovered that cooling down the experiments quickly (in a few seconds) prevents this back reaction. The final composition analysis indicated that high conversions ( almost 100 %) are obtained at higher temperatures. So, if there is back reaction, its effect is small.

The equilibrium constant was calculated using equation 5.10 on case #1$\left( K_{eq} = \frac{x^2}{(\mathrm{n_o} - 2\mathrm{x})^2} \right)$. To solve for the equilibrium constant, we determined the final concentrations of the bicarbonate and carbonate.

## 5.3 Analysis of the final solution. Calculation of the conversion and equilibrium constant

The conversion of the bicarbonate was calculated by analyzing the sample in three different ways:

**5.3.1** **Measure of the final pH:** This is a semi-quantitative way of measuring the sample because the accuracy of this method is low. We relate the pH-measurement to the final composition.

**5.3.2** **TG-MS:** A sample of half of the remaining electrolyte was dried in an oven at 90°C under vacuum. The precipitate (the bicarbonate/carbonate crystals) was sent to Hungary for TG-MS analysis. The data of the crystals composition are extracted from the TG-MS.

**5.3.3** **Titration:** The sample was titrated so that we get final solution composition.

Once the final composition is obtained and assuming case #1 (i.e. Assume that there is no back reaction and all the $CO_2$ is released and escapes when the vessel is open), the conversion and equilibrium constant can be directly obtained using the equations that apply to this case (Equation 5.10, $K_{eq} = \frac{x^2}{(\mathrm{n_o} - 2\mathrm{x})^2}$)

- moles $KHCO_3 = n_o - 2x$
- moles $K_2CO_3 = x$

Or in terms of conversion:

$$moles\ KHCO_{3_{final}} = moles\ KHCO_{3_o} \cdot (1 - Conversion\ KHCO_3) \qquad \text{Equation 5.13}$$

$$moles\ K_2CO_{3_{final}} = moles\ CO_{2_{final}} = \frac{moles\ KHCO_{3_o} \cdot Conversion\ KHCO_3}{2} \qquad \text{Equation 5.14}$$

And therefore, the equilibrium constant can be calculated as

$$K_{eq} = \frac{[K_2CO_3][CO_2]}{[KHCO_3]^2} = \frac{n_{K_2CO_3} \cdot n_{CO_2}}{{n_{KHCO_3}}^2} = \frac{\left(\frac{moles\ KHCO_{3_o} \cdot Conversion\ KHCO_3}{2}\right)^2}{\left(moles\ KHCO_{3_o} \cdot (1 - Conversion\ KHCO_3)\right)^2}$$

$$= \left(\frac{Conversion\ KHCO_3}{2\ \cdot (1 - Conversion\ KHCO_3)}\right)^2 \qquad \text{Equation 5.15}$$

Where $K_{eq}$ depends on the temperature and ionic medium and is defined as $K_{eq} = {K_{eq}}^o \frac{\left(\gamma_{HCO_3^-}\right)^2}{\gamma_{CO_2}\gamma_{{CO_3}^{2-}}}$.

Figure 5.7 shows the graph $K_{eq}$ vs. Conversion of bicarbonate from 0 to 90% of conversion

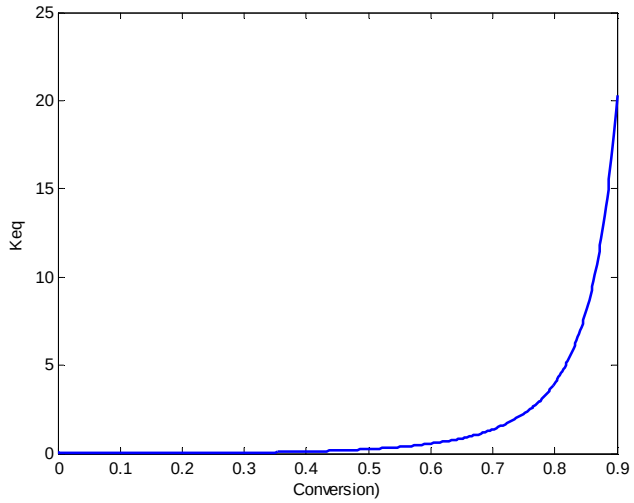


**Figure 5.7 Keq vs. Conversion of bicarbonate in reaction, $2HCO_3^- \leftrightarrow CO_3^{2-} + CO_2 + H_2O$**

Figure 5.7 shows that the equilibrium constant increases with the conversion. At low conversions, the equilibrium constant is low and it does not increase significantly with the conversion. However, at conversions over 70%, a small variation of the conversion means a large variation in the equilibrium constant, i.e the equilibrium constant is very sensitive with the conversion.

### *5.3.1 Measure of the final pH*

**Determine the curve pH vs. Conversion**

Once the pH of the experimental solution is measured, it needs to be related to the conversion of the reaction. As the bicarbonate initial concentration and the stoichiometry of the bicarbonate decomposition reaction are known, the final bicarbonate and carbonate concentrations can be

calculated as long as the conversion of the reaction is known. For example, beginning with an initial potassium bicarbonate concentration of 1molal (0.1 mol potassium bicarbonate in 100g water) and assuming conversions from 0 to 100 % of the reaction 5.3, $2\mathrm{HCO_3}^- \leftrightarrow \mathrm{CO_3}^{2-} + \mathrm{CO_2} + \mathrm{H_2O}$. I calculated the makeup of the product solution. In this calculation, I assumed that all the $CO_2$ formed escapes from the solution (Case #1). Based on the calculated results, I prepared final solutions representing the calculated product mixture and measured their pHs. Under all these assumptions, the number of moles and volume of the final solutions are calculated and tabulated in table 5.4. The measured pHs of these solutions are also tabulated in table 5.4.

**Table 5.4 Experimental pH of mixtures of potassium carbonate/bicarbonate representing the products of reaction 5.3 at different conversions beginning with a 1 molal initial potassium bicarbonate solution**

| Conversion of reaction (%) | mol $KHCO_3$ | mol $K_2CO_3$ | mol $H_2O$ | V $H_2O$ due to rxn (L) | V final (mL) | Calculated product mixture mass $KHCO_3$ (g) | mass $K_2CO_3$ (g) | pH |
|---|---|---|---|---|---|---|---|---|
| 0 | 0.1 | 0 | 0 | 0 | 100 | 10.012 | 0 | **8.05** |
| 20 | 0.08 | 0.01 | 0.01 | 0.00018 | 100.18 | 8.0096 | 1.3821 | **8.99** |
| 40 | 0.06 | 0.02 | 0.02 | 0.00036 | 100.36 | 6.0072 | 2.7642 | **9.41** |
| 60 | 0.04 | 0.03 | 0.03 | 0.00054 | 100.54 | 4.0048 | 4.1463 | **9.75** |
| 80 | 0.02 | 0.04 | 0.04 | 0.00072 | 100.72 | 2.0024 | 5.5284 | **10.2** |
| 90 | 0.01 | 0.045 | 0.045 | 0.00081 | 100.81 | 1.0012 | 6.21945 | **10.52** |
| 100 | 0 | 0.05 | 0.05 | 0.0009 | 100.9 | 0 | 6.9105 | **11.48** |

The same procedure has been done beginning with an initial potassium bicarbonate concentration of 0.1molal (0.01 mol potassium bicarbonate in 100g water). The number of moles ,volume of the final solutions and the measured pHs of the 0.01 molal initial solutions are tabulated in table 5.5.

**Table 5.5 Experimental pH of mixtures of potassium carbonate/bicarbonate representing the products of reaction 5.3 at different conversions beginning with a 0.1 molal initial potassium bicarbonate solution**

| Conversion of reaction (%) | mol $KHCO_3$ | mol $K_2CO_3$ | mol $H_2O$ | V $H_2O$ due to rxn (L) | V final (mL) | Calculated product mixture mass $KHCO_3$ (g) | mass $K_2CO_3$ (g) | pH |
|---|---|---|---|---|---|---|---|---|
| 0 | 0.01 | 0 | 0 | 0.0E+00 | 100.00 | 1.0012 | 0 | **8.23** |
| 20 | 0.008 | 0.001 | 0.001 | 1.8E-05 | 100.02 | 0.80096 | 0.13821 | **9.2** |
| 40 | 0.006 | 0.002 | 0.002 | 3.6E-05 | 100.04 | 0.60072 | 0.27642 | **9.66** |
| 60 | 0.004 | 0.003 | 0.003 | 5.4E-05 | 100.05 | 0.40048 | 0.41463 | **10.03** |
| 80 | 0.002 | 0.004 | 0.004 | 7.2E-05 | 100.07 | 0.20024 | 0.55284 | **10.45** |
| 90 | 0.001 | 0.0045 | 0.0045 | 8.1E-05 | 100.08 | 0.10012 | 0.621945 | **10.77** |
| 100 | 0 | 0.005 | 0.005 | 9.0E-05 | 100.09 | 0 | 0.69105 | **11.38** |

The conversion is defined as

$$Conversion\ KHCO_3 \equiv X = \frac{n_{o,KHCO_3} - n_{f,KHCO_3}}{n_{o,KHCO_3}} \qquad \text{Equation 5.16}$$

Where $n_{o,KHCO_3}$=initial moles of potassium bicarbonate; $n_{f,KHCO_3}$=final moles of potassium bicarbonate. The change in volume due to the formation of water is not taken into account because it is very small. Figure 5.8 shows the pH-conversion values displayed in Tables 5.4 and 5.5 denoted as '1M exp' and '0.1 M exp' respectively. The theoretical data for initial bicarbonate concentrations of 1, 0.1 and 0.01 M are also calculated from the following equilibrium, mass balance and charge balance equations and plotted in figure 5.8 as well.

**Equations**

After the bicarbonate decomposition reaction, the final solution consists in a mixture of bicarbonate and carbonate. The bicarbonate and carbonate are completely dissociated in solution

$$KHCO_3 \leftrightarrow K^+ + HCO_3^- \qquad \text{Reaction 5.4}$$

$$K_2CO_3 \leftrightarrow 2K^+ + CO_3^{2-} \qquad \text{Reaction 5.7}$$

In solution, the bicarbonate, carbonate and $CO_2$ (aq) are in equilibrium and the concentrations can be determined by the $CO_3^{2-}$- $HCO_3^-$- $H_2CO_3$ equilibrium equations, mass balances on carbon and potassium and a charge balance. Remember that at equilibrium [$H_2CO_3$] is only about $10^{-3}$ as large as [$CO_2$] and has no special significance in the acid-base equilibria, since both are uncharged. Hence, [$H_2CO_3$]+[$CO_2$] is written simply as [$CO_2$] .

Equilibria and charge balance

The equilibrium expressions (Reactions 5.5 and 5.6) and the charge balance are given by the previous equations 5.1, 5.2 and 5.5

$$H_2CO_3 \leftrightarrow H^+ + HCO_3^- \qquad K_{a1} = \frac{[H^+][HCO_3^-]}{[CO_2]} \qquad \text{Eq. 5.1}$$

$$HCO_3^- \leftrightarrow H^+ + CO_3^{2-} \qquad K_{a2} = \frac{[H^+][CO_3^{2-}]}{[HCO_3^-]} \qquad \text{Eq. 5.2}$$

$$[K^+] + [H^+] = [HCO_3^- ] + 2[CO_3^{2-}] + [OH^-] \quad \text{Eq. 5.5}$$

Mass balance on carbon and potassium

$$Cb + Ca = [CO_2 ] + [HCO_3^- ] + [CO_3^{2-}] \quad \text{Equation 5.17}$$

$$[K^+] = Ca + 2Cb \quad \text{Equation 5.18}$$

Where $Ca$ and $Cb$ are the molar concentrations of the bicarbonate solution and carbonate solutions respectively. Manipulating these six equations and relating the concentration of $OH^-$ to the concentration of $H^+$ by the dissociation constant of water, $Kw$, $[OH^-] = Kw/[H^+]$ (eq.5.6), we obtain a final equation 5.19

$$Ca + 2Cb + [H^+] = (Ca + Cb)\frac{K_{a1}[H^+]+2K_{a1}K_{a2}}{[H^+]^2 + K_{a1}[H^+] + K_{a1}K_{a2}} + \frac{Kw}{[H^+]} \quad \text{Equation 5.19}$$

Where the equilibrium constants, $K_{a1}$ and $K_{a2}$, and the dissociation constant of water, $Kw$, depend mainly on the temperature and the ionic medium, and are calculated with equations in chapter 3 (3.9, 3.15 and 3.16).

$$pK_w = pK_w^o - 1.0\, f(I) \quad (3.9)$$

$$pK_{a1} = pK_{a1}^o - 1.0\, f(I) - bI \quad (3.15)$$

$$pK_{a2} = pK_{a2}^o - 2.0\, f(I) \quad (3.17)$$

Where *f(I)* is determined by Davies equation (Chapter 3, equation 3.5), *b* is a constant (a typical value of 0.10 is used [71, 80],*I* is the ionic strength and is calculated with the Debye-Hückel equation as

$$I = \frac{1}{2}\left([K^+]1^2 + [HCO_3{}^-]1^2 + \left[CO_3{}^{2-}\right]2^2\right) = \frac{1}{2}(Ca + 2Cb + Ca + 4Cb) = Ca + 3Cb$$

and $pK_w^o$, $pK_{a1}^o$ and $pK_{a2}^o$ are the equilibrium constants at ionic strength zero. $pK_{a1}^o$ and $pK_{a2}^o$ and $pK_w^o$ are taken from Stumm,W. and Morgan (1981)[64](See chapter 3, table 3.1) at room temperature(25°C) ($pK_{a1}^o = 6.352$, $pK_{a2}^o = 10.329$ and $pK_w^o = 13.999$). The initial potassium bicarbonate and carbonate concentrations, $Ca$ and $Cb$ are known and related to the conversion by equations:

$$Ca = [\,KHCO_3]_o \cdot (1 - Conversion\ KHCO_3) \quad \text{Equation 5.20}$$

$$Cb = \frac{[\,KHCO_3]_o \cdot Conversion\ KHCO_3}{2} \qquad \text{Equation 5.21}$$

Where $[\,\mathrm{KHCO_3}]_o$ is the bicarbonate concentration before running the experiment (1, 0.1 and 0.01 M). Then, specifying the temperature, the bicarbonate concentration before running the experiment tand the conversion, the only unknown in equation 5.19 is the $H^+$ concentration ($[H^+]$). Solving for the $H^+$ concentration in MatLab for different conversion values, the pH is directly determined by equation 5.8, $pH = -log\ a_{H^+} = -\log(\gamma_+) - \log[H^+]$, where $\log(\gamma_+)$ is given by Davies equation. These analytical results are plotted in figure 5.8 as well as the experimental values displayed in tables 5.4 and 5.5

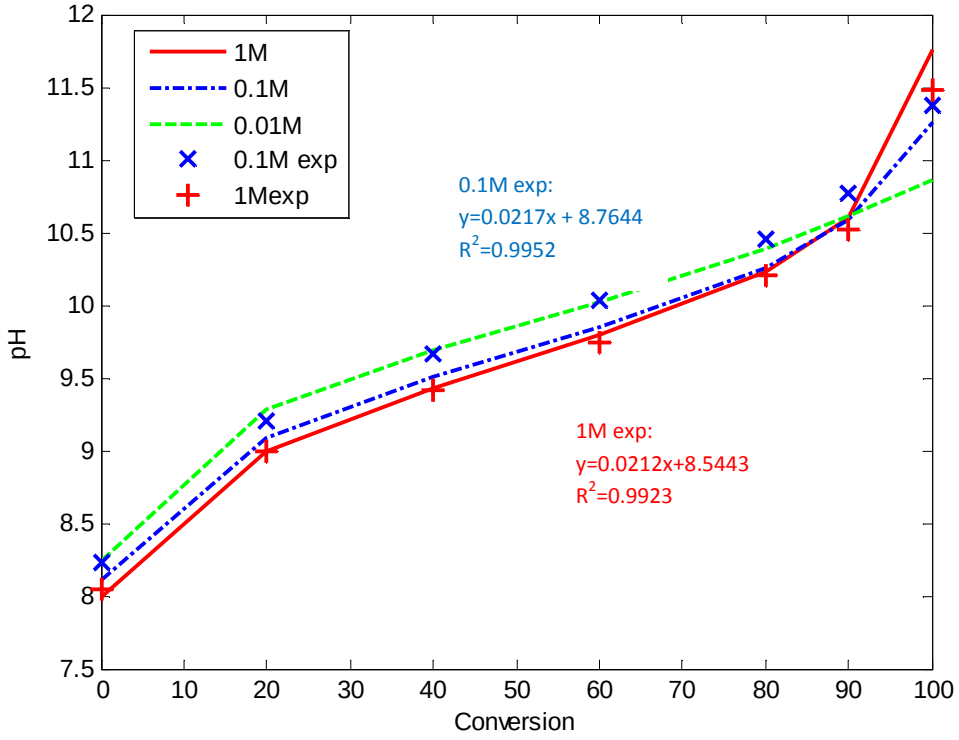


**Figure 5.8 pH vs. conversion . Analytical results for an initial bicarbonate concentration of 1 M , 0.1 M and 0.01 M and experimental results for an initial bicarbonate concentration of 1 M and 0.1 M**

The experimental results of the carbonate-bicarbonate mixtures formed from an initial 1M bicarbonate solution fits the analytical data very well, the difference between the experimental and analytical pH is between 0.003 and 0.06, with the exception of 100 % conversion whose difference is 0.2. In the case of a 0.1M bicarbonate solution, the experimental data are higher than the analytical data, the difference between the experimental and analytical pH is between 0.11 and 0.17. The analytical pHs of the carbonate-bicarbonate mixtures formed from initial 1M bicarbonate are lower than the ones that come

from an initial 0.1M bicarbonate solution (except for the case of 100 % conversion), this agrees with the experimental results we obtained. We observe that the pH-conversion experimental data follows a linear function between 20 and 90 % conversion. The equations displayed in figure 5.8 correspond to the experimental linear fit for initial bicarbonate concentrations of 1M and 0.1 M and are used to calculate the conversion once the pH is measured. This equation is used in the range of conversion 20 %-90 %. In the range of conversion, 90-100% we interpolate.

For a 1M initial bicarbonate solution, the experimental pH-conversion equation is $\mathrm{pH} = 0.0212 \cdot \mathrm{Conversion} + 8.5443$, and is valid when the pH is between 8.99 (20 % conversion) and 10.52(90 % conversion). For a 0.1M initial bicarbonate solution, the experimental pH-conversion equation is $\mathrm{pH} = 0.0217 \cdot \mathrm{Conversion} + 8.7644$, and is valid when the pH is between 9.2 (20 % conversion) and 10.77(90 % conversion). Once the conversion in known, the final composition and equilibrium constant are calculated using the previous equations 5.15, 5.20 and 5.21

Bicarbonate concentration: $Ca = [\,KHCO_3]_o \cdot (1 - Conversion\ KHCO_3)$ Eq. 5.20

Carbonate concentration: $Cb = \dfrac{[\,KHCO_3]_o \cdot Conversion\ KHCO_3}{2}$ Eq. 5.21

$$K_{eq} = \left(\frac{Conversion\ KHCO_3}{2\ \cdot (1 - Conversion\ KHCO_3)}\right)^2 \quad \text{Eq. 5.15}$$

*Ca* and *Cb* are the bicarbonate and carbonate concentration respectively. $K_{eq}$ depends on the temperature and ionic medium $K_{eq} = {K_{eq}}^{o} \frac{\left(\gamma_{HCO_3^-}\right)^2}{\gamma_{CO_2}\gamma_{{CO_3}^{2-}}}$ (see equation 5.9). To examine the reliability of the pH method, the accuracy of the conversion and the concentrations obtained with the pH method is studied.

**Accuracy of the pH –Conversion data and pH-Concentration data**

A Mettler Toledo 'Seven easy' pH meter was used for the pH measurements. The 'Seven easy' pH –meter and its electrodes were purchased in 2010 as they were recommended by Mettler as their best available. The pH and temperature relative accuracies are specified by Mettler Toledo as ±0.01 and ±0.05 respectively. The calibration of the pH-meter was done by following the R3Lab Analytical Calibration Procedure written by Joseph Lichwa in "Determination of Carbohydrates, HMF, and Furfural in Biomass by HPLC" [82] introducing small modifications to adapt the calibration method to the pH

calibration. The pH-meter is calibrated with a first set of Mettler Toledo standards or Calibration Standards (CAL) with pHs of 4.01, 7 and 10 (Ref.51302069). To verify that the initial calibration curve prepared from the first set of standards is accurate, a second buffer from a different lot called Calibration Verification Standard (CVS) with known pH is tested. This CVS consists of a Buffer 'BDH' Beckman of a stated pH of 12.45 (Cat. No. BDH 5092-500ML). Once the pH –meter is calibrated with the CAL and CVS, the pH of two known solutions - Method Verification Standard (MVS) and Continuing Calibration Verification Standard (CCV) - are measured every week. The MVS is a well characterized standard reference material similar in composition to the samples being analyzed. We used a solution of 5M potassium carbonate prepared by dissolving potassium carbonate sesquihydrate from *Fisher Chemical* (LOT 090226) in DI water. It is analyzed along with other samples in the batch to test the reproducibility of the method as a whole [82]. The CCV is another buffer prepared by us which consists in a mixture of 50 mL 0.2 M potassium chloride (KCl from *Fisher Chemical* LOT 871601) and 40.8 mL of 0.2 M sodium hydroxide (NaOH from *EM Science* LOT 41268144). This is used to verify that the initial calibration curve is still valid on a day to day basis without any bias that may be introduced from a second source standard [82]. To check the accuracy of the pH-meter, a calibration form that keeps track of the pHs every week is created. Tables 5.6 and 5.7 contain the data of the calibration forms of two different electrodes.

**Table 5.6 Calibration form for the 1st electrode**

| Date | pH (CCV) | pH (MVS) |
|---|---|---|
| 02/23/2011 | 12.63 | 13.24 |
| 03/09/2011 | 12.50 | 13.21 |
| 03/17/2011 | 12.30 | 13.19 |
| 03/22/2011 | 12.57 | 12.94 |
| 03/31/2011 | 12.60 | 13.01 |
| 04/08/2011 | 12.59 | 12.97 |
| 05/13/2011 | 12.33 | 12.84 |
| 05/31/2011 | 12.04 | 12.76 |
| 06/03/2011 | 12.03 | 12.88 |
| 06/17/2011 | 11.60 | 12.80 |
| 06/20/2011 | 13.04( New CCV) | |
| 06/25/2011 | 13.00 | 12.87 |
| 06/30/2011 | 12.96 | 12.77 |
| 07/15/2011 | 12.97 | 12.80 |
| 07/22/2011 | 12.90 | 12.75 |
| 08/08/2011 | 12.85 | 12.70 |
| 09/01/2011 | 12.73 | 12.66 |

**Table 5.7 Calibration form for the 2nd electrode**

| Date | pH (CCV) | pH (MVS) |
|---|---|---|
| 12/06/2011 | 12.90 | 13.12 (Change storage) |
| 12/13/2011 | 12.87 | 13.15 |
| 01/09/2012 | 12.81 | 13.27 |
| 01/13/2012 | 12.67 | 13.25 |
| 01/19/2012 | 12.59 (Change storage) | 13.06 |
| 01/30/2012 | 12.57 | 13.08 |
| 02/01/2012 | 12.65 | 13.10 |
| 02/13/2012 | 12.60 | 13.11 |
| 02/17/2012 | 12.65 | 13.09 |

Table 5.6 shows a decrease of the pH with time. The decrease in the pH caused us to wonder if the electrode was drifting or the storage of the sample was not adequate. A new CCV was prepared in 06/20/2011 and the pH was measured. The pH was instantaneously corrected which suggested that the electrode was working properly and the storage of the samples was not adequate. Table 5.7 shows the CCV and MVS pHs with a second electrode. The CCV and MVS samples were stored in capped glass bottles. We changed the storage of the MVS to a smaller bottle in 12/06/2011, the new 100mL glass

bottle was almost full, therefore, the amount of air in the close system was significantly reduced and the drift in the pH values disappeared. The storage of the CCV was changed later, in 01/19/2012 and as soon as the storage changed, we observed the correction in the pH drifting. We concluded that the $CO_2$ from the air dissolves in the sample and as a result, the sample becomes more acidic and the pH lowers. In order to store the CCV and MVS properly, bottles must be capped and only a small amount of air can be allowed in the closed system.

Taking into account the pH data of tables 5.6 and 5.7 (we took into account the data after changing the storage of the sample), the absolute accuracy of the pH-meter is calculated. The CCV pH is 12.61±0.04 and the MVS pH is 12.16±0.11. Considering the worst case scenario, the pH-meter absolute accuracy is considered ±0.11. This value agrees with the pH bicarbonate measurements of 1M bicarbonate solutions. Table 5.10 shows the initial experimental pH, which corresponds to the pH of 1M potassium bicarbonate solutions. The pH values vary from 8.02 to 8.24 (pH=8.13±0.11), showing a ±0.11 pH absolute accuracy.

Once the pH-meter accuracy is known, the conversion accuracy is calculated. The pH is related to the conversion by equation $pH = 0.0212 Conversion(\%) + 8.5443$. Therefore, the conversion absolute accuracy ($\Delta Conversion$) and the pH absolute accuracy ($\Delta pH$) are related with the following equation

$$\Delta pH = 0.0212 \cdot \Delta Conversion \qquad \text{Equation 5.22}$$

Solving for $\Delta Conversion(\%)$ with $\Delta pH = \pm 0.11$

$$\Delta Conversion(\%) = \frac{\Delta pH}{0.0212} = \frac{\pm 0.11}{0.0212} = \pm 5.19\% \qquad \text{Equation 5.23}$$

The absolute accuracy of $\pm 5.19\%$ in the conversion indicates the error in the conversion we can get by using the pH-conversion equation. This error in the conversion also introduces an error in the bicarbonate and carbonate concentration calculations. The bicarbonate and carbonate compositions depend on the conversion and the concentrations are given by equations 5.20 ($[KHCO_3] = [\,KHCO_3]_o \cdot (1 - Conversion\ KHCO_3)$ ), and 5.21, ($[K_2CO_3] = \frac{[\,KHCO_3]_o \cdot Conversion\ KHCO_3}{2}$). As the conversion absolute accuracy is $\pm 5.19\%$, the bicarbonate concentration , for example, can range between $[KHCO_3] = [\,KHCO_3]_o(1 - (Conversion\ KHCO_3 + 0.0519))$ and $[KHCO_3] = [\,KHCO_3]_o(1 - (Conversion\ KHCO_3 - 0.0519))$

Or $$[KHCO_3] = [\,KHCO_3]_o \cdot (1 - (Conversion\ KHCO_3 \pm 0.0519))$$ Equation 5.24

Following the same reasoning for the carbonate concentration

$$[K_2CO_3] = \frac{[\,KHCO_3]_o \cdot (Conversion\ KHCO_3 \pm 0.0519)}{2}$$ Equation 5.25

The relative accuracy for the carbonate and bicarbonate concentrations is given by equation 5.26

$$Accuracy\ (\%) = \left|\frac{Calculated\ Molarity - Real\ Molarity}{Real\ Molarity}\right| 100$$ Equation 5.26

The $Real\ Molarity$ is specified by equations 5.20 and 5.21 and is the exact molarity (i.e molarity when the accuracy is 0%), the calculated molarity is the one given introducing an absolute accuracy in the conversion of $\pm 5.19\%$ (worst case scenario) and is given by equations 5.24 and 5.25. If these equations are substituted in the accuracy equation, the final expressions obtained for the bicarbonate and carbonate accuracies are:

$$Accuracy\ KHCO_3(\%) = \frac{\Delta Conversion}{1 - Conversion} 100$$ Equation 5.27

$$Accuracy\ K_2CO_3(\%) = \frac{\Delta Conversion}{Conversion} 100$$ Equation 5.28

$\Delta Conversion$ is the absolute accuracy in the conversion, $\Delta Conversion = \pm 5.19\%$ .

The relative accuracy in the bicarbonate and carbonate concentrations (Equations 5.27 and 5.28), does not depend on the initial bicarbonate concentration but it is a function of the conversion. Table 5.8 shows the exact concentration in mol/L of bicarbonate and carbonate given a value of conversion (Equations 5.20 and 5.21) and the accuracy of the concentration of bicarbonate and carbonate for different values of conversion(Equations 5.27 and 5.28) . The bicarbonate and carbonate concentrations are the concentrations when there is no error introduced in their calculation, also denominated as real molarity. The concentrations are calculated considering an initial experimental bicarbonate solution of 1M.

**Table 5.8 Bicarbonate and Carbonate concentrations of reaction $2HCO_3^-(aq) \leftrightarrow CO_3^{2-}(aq) + CO_2(aq) + H_2O$ for different conversions given an initial 1M bicarbonate solution and accuracies of bicarbonate and carbonate concentrations using the pH –conversion model**

| Conversion | [$KHCO_3$] | [$K_2CO_3$] | Accuracy $KHCO_3$ (%) | Accuracy $K_2CO_3$ (%) |
|---|---|---|---|---|
| 0 | 1 | 0 | 5.19 | -- |
| 0.1 | 0.9 | 0.05 | 5.77 | 51.89 |
| 0.2 | 0.8 | 0.1 | 6.49 | 25.94 |
| 0.3 | 0.7 | 0.15 | 7.41 | 17.30 |
| 0.4 | 0.6 | 0.2 | 8.65 | 12.97 |
| 0.5 | 0.5 | 0.25 | 10.38 | 10.38 |
| 0.6 | 0.4 | 0.3 | 12.97 | 8.65 |
| 0.7 | 0.3 | 0.35 | 17.30 | 7.41 |
| 0.8 | 0.2 | 0.4 | 25.94 | 6.49 |
| 0.9 | 0.1 | 0.45 | 51.89 | 5.77 |
| 1 | 0 | 0.5 | -- | 5.19 |

The relative accuracy in the bicarbonate concentration is good at conversions below 60 %, with accuracies from 5 to 12 % at conversions lower than 60 %. However, the accuracy gets worse at higher conversions. At conversions of 70 to 90 %, the relative accuracy increase from 17 to 51 %. The situation is the opposite for the carbonate concentrations; we get good accuracies at higher concentrations, from 5 to 12 % at conversions higher than 40 %. And the relative accuracy introduced increase from 17 to 51 % when the conversion is 30% and lower. We conclude from this study that the pH method accuracy is not very reliable. However, it helped us to estimate the impacts of cooling and estimate the time to reach equilibrium and the conversion in equilibrium.

**Determination of the effect of cooling**

The first effect to analyze by measuring the pH is the cooling of the canister after running the experiment. We were afraid that the $CO_2$ formed from the decomposition back reacted and the bicarbonate was produced again. Therefore, three ways of cooling were analyzed: (1) Cooling the vessel naturally (1h) ,(2) With a fan (5-10 min) and (3) Immediately submerging the vessel in cool water ( ≈30 sec). Table 5.9 contains some results of the experiments run to determine the effect of cooling. It can be seen that in run #4, the final pH is the highest. This means that the conversion of the bicarbonate in run 4 is the highest and we can conclude that a quick cool down reduces the $CO_2$ that back reacts.

**Table 5.9 Determination of the effect of cooling. Set of experiments #1.**

| Run n° | Temperature (◦C) | [$KHCO_3$] | $t_{exposed}$ (h) | Cooling method | Results pH Initial | pH Final |
|---|---|---|---|---|---|---|
| 1 | 300 | 1 | 2 | Without a fan,1h | 8.06 | 9.73 |
| 2 | 300 | 1 | 2 | Fan,5min; $T_{vessel\ open}$=100◦C | 8.15 | 9.93 |
| 3 | 320 | 1 | 4 | Fan,5min; $T_{vessel\ open}$=100◦C | 8.25 | 10.16 |
| 4 | 320 | 1 | 4 | Bucket cool water; $T_{vessel\ open}$=100◦C | 8.05 | 12.42 |

The experiments in table 5.9 show the important effect of the cooling method, we could observe higher pHs when the bucket was cooled down quickly as we minimize the $CO_2$ that back reacts. The vessel in all the experiments after run #4 was submerged in a bucket of cool water.

**Determination of equilibrium conversion and time to reach equilibrium**

In the next set of experiments (Set #2), the conversion and time to reach equilibrium vs. temperature is determined for an initial bicarbonate concentration of 1M. Table 5.10 contains the data of the initial and final pH of the experiments starting with a 1M potassium bicarbonate solution. Based on the experimental data displayed on table 5.4 and plotted in figure 5.8, the conversion based on the final pH has been calculated using equation $\mathrm{pH} = 0.0212 \cdot \mathrm{Conversion} + 8.5443$ (figure 5.8) when the pH is between 8.99 (20 % conversion) and 10.52 (90 % conversion).The conversion is interpolated when the pH is between 10.52 (90 % conversion)and 11.48 (100 % conversion).

**Table 5.10 Experiment conditions and final pH and conversion. All the experiments have been cooled down by immersion in a bucket of cool water. The initial concentration of the bicarbonate of all experiments is 1M. The final solution of all experiments is colorless. Set of experiments #2.**

| Run # | Temperature (◦C) | $[KHCO_3]_o$ | $t_{exposed}$ (h) | Results | | |
|---|---|---|---|---|---|---|
| | | | | pH initial | pH final | Conversion (%) Based on Final pH |
| 1 | 320 | 1 | 2 | 8.10 | 10.66 | 91.46 |
| 2 | 320 | 1 | 4 | 8.02 | 12.42 | >100 % |
| 3 | 320 | 1 | 4 | 8.10 | 13.40 | >100 % |
| 4 | 250 | 1 | 2 | | 10.09 | 72.91 |
| 5 | 250 | 1 | 4 | 8.24 | 10.06 | 71.50 |
| 6 | 250 | 1 | 4 | 8.05 | 10.01 | 69.14 |
| 7 | 200 | 1 | 2 | 8.17 | 9.92 | 64.89 |
| 8 | 200 | 1 | 4 | 8.12 | 10.15 | 75.74 |
| 9 | 150 | 1 | 2 | 8.07 | 9.03 | 22.91 |
| 10 | 150 | 1 | 4 | 8.08 | 9.99 | 68.19 |
| 11 | 150 | 1 | 8 | 8.11 | 9.90 | 63.95 |

At 150°C and 200°C, the equilibrium of the reaction of decomposition of bicarbonate- $2HCO_3^-(aq) \leftrightarrow CO_3^{2-}(aq) + CO_2(aq) + H_2O$- was reached by 4 hours. At 250°C, the equilibrium of the reaction of decomposition of bicarbonate- $2HCO_3^-(aq) \leftrightarrow CO_3^{2-}(aq) + CO_2(aq) + H_2O$- was reached by 2 hours. From 200 to 250 °C, we observe no increase in the pH and therefore in the conversion. The cause of this plateau can be explained because the decomposition reaction is complete. That means that the final conversion is 100 % instead of 75 % and low value in conversion is because the $CO_2$ back reacts.

At 320°C and 4 hours of time of reaction, we notice an increase in the pH to more than 12, the pH is higher that the correspondent pH for 100 % conversion, which implies that another reaction is causing that the solution becomes more basic. The candidate is $CO_3^{2-}(aq) + H_2O \leftrightarrow CO_2(aq) + 2OH^-(aq)$. So, after all the bicarbonate has been decomposed into carbonate and water, the carbonate may decompose into $CO_2$ and $OH^-$. The $CO_2$ escapes and the solution becomes more alkaline because of the $OH^-$ produced. So, this suggests that while the decomposition of dry carbonate occurs at 900°C as it is shown in the TG-MS (Figure 5.2), the carbonate can decompose at much lower temperatures in solution. To prove this hypothesis, we analyzed the solution by titration and check if the carbonate decomposes at these conditions into hydroxide and $CO_2$ or it did not. The titration analysis indicated that the carbonate did not decompose further.

In the next set of experiments (Set #3), the equilibrium conversion vs. temperature is determined for an initial bicarbonate concentration of 0.1M. Table 5.11 contains the data of the initial and final pH of the experiments starting with a 0.1M potassium bicarbonate solution. Based on the experimental data diplayed on table 5.5 and plotted in figure 5.8, the conversion based on the final pH has been calculated using equation $\mathrm{pH} = 0.0217 \cdot \mathrm{Conversion} + 8.7664$ (figure 5.8) when the pH is between 9.2 (20 % conversion) and 10.77 (90 % conversion).The conversion is interpolated when the pH is between 10.77 (90 % conversion)and 11.38 (100 % conversion).

**Table 5.11 Experiment conditions and final pH and conversion. All the experiments have been cooled down by immersion in a bucket of cool water. The initial concentration of the bicarbonate of all experiments is 0.1M. The final solution of all experiments is colorless. Set of experiments #3.**

| Run # | Temperature (◦C) | $[KHCO_3]_o$ | $t_{exposed}$ (h) | Results | | |
|---|---|---|---|---|---|---|
| | | | | pH initial | pH final | Conversion (%) Based on Final pH |
| 1 | 320 | 0.1 | 4 | 8.20 | 12.08 | >100% |
| 2 | 320 | 0.1 | 2 | 8.34 | 10.47 | 78.60 |
| 3 | 250 | 0.1 | 2 | 8.30 | 10.66 | 87.35 |
| 4 | 200 | 0.1 | 2 | 8.30 | 10.36 | 73.53 |

At the same temperature and time of reaction conditions, the experiments carried out with 0.1M potassium bicarbonate solution give higher conversions than experiments carried out with a 1M potassium bicarbonate. At 320°C, the equilibrium and 4 hours of time of reaction, the equilibrium pH is higher that the correspondent pH for 100 % conversion. This high value can be explained because at 320 °C, the carbonate decomposition also takes place, $\mathrm{CO_3}^{-}(\mathrm{aq}) + \mathrm{H_2O} \leftrightarrow \mathrm{CO_2(aq)} + 2\mathrm{OH}^{-}$. Due to the low accuracy of the pH method, two other methods are used to determine the conversion and crystals composition: TG-MS of the dried crystals and Titration.

### *5.3.2 TG-MS of the dried crystals*

We dried one third of the samples at 90°C under vacuum and send them to Hungary for TG-MS. The reason of drying the sample under vacuum is to avoid the absorption of the $CO_2$ in the air by reactions as observed in literature

$$\mathrm{CO_2(g)} \leftrightarrow \mathrm{CO_2(aq)}$$

$$\mathrm{CO_3}^{2-}(\mathrm{aq}) + \mathrm{CO_2(aq)} + \mathrm{H_2O} \leftrightarrow 2\mathrm{HCO_3}^{-}(\mathrm{aq})$$

For mixtures carbonate-bicarbonate (experiments carried out at temperatures from 150 to 250 °C), the total decomposition of bicarbonate can be observed and quantified by TG-MS as it happens at temperatures between 150 and 240°C. However, the carbonate cannot be quantified directly. The highest temperature reached by the Hungarian TG-MS instrument is 1000°C and the dry $K_2CO_3$ starts to decompose at 900°C. By 1000°C, we did not obtain total decomposition of the carbonate. The TG-MS done in Hungary can just show the beginning of the decomposition. The carbonate mass is determined by the difference between the total initial mass (after complete drying of the crystals) and the bicarbonate mass. The mixtures carbonate-hydroxide composition, on the other hand, cannot be determined (experiments carried out at temperatures at 320 °C) as the temperature to see total decomposition of carbonate is over the maximum temperature of the instrument and the hydroxide remains stable all this range.

The sample crystals as well as three controls of known composition were sent to the Hungarian Academy of Science. Table 5.12 shows the mass composition determined from the TG-MS analysis of the three controls.

**Table 5.12 Mass composition from TG-MS of three known controls**

| # | Date | Composition of solution | pH final | Results of TG-MS |
|---|---|---|---|---|
| | | | | mass %KHCO3 (dry) |
| **1** | 110915 | CONTROL I (Potassium Bicarbonate Wet and subsequently dried) | 8.09 | 45.8 |
| | | 1.7g $KHCO_3$ in 17 mL $H_2O$ | | |
| **2** | 110916 | CONTROL II (50 % wt Potassium Bicarbonate/50 % wt Potassium Carbonate Wet and subsequently dried) | 9.81 | 35.2 |
| | | 0.85g $KHCO_3$ /0.85g $K_2CO_3$ in 17 mL $H_2O$ ([KHCO3]/[K2CO3]=0.5M/0.36M | | |
| **3** | 110919 | CONTROL III (90 % wt Potassium Carbonate/10 % wt Potassium Hydroxide Wet and subsequently dried) | 13.07 | |
| | | 0.9g $K_2CO_3$/0.1g KOH in 20 mL $H_2O$ | | |

The composition of control III cannot be determined. The high temperature limit of the TG-MS instrument is 1000 °C. At this temperature, it was impossible to see total decomposition of neither hydroxide nor carbonate. However, no peak of bicarbonate was observed in the TG-MS, which means that the crystals consisted of a mixture carbonate-hydroxide. The composition of control I ($KHCO_3$ wet and dried) and control II (50%$KHCO_3$ 50%$K_2CO_3$ wet and dry) crystals were not as expected. Control I

contained about 46% $KHCO_3$, while it should have been 100%, control II contained about 35% $KHCO_3$, while it should have been 50%; a dry sample of bicarbonate without being dissolved gave 100 % bicarbonate so this taught us that the drying of the sample changed the final composition of the solution. The reason of this disagreement could be explained by the equilibrium:

$$2HCO_3^-(aq) \leftrightarrow CO_3^{2-}(aq) + CO_2(aq) + H_2O$$

$$CO_2(aq) \leftrightarrow CO_2(g)$$

As the sample was dried in vacuum oven, the partial pressure of $CO_2$ was very low during the drying procedure. It promoted the carbon dioxide to enter into the gas phase, therefore the equilibrium shifts to the direction of $CO_3^{2-}$ formation. So, when the solution is dried under vacuum, the absorption of the $CO_2$ of the air into the sample is avoided, but the equilibrium is shifted in the opposite direction and we didn't obtain a representative sample. This led us to find the third way of determining the composition of the final solution: Titration of the sample.

### *5.3.3 Titration of the sample*

As said previously, in our Bicarbonate Tubing Bomb, the final experimental solutions consist of either a mixture of potassium carbonate and bicarbonate or a mixture of potassium carbonate and potassium hydroxide. Experimentally, a final mixture carbonate-bicarbonate is obtained when the pressure vessel was heated at temperatures between 150 to 250 °C as a result of the bicarbonate decomposition reaction, $2HCO_3^- \rightarrow CO_3^{2-} + CO_2 + H_2O$. When the pressure vessel was heated to 320 °C, the mixture carbonate-hydroxide is obtained due to the decomposition of carbonate, $CO_3^{2-} + H_2O \rightarrow CO_2 + 2OH^-$ .

The carbonate-bicarbonate or carbonate-hydroxide concentrations are calculated by titration following the standard method reported by the American Public health Association [83]. In this method, an acid (the titrant) is added in small increments to the alkaline sample and the pHs after each addition are measured. A potentiometric curve (pH-Volume of titrant) is built and the concentration of bicarbonate and carbonate or carbonate and hydroxide is calculated with the equivalence points of this potentiometric curve.

**Experimental procedure: Potentiometric titration curve and apparatus**

To build the potentiometric curve, first I rinsed the electrodes and the titration vessel with distilled water and drained it. Then, I measured the sample pH. I added the titrant, standard HCl 0.1 or 0.02N, in increments of 1 mL or less (near the equivalence points, add drop by drop), such that a change of less than 0.2 pH units occurred per increment. The sample and titrant were mixed thoroughly but gently with the magnetic stirrer without splashing. I recorded the pH when a constant reading is obtained. I continued adding titrant and measured pH until pH 4.5 or lower was reached. I constructed the titration curve by plotting observed pH values versus cumulative milliliters titrant added. A smooth curve showing two inflections was obtained. A ragged or erratic curve indicated that equilibrium was not reached between successive alkali additions. Although the inflection points can be determined by the titration curve, the phenolphthalein and bromocresol indicators were used to corroborate the pH inflection points as their change in color occur at approximately the same pH as the inflection points. The pH-$V_{HCl}$ given by the inflection points was used to determine the bicarbonate-carbonate or carbonate-hydroxide concentrations.

Figure 5.9 shows a schematic diagram of the titration apparatus. The titration vessel is a beaker with a magnetic stirrer which allows the good mixture between titrant and sample, the titrant is added through a 25 mL glass buret to the beaker. And the pH is measured by the electrometric titrator which is a pH-meter Seven Easy Mettler Toledo. The potentiometric curve (pH vs. Volume of titrant) is built.

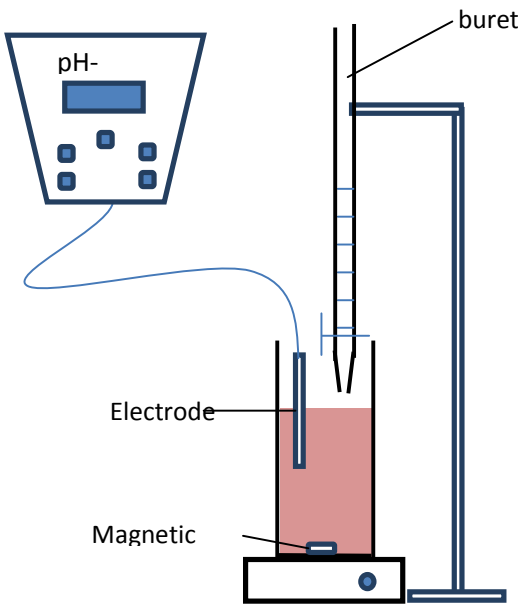


**Figure 5.9 Schematic diagram of the titration apparatus**

**Reagents and indicators**

Standard NaOH solution: A ~0.1 N NaOH solution was prepared by diluting a standard Aldrich, Sodium Hydroxide , volumetric standard 1.041 N solution in water (CAS 1310-73-2). This standard was used to standardize the HCl titrant

Standard hydrochloric acid: ~0.1 N HCl solution was used as the titrant. Three hydrochloric acid solutions were used. The first one was a 0.1 N HCl solution prepared by diluting with deionized HPLC grade water Fisher Scientific 12.1 N HCl (CAS 7647-01-0, Lot # 074064) and standardized with the standard 0.1 N NaOH. The bicarbonate-carbonate and carbonate-hydroxide controls (see below) were titrated with this solution. The second standard was an Alfa Aesar 0.100 N standardized solution (Lot # G21X031) and the third one was another standard 0.100 N HCl solution prepared from a standard volumetric concentrate solution from Acculute Anachemia (Lot # 90605). The concentrate solution was transferred to a 1L volumetric flask and it was diluted to the line mark with deionized water at 20 °C. The second and third standard solutions were used to verify the concentration of the standard 0.1 N NaOH solution and the Acculute standard was also used to titrate the experimental samples.

Bromocresol green indicator solution: The bromocresol green indicator was prepared by dissolving 100 mg bromocresol green, sodium salt, in 100 mL deionized water. The change in color occurs at pH≔4.5 from blue to yellow.

Phenolphthalein solution, alcoholic: To prepare the phenolphthalein indicator, I weighed 0.5 g of phenolphthalein and dissolved it in a 50% ethanol solution that consists in 50ml ethanol and 50 ml water. The change in color occurs at pH≔8.3 from pink to colorless.

Verification of the standard solutions

As stated previously, the second and third standard 0.1 N HCl standards (Alfa Aesar and Acculute Anachemia )were used to verify the concentration of the ~0.1 N NaOH. I prepared two ~0.1 N NaOH solutions by diluting 10 mL of NaOH (Stated Molarity=1.041 M) into 100 mL. I took 25 mL of these NaOH ~ 0.1041 N solutions and titrated with the two standard HCl 0.1 N solutions (Acculute HCl and Alfa Aesar HCl). In the titrations, the NaOH reacts with the HCl to produce NaCl ($NaOH + HCl \rightarrow NaCl + H_2O$).When

all the NaOH reacts with HCl, the final pH will be pH=7. The moles of HCl needed to get pH=7 correspond to the initial moles of NaOH. Therefore, the NaOH concentration is calculated dividing the moles to the

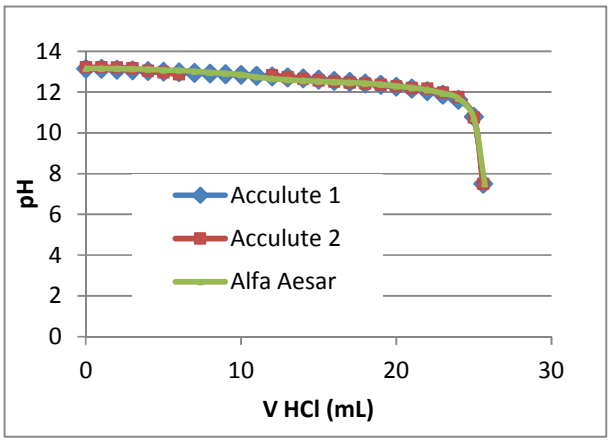


**Figure 5.10 Titration curves to verify standard 0.1 M NaOH (Solution I)**

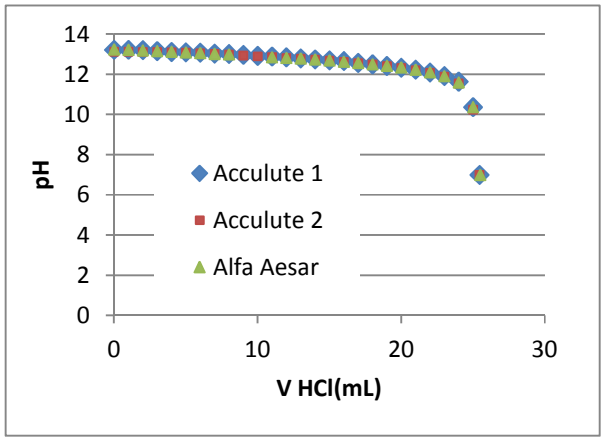


**Figure 5.11 Titration curves to verify standard 0.1 M NaOH (Solution II)**

initial volume. The titration curves of two 0.1 N NaOH solutions are plotted in figures 5.10 and 5.11. The concentration of the NaOH solution is then calculated

The volume of NaOH taken in both figures is 25 mL. The volume of the 0.1 N HCl spent in figure 5.10 is 25.6(Acculute 1 and Acculute 2 titrations) and 25.7 ml (Alfa Aesar titration), which gives a NaOH concentration of:

[NaOH]=0.1 x 25.6/25=0.102 M Acculute 1, Acculute 2

[NaOH]=0.1 x 25.7/25=0.103 M Alfa Aesar

The NaOH has a stated concentration of 0.1041 M which gives an accuracy of

$$Accuracy\ (\%) = \frac{|0.1041 - 0.102|}{0.1041} \cdot 100 = 1.63\ \%$$ Acculute 1, Acculute 2

$$Accuracy\ (\%) = \frac{|0.1041 - 0.1023|}{0.1041} \cdot 100 = 1.25\ \%$$ Alfa Aesar

In figure 5.11, the volume of HCl spent is 25.45(Acculute 1 and Acculute 2 titrations) and 25.5 ml (Alfa Aesar titration) which gives a NaOH concentration of:

[NaOH]=0.1 x 25.45/25=0.102 M Acculute 1, Acculute 2

[NaOH]=0.1 x 25.5/25=0.102 M Alfa Aesar

The accuracy of the NaOH concentration is

$$Accuracy\ (\%) = \frac{|0.1041 - 0.102|}{0.1041} \cdot 100 = 2.21\% \qquad \text{Acculute 1, Acculute 2}$$

$$Accuracy\ (\%) = \frac{|0.1041 - 0.102|}{0.1041} \cdot 100 = 2.02\ \% \qquad \text{Alfa Aesar}$$

The reproducibility of the titrations is very good. The titrations with the same and the different HCl standard bottles give almost the same titration curves which gives faith to the HCl standard used. The number of significant figures that agree in the six titrations is three. So, we can state that the NaOH concentration is 0.103±0.001 M (mol/L) and the HCl concentration is 0.100 M.

**Equations to calculate carbonate-bicarbonate and carbonate-hydroxide concentrations**

Experimentally, we saw two possible solutions after running the experiment: Mixture carbonate-hydroxide (experiments run at temperatures over 250 °C) and mixture carbonate-bicarbonate (experiments run from 150 to 250 °C). The calculation of the concentrations of the Carbonate-Bicarbonate mixture and Carbonate- Hydroxide mixture are presented in the following section.

Calculation of the Potassium Carbonate –Bicarbonate Concentrations

To titrate the samples, I used HCl 0.1M to neutralize the carbonate and bicarbonate. The stronger the base, the easier it reacts with acid. In this case, the $K_2CO_3$ is the strongest base, so it will be neutralized first (Reaction 5.8). When all the carbonate -$CO_3^{2-}$ -is converted to bicarbonate –$HCO_3^-$-, this bicarbonate and the bicarbonate of the initial sample will react with HCl (Reaction 5.9).

$$K_2CO_3 + HCl \rightarrow KHCO_3 + KCl \qquad \text{Reaction 5.8}$$

$$KHCO_3 + HCl \rightarrow H_2O + CO_2(aq) + KCl \qquad \text{Reaction 5.9}$$

Figures 5.15 to 5.21 show the titration curves of carbonate-bicarbonate mixtures. The first inflection point observed in these figures is obtained after all the $K_2CO_3$ has reacted with the HCl (Reaction 5.8). The pH of the solution will be the pH of the potassium bicarbonate solution. The bicarbonate concentration, just after the first inflection point, will be the sum of the initial concentration of bicarbonate and the concentration of the carbonate (as everything converted into bicarbonate). Figure 5.12 shows the calculated pH of a potassium bicarbonate solution when the concentration is between 0.01 and 1M. This pH has been calculated in MatLab with the previous equilibria, mass balance and

charge balance equations 5.4 to 5.8. The pH within this range will be between 8.25 and 8. This pH inflection point is clear and it happens in the areas where phenolphthalein changes its color from pink to colorless (pH=8.2).

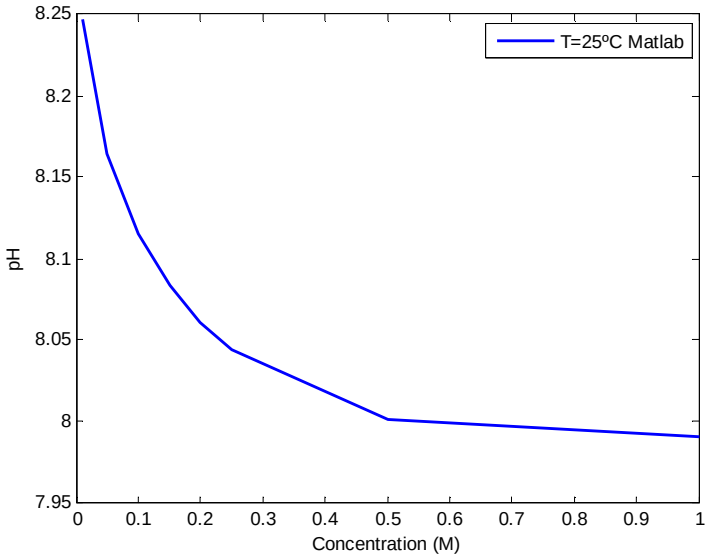


**Figure5.12 pH vs. Potassium Bucarbonate concentration**

I called $V_1$ the volume of HCl needed to reach the first inflection point. After this first inflection point, the $KHCO_3$ reacts with HCl to form KCl and carbonic acid($CO_2$ and $H_2O$) (Reaction 5.9).After all the KHCO3 has reacted with the HCl, the pH of the solution will be the pH of carbonic acid ($CO_2$+$H_2O$) solution and a second inflection point is observed. If $CO_2$ does not escape, the concentration of this solution will be the same as the bicarbonate. Figure 5.13 shows the pH of a carbonic acid solution when the concentration is between 0.01 and 1M. The indicator used is bromocresol green (pH at which it changes color from blue to yellow is 4.5). However, the pH of changing color is above the actual change. So if we titrate until color changes, we cannot be sure we are left with a solution of $H_2CO_3$ and an uncertainty in the calculation is introduced.

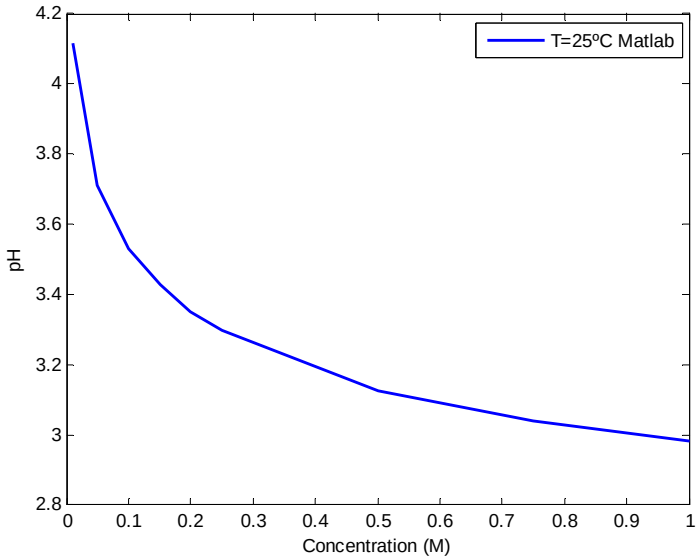


**Figure 5.13 pH vs. Carbonic acid concentration**

I called $V_2$ the volume of HCl needed to reach the second inflection point, i.e. the volume of HCl needed to titrate the sum of potassium carbonate and bicarbonate. The potassium carbonate and potassium bicarbonate moles are calculated from $V_1$ and $V_2$. In summary, the titration reactions and volume of HCl spent in the first and second equivalence point are

$$K_2CO_3 + HCl \rightarrow KHCO_3 + KCl \qquad \text{Reaction 5.8}$$

$$KHCO_3 + HCl \rightarrow H_2O + CO_2(aq) + KCl \qquad \text{Reaction 5.9}$$

$V_1$= Volume of HCl to titrate potassium carbonate. This means $V_{HCl}$ after reaction 5.8

$V_2$= Volume of HCl to titrate sum of potassium carbonate and bicarbonate. This means $V_{HCl}$ after reactions 5.8 and 5.9.

To calculate the potassium carbonate and bicarbonate concentrations, the concept of Phenolphthalein (*P*) and Total alkalinity (*T*) used by Eaton et al. [9] is introduced. The Phenolphthalein is defined as the $H^+$ equivalents spent in the titration to reach the first inflection point, the Total alkalinity is defined as the $H^+$ equivalents spent in the titration to reach the second inflection point. The $H^+$ equivalents correspond to the HCl moles that reacted and are expressed as

$$P = eq\ H^+\ to\ titrate\ carbonate = V_1(L)\ \cdot N_{HCl}$$

$$T = \ eq\ H^{+}\ \ to\ titrate\ sum\ of\ potassium\ carbonate\ and\ bicarbonate = V_2(L)\ \cdot N_{HCl}$$

The moles of carbonate and bicarbonate are calculated as:

$$Moles\ K2CO3 = P$$

$$Moles\ KHCO3 = T - 2P$$

*P* corresponds to the moles of potassium carbonate. *T* corresponds to the bicarbonate moles plus twice the carbonate moles (moles of $H^+$ used to convert them into bicarbonate and then into carbonic acid)

Calculation of the Carbonate –Hydroxide concentrations

In this case, the KOH is the strongest base, so it will be neutralized first (Reaction 5.10). The next base to be neutralized is $CO_3^{2-}$ (Previous reaction 5.8), when all the carbonate - $CO_3^{2-}$ -is converted to bicarbonate - $HCO_3^-$-, the bicarbonate will react with HCl (Previous reaction 5.9).

$$KOH\ +\ HCl \rightarrow KCl\ +\ H_2O \qquad \text{Reaction 5.10}$$

$$K_2CO_3\ + HCl \rightarrow KHCO_3 +\ KCl \qquad \text{Reaction 5.8}$$

$$KHCO_3 + HCl \rightarrow H_2O + CO_2 + KCl \qquad \text{Reaction 5.9}$$

In this case the first inflection point is shown after the KOH reacts with HCl to form KCl and water (Reaction 5.10). This inflection point indicates the disappearance of KOH, leaving only $K_2CO_3$. The potassium carbonate concentration after reaction 5.10 will be the initial carbonate concentration. Figure 5.14 shows the pH of a potassium carbonate solution when the concentration is between 0.01 and 0.5. The pH within this range will be between 10.99 and 11.75. The carbonate-hydroxide titration curves show n inflection point at this pH. However, this inflection point is not very clear and can't be detected using pH indicators [84].

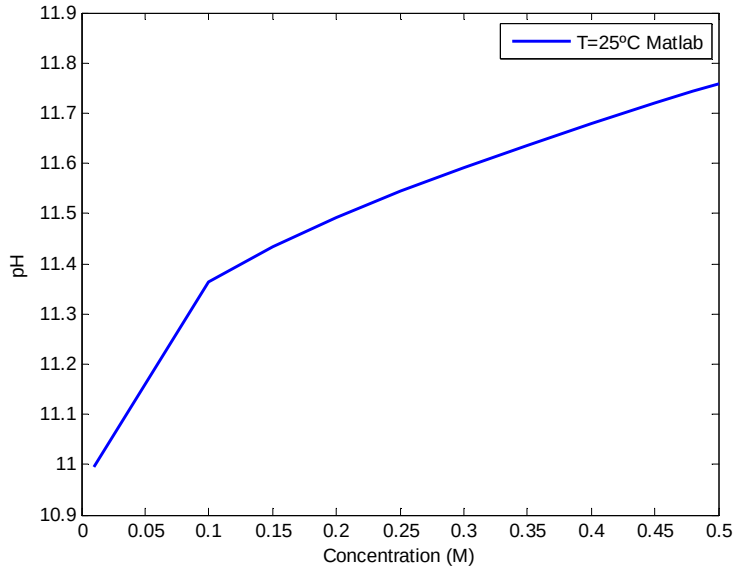


**Figure 5.14 pH vs. Concentration Potassium Carbonate (M)**

After this inflection point, the $K_2CO_3$ reacts with HCl to form KCl and $KHCO_3$ (Reaction 5.8). After all the $K_2CO_3$ has reacted with the HCl, the pH of the solution will be the pH of the potassium bicarbonate solution. The concentration of the potassium bicarbonate solution is equal to the concentration of the carbonate after reaction 5.10 happened. The pH within this range will be around 8-8.2 (Figure 5.12). This means after adding $V_1$ of the titrant we have titrated the sum of potassium hydroxide and potassium carbonate. This $V_1$ was the volume to get pH≃8.2in the pH-meter. Finally, the $KHCO_3$ reacts with HCl to form KCl, $CO_2$ and $H_2O$ (Reaction 5.9). After all the KHCO3 has reacted with the HCl, the pH of the solution will be the pH of carbonic acid ($CO_2$+$H_2O$) solution (Figure 5.13). After adding $V_2$ of the titrant we have titrated sum of potassium hydroxide, potassium carbonate and bicarbonate. From $V_1$ and $V_2$, the potassium carbonate and potassium hydroxide concentrations are calculated. In summary, the titration reactions and volume of HCl spent in the first and second detectable equivalence points are

$$KOH + HCl \rightarrow KCl + H_2O \qquad \text{Reaction 5.10}$$

$$K_2CO_3 + HCl \rightarrow KHCO_3 + KCl \qquad \text{Reaction 5.8}$$

$$KHCO_3 + HCl \rightarrow H_2O + CO_2 + KCl \qquad \text{Reaction 5.9}$$

$V_1$= Volume of HCl to titrate sum of potassium hydroxide and carbonate. This means $V_{HCl}$ after reactions 5.10 and 5.8

$V_2$= Volume of HCl to titrate sum of potassium hydroxide, carbonate and bicarbonate. This means $V_{HCl}$ after reactions 5.10, 5.8 and 5.9

The $H^+$ equivalents correspond to the moles of HCl spent to reach the first an second inflection points and are expressed as

$$P = \ eq\ H^+\ to\ titrate\ potassium\ hydroxide\ and\ carbonate(rxns\ 5.10\ and\ 5.8) = V_1(L)\ \cdot N_{HCl}$$

$$T = \ eq\ H^+\ \ to\ titrate\ sum\ of\ \ hydroxide, carbonate\ and\ bicarbonate(rxns\ 5.8\ and\ 5.9)$$
$$= V_2(L)\ \cdot N_{HCl}$$

P and T are the Phenolphthalein and Total alkalinity respectively. The moles of carbonate and hydroxide are calculated as:

$$Moles\ K_2CO_3 = T - P$$

$$Moles\ KOH = 2P - T$$

After reactions 5.10 and 5.8, all the carbonate has been converted into bicarbonate, so the moles of bicarbonate titrated ( T-P) correspond to the initial carbonate moles. The moles of KOH are the moles of carbonate and KOH titrated (P) minus the carbonate moles (T-P).

**Accuracy of the titration method**

To improve and validate the titration procedure, bicarbonate-carbonate and carbonate-hydroxide known solutions were prepared. The concentrations determined by the titration method were compared to the known concentration values and the accuracy of the titration method is calculated. 25 mL controls of known carbonate-hydroxide and carbonate-bicarbonate solutions were prepared and titrated with a standardized ~0.1 M (mol/L) solution of HCl. In this case, the HCl titrant was prepared by diluting the 12.1 N Fisher Scientific HCl. The standardization of the HCl was made by titrating 25 mL of standard 0.103 M (mol/L) solution of NaOH with the HCl until phenolphthalein change of color. The controls were then titrated with the standardized HCl and the potentiometric titration curve was built. The carbonate-bicarbonate and carbonate-hydroxide moles are calculated based on the results of the titrations curves (Figures 5.15 to 5.21 for carbonate-bicarbonate mixtures and Figures 5.22 to 5.24 for carbonate-hydroxide mixtures) and compared to the known values and the accuracy is finally determined.

Titration curves of potassium carbonate-bicarbonate controls

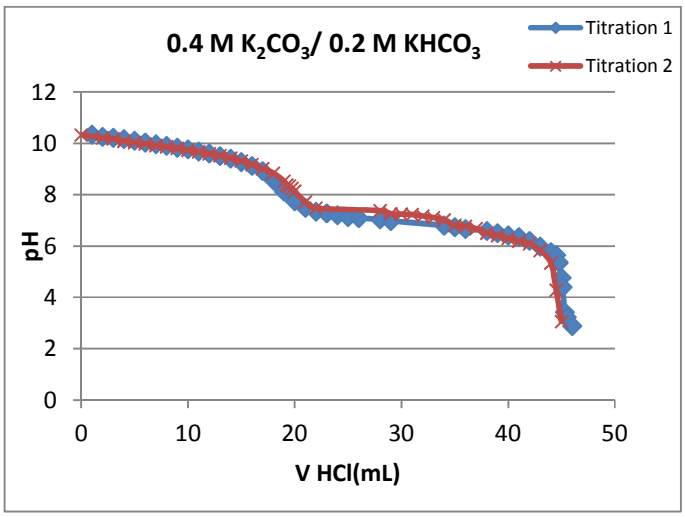


**Figure 5.15 Titration of a 0.4M $K_2CO_3$/0.2M $KHCO_3$ control solution**

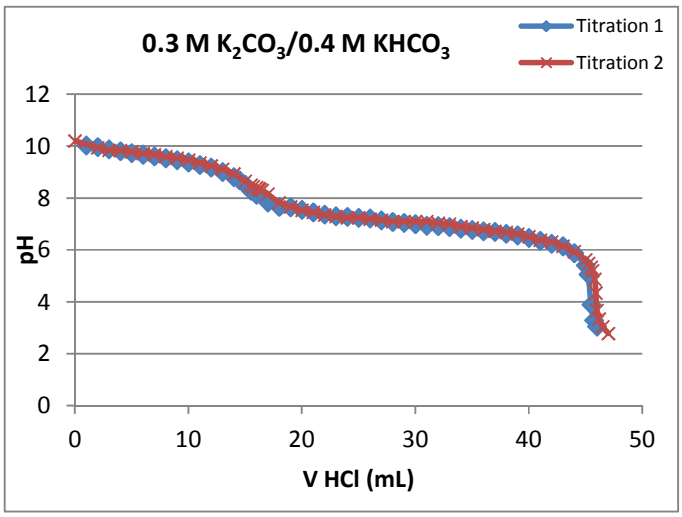


**Figure 5.16 Titration of a 0.3M $K_2CO_3$/0.4M $KHCO_3$ control solution**

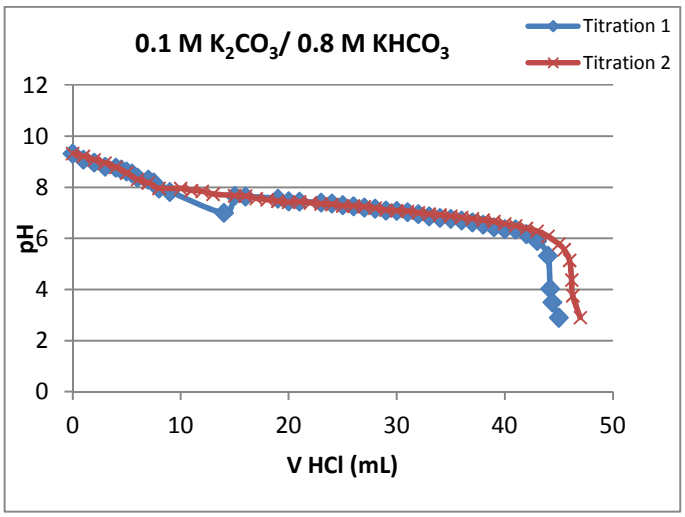


**Figure 5.17 Titration of a 0.1M $K_2CO_3$/0.8M $KHCO_3$ control solution**

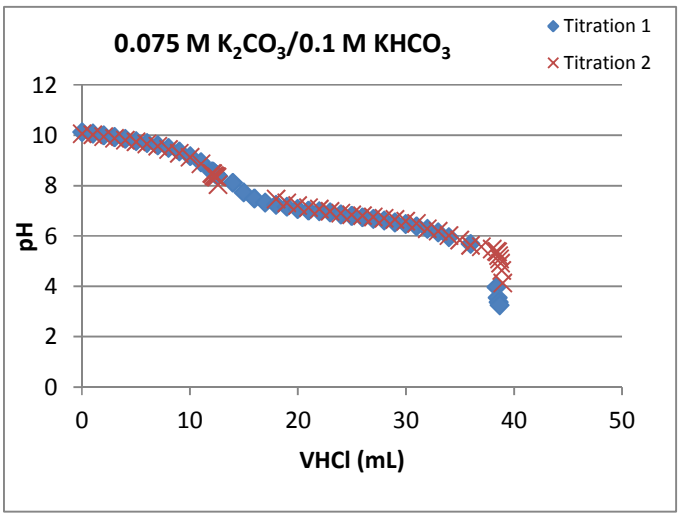


**Figure 5.18 Titration of a 0.075M $K_2CO_3$/0.1M $KHCO_3$ control solution Concentration titrant [HCl]=0.122M**

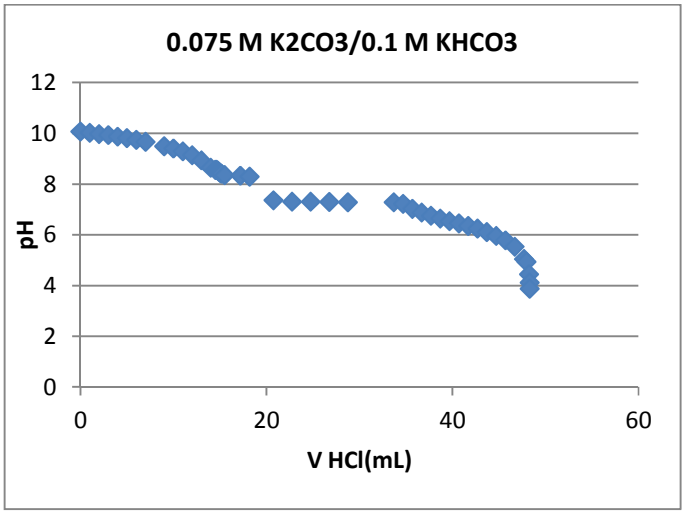


**Figure 5.19 Titration of a 0.075M $K_2CO_3$/0.1M $KHCO_3$ control solution Concentration titrant [HCl]=0.096M**

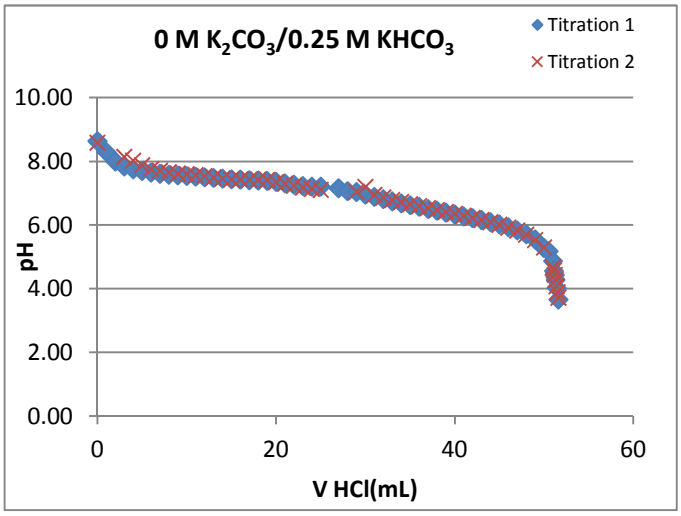


**Figure 5.20 Titration of a 0 M $K_2CO_3$/0.25M $KHCO_3$ control solution**

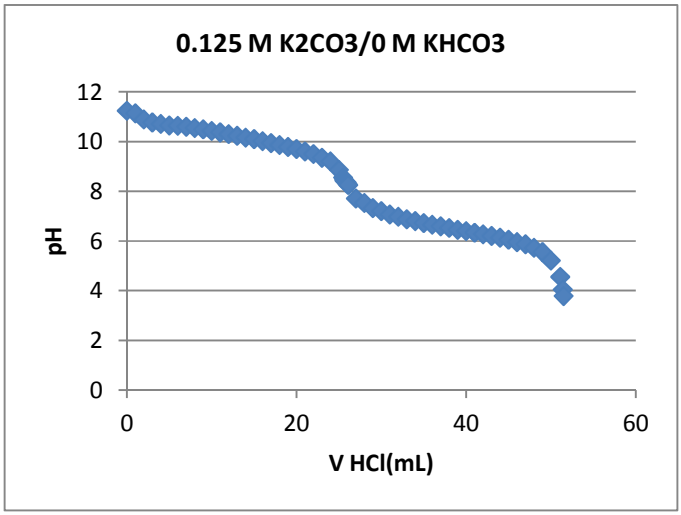


**Figure 5.21 Titration of a 0.125M $K_2CO_3$/0 M $KHCO_3$ control solution**

The HCl molarity is 0.111M for figures 5.15 to 5.17, 0.122 M for figure 5.18, 0.096 M for figure 5.19 and 0.0947 M for figures 5.20 and 5.21.The initial volume of bicarbonate-carbonate titrated is 5 mL for figures 5.15 to 5.17 and 20 mL for figures 5.18 to 5.21. The initial concentrations of the bicarbonate and carbonate mixtures used for the titrations are based on different conversions of a solution of just bicarbonate that decomposed into carbonate and $CO_2$ and the $CO_2$ escaped. Figures 5.15 to 5.17 use 0.4M $K_2CO_3$/0.2M $KHCO_3$ (figure 5.17), 0.3M $K_2CO_3$/0.4M $KHCO_3$ (figure 5.18) and 0.1M $K_2CO_3$/0.8M $KHCO_3$ (figure 5.19) which represent the product solution of an initial 1M $KHCO_3$ that suffered 80%, 60% and 20 % conversions. Figures 5.18 to 5.21 use 0.075M $K_2CO_3$/0.1M $KHCO_3$ (figures 5.18 and 5.19), 0M$K_2CO_3$/0.25M $KHCO_3$ (figure 5.20) and 0.125M $K_2CO_3$/0M $KHCO_3$ (figure 5.21) which represent the

product solution of an initial 0.25M $KHCO_3$ that suffered 60%, 100% and 0 % conversions. 0.075M $K_2CO_3$/0.1M $KHCO_3$ (figures 5.18 and 5.19) was titrated twice to check the reliability of the values due to the first strange graph obtained (figure 5.19). The volumes for the first and second inflection points, $V_1$ and $V_2$, were taken from the graphs. The concentrations of the species are calculated using the Phenolphthalein (*P*) and Total alkalinity (*T*) points. The moles of the carbonate-bicarbonate and carbonate-bicarbonate are calculated as

- $K_2CO_3$ - $KHCO_3$ mixture: Moles $K_2CO_3$=P, Moles $KHCO_3$=T-2P

The calculated concentration ($Calculated\ Molarity$) is calculated dividing the moles of carbonate and bicarbonate given by the titration curves by the volume of initial sample, the real concentration($Real\ Molarity$ ) is the calculated dividing the mass of carbonate and bicarbonate weighted by the volume, the relative accuracy and the absolute error are evaluated for different carbonate-bicarbonate and carbonate-hydroxide mixtures and tabulated from tables 5.13 to 5.19. The relative accuracy and absolute error are defined as

$$Accuracy\ (\%)\ = \left|\frac{Calculated\ Molarity - Real\ Molarity}{Real\ Molarity}\right|$$

$$Absolute\ error\ = |Calculated\ Molarity - Real\ Molarity|$$

**Table 5.13 Accuracy of the titration of a 0.4M $K_2CO_3$/0.2M $KHCO_3$ solution (figure 5.15) with the alkalinity method**

| | Molarities | | | Accuracy(%) | | Absolute error | |
|---|---|---|---|---|---|---|---|
| | **Titration 1** | **Titration 2** | **Real** | **Titration 1** | **Titration 2** | **Titration 1** | **Titration 2** |
| **M K2CO3** | 0.40 | 0.42 | **0.4** | 0.01 | 5.54 | 0.00 | 0.02 |
| **M KHCO3** | 0.19 | 0.16 | **0.20** | 5.57 | 21.12 | 0.01 | 0.04 |

**Table 5.14 Accuracy of the titration of a 0.3M $K_2CO_3$/0.4 M $KHCO_3$ solution (figure 5.16) with the alkalinity method**

| | Molarities | | | Accuracy(%) | | Absolute error | |
|---|---|---|---|---|---|---|---|
| | **Titration 1** | **Titration 2** | **Real** | **Titration 1** | **Titration 2** | **Titration 1** | **Titration 2** |
| **M K2CO3** | 0.32 | 0.33 | **0.3** | 7.40 | 11.10 | 0.02 | 0.03 |
| **M KHCO3** | 0.37 | 0.36 | **0.4** | 6.95 | 10.01 | 0.03 | 0.04 |

**Table 5.15 Accuracy of the titration of a 0.1M $K_2CO_3$/0.8 M $KHCO_3$ solution (figure 5.17) with the alkalinity method**

| | Molarities | | | Accuracy(%) | | Absolute error | |
|---|---|---|---|---|---|---|---|
| | Titration 1 | Titration 2 | Real | Titration 1 | Titration 2 | Titration 1 | Titration 2 |
| M K2CO3 | 0.11 | 0.11 | **0.1** | 11.10 | 11.10 | 0.01 | 0.01 |
| M KHCO3 | 0.76 | 0.81 | **0.8** | 4.45 | 0.82 | 0.04 | 0.01 |

**Table 5.16 Accuracy of the titration of a 0.075M $K_2CO_3$/0.1 M $KHCO_3$ solution (figure 5.18) with the alkalinity method**

| | Molarities | | | Accuracy(%) | | Absolute error | |
|---|---|---|---|---|---|---|---|
| | Titration 1 | Titration 2 | Real | Titration 1 | Titration 2 | Titration 1 | Titration 2 |
| M K2CO3 | 0.074 | 0.074 | **0.075** | 1.961 | 1.961 | 0.001 | 0.001 |
| M KHCO3 | 0.090 | 0.092 | **0.100** | 10.287 | 8.496 | 0.010 | 0.008 |

**Table 5.17 Accuracy of the titration of a 0.075M $K_2CO_3$/0.1 M $KHCO_3$ solution (figure 5.19) with the alkalinity method**

| | Molarities | | Accuracy(%) | Absolute error |
|---|---|---|---|---|
| | Titration 1 | Real | Titration 1 | Titration 1 |
| M K2CO3 | 0.072 | **0.075** | 3.846 | 0.003 |
| M KHCO3 | 0.088 | **0.100** | 11.971 | 0.012 |

**Table 5.18 Accuracy of the titration of a 0M $K_2CO_3$/0.25 M $KHCO_3$ solution (figure 5.20) with the alkalinity method**

| | Molarities | | | Accuracy(%) | | Absolute error | |
|---|---|---|---|---|---|---|---|
| | Titration 1 | Titration 2 | Real | Titration 1 | Titration 2 | Titration 1 | Titration 2 |
| M KHCO3 | 0.24 | 0.24 | **0.25** | 2.65 | 2.65 | 0.01 | 0.01 |

**Table 5.19 Accuracy of the titration of a 0.125M $K_2CO_3$/0 M $KHCO_3$ solution (figure 5.21) with the alkalinity method**

| | Molarities | | Accuracy(%) | Absolute error |
|---|---|---|---|---|
| | Titration 1 | Real | Titration 1 | Titration 1 |
| M K2CO3(from P) | 0.121 | 0.125 | 3.41 | 0.004 |

The carbonate accuracy varies from 0.01 to 11.10% and the bicarbonate from 0.82 to 11.97 %. There is one value that presents a 21.12 % accuracy.

Similarly, carbonate-hydroxide mixtures are prepared, the titration curves are built (Figure 5.22 to 5.24) and the moles of the carbonate-hydroxide are calculated from the titration curves as

- $K_2CO_3$ –KOH mixture: Moles $K_2CO_3$=T-P, Moles KOH=2P-T

The accuracy and absolute error is tabulated

Titrations curves of potassium carbonate-hydroxide controls

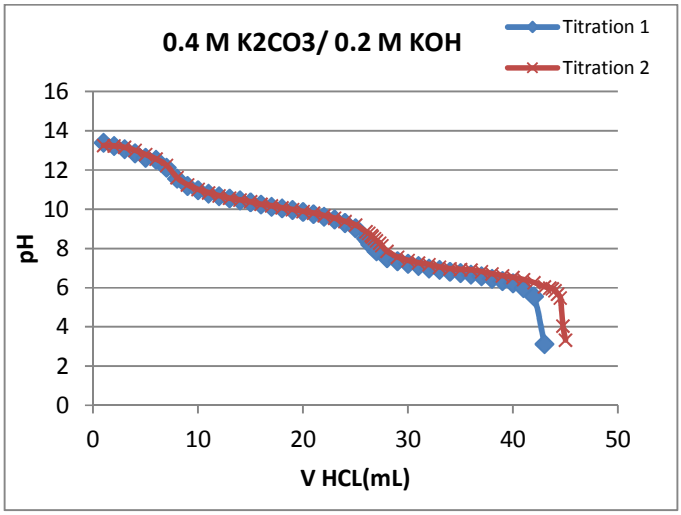


**Figure 5.22 Titration of a 0.4 M $K_2CO_3$/0.2 M KOH control solution**

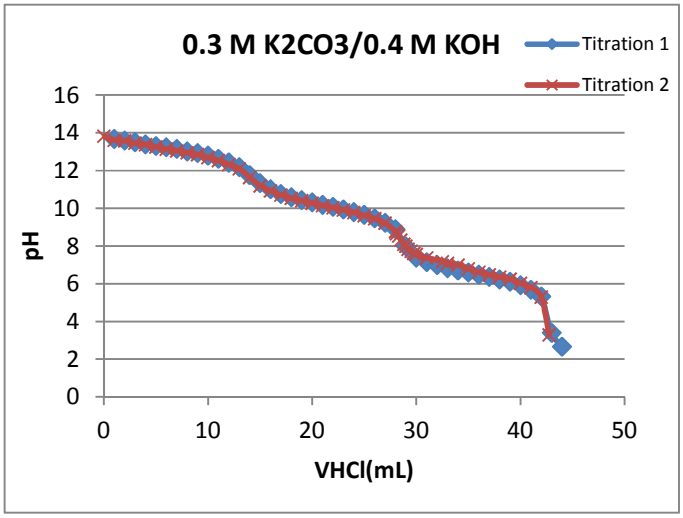


**Figure 5.23 Titration of a 0.3 M $K_2CO_3$/0.4 M KOH control solution**

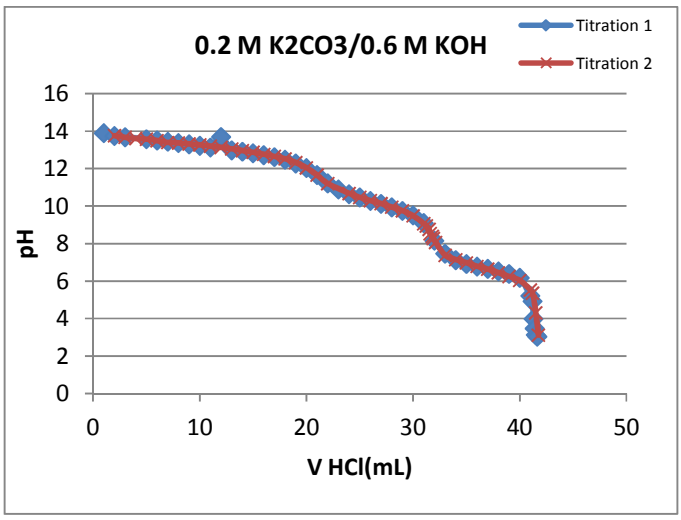


**Figure 5.24 Titration of a 0.2 M $K_2CO_3$/0.6 M KOH control solution**

The following tables show the $Calculated\ Molarity$, the $Real\ Molarity$ , the relative accuracy and the absolute error for different carbonate-hydroxide mixtures

**Table 5.20 Accuracy of the titration of a 0.4M $K_2CO_3$/0.2 M KOH control solution (figure 5.22) with the alkalinity method**

| | Molarities | | | Accuracy(%) | | Absolute error | |
|---|---|---|---|---|---|---|---|
| | Titration 1 | Titration 2 | Real | Titration 1 | Titration 2 | Titration 1 | Titration 2 |
| **M K2CO3** | 0.42 | 0.40 | **0.4** | 4.06 | 0.18 | 0.02 | 0.00 |
| **M KOH** | 0.16 | 0.19 | **0.2** | 19.53 | 3.99 | 0.04 | 0.01 |

**Table 5.21 Accuracy of the titration of a 0.3M $K_2CO_3$/0.4 M KOH control solution (figure 5.23) with the alkalinity method**

| | Molarities | | | Accuracy(%) | | Absolute error | |
|---|---|---|---|---|---|---|---|
| | Titration 1 | Titration 2 | Real | Titration 1 | Titration 2 | Titration 1 | Titration 2 |
| **M K2CO3** | 0.32 | 0.32 | **0.3** | 7.40 | 7.03 | 0.02 | 0.02 |
| **M KOH** | 0.31 | 0.31 | **0.4** | 22.23 | 23.06 | 0.09 | 0.09 |

**Table 5.22 Accuracy of the titration of a 0.2M $K_2CO_3$/0.6 M KOH control solution (figure 5.24) with the alkalinity method**

| | Molarities | | | Accuracy(%) | | Absolute error | |
|---|---|---|---|---|---|---|---|
| | Titration 1 | Titration 2 | Real | Titration 1 | Titration 2 | Titration 1 | Titration 2 |
| **M K2CO3** | 0.22 | 0.23 | **0.2** | 8.88 | 12.77 | 0.02 | 0.03 |
| **M KOH** | 0.48 | 0.48 | **0.6** | 19.64 | 20.56 | 0.12 | 0.12 |

The carbonate accuracy varies from 0.18 to 12.77% and the hydroxide from 3.99 to 23.06%. The hydroxide accuracy is not very good.

**Precision and Bias**

The precision and bias of this method is described in the literature by Eaton et al. [83]. No general statement can be made about precision because of the great variation in sample characteristics. The precision of the titration is likely to be much greater than the uncertainties involved in sampling and sample handling before the analysis. Eaton et al. [83] included that in the range of 10 to 500 mg/L, when the alkalinity is due entirely to carbonates or bicarbonates, a standard deviation of 1 mg CaCO3/L can be achieved. Forty analysts in 17 laboratories analyzed synthetic samples containing increments of bicarbonate equivalent to 120 mg CaCO3/L. The titration procedure of potentiometric titration curve was used, with an end point pH of 4.5. The standard deviation was 5 mg/L and the average bias (lower than the true value) was 9 mg/L. Sodium carbonate solutions equivalent to 80 and 65 mg CaCO3/L were analyzed by 12 laboratories according to the procedure of potentiometric titration to preselected pH. The standard deviations were 8 and 5 mg/L, respectively, with negligible bias. Four laboratories analyzed six samples having total alkalinities of about 1000 mg $CaCO_3$/L and containing various ratios of

carbonate/bicarbonate by the procedures of both color change and potentiometric titration to preselected pH. The pooled standard deviation was 40 mg/L, with negligible difference between procedures.

**Results of the titration method of the experimental solutions**

Unfortunately, all the experiments samples ran with a 0.1 M potassium bicarbonate solution (experiments from Table 5.8) were lost as all the sample was dried to do the TG-MS analysis. Some of the experiments ran with a 1 M potassium bicarbonate solution (Runs 1, 6, 7 and 9 from Table 5.7) were also lost. The rest of the experimental samples were stored and analyzed by titration. Titration curves of the experiments are done and the composition of the solution is determined. As stated before, the composition of a bicarbonate-carbonate solution is given by the two equivalences points of the titration curve:

$K_2CO_3$ - $KHCO_3$ mixture: Moles $K_2CO_3$=P,Moles $KHCO_3$=T-2P. Where P is the Phenolphthalein alkalinity and T the Total alkalinity

Once the composition is known, it can be related to the conversion as

$$moles\ KHCO_{3_{final}} = moles\ KHCO_{3_o} \cdot (1 - Conversion\ KHCO_3)$$

$$moles\ K_2CO_{3_{final}} = \frac{moles\ KHCO_{3_o} \cdot Conversion\ KHCO_3}{2}$$

If the % of the species in the products are written in terms of conversion

$$\%\ KHCO_3 = \frac{moles\ KHCO_{3_o} \cdot (1 - Conversion\ KHCO_3)}{moles\ KHCO_{3_o} \cdot (1 - Conversion\ KHCO_3) + \frac{moles\ KHCO_{3_o} \cdot Conversion\ KHCO_3}{2}} 100$$

$$\%\ KHCO_3 = \frac{1 - Conversion\ KHCO_3}{1 - \frac{Conversion\ KHCO_3}{2}} 100$$

$$\%\ K_2CO_3 = \frac{\frac{Conversion\ KHCO_3}{2}}{1 - \frac{Conversion\ KHCO_3}{2}} \cdot 100$$

So, the conversion for the species is then calculated as

$$Conversion = \frac{2\left(\%\frac{K_2CO_3}{100}\right)}{\left(1+\%\frac{K_2CO_3}{100}\right)}$$

A 0.1 M HCl standardized solution (Acculute Anachemia R-2820 F (46432-00) Lot 90605) is used in these titrations .Figure 5.25 shows the composition and conversion of run #2 calculated from the phenolphthalein and total alkalinities points (P and T) of the titration curve.

Run #2 (Temperature 320 °C, [$KHCO_3$=1M], $t_{exposed}$=4h)

First equivalence point: P=35mL*0.02M=0.70 mmoles

Second equivalence point: T=76mL*0.02M=1.52 mmoles

Moles carbonate =P=0.70 mmoles

Moles bicarbonate=T-2P=0.12 mmoles

$$\%Carbonate = \frac{0.7}{0.7+0.12}\cdot 100 = 85.4\ \%$$

$$\%Bicarbonate = \frac{0.12}{0.12+0.7}\cdot 100 = 14.3\ \%$$

$$Conversion = \frac{2(\%\frac{K_2CO_3}{100})}{(1+\%\,K_2CO_3)} = 92\%$$

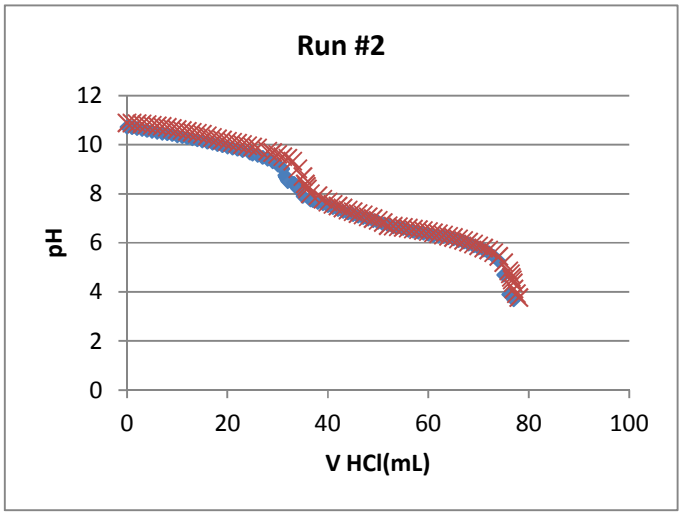


**Figure 5.25 Titration curve of experimental run #2**

Similarly, the composition and conversions of the rest of the experimental samples have been calculated from their respective titration curve and tabulated in table 5.23. Figure 5.26 to 5.31 show the titration curves of the runs.

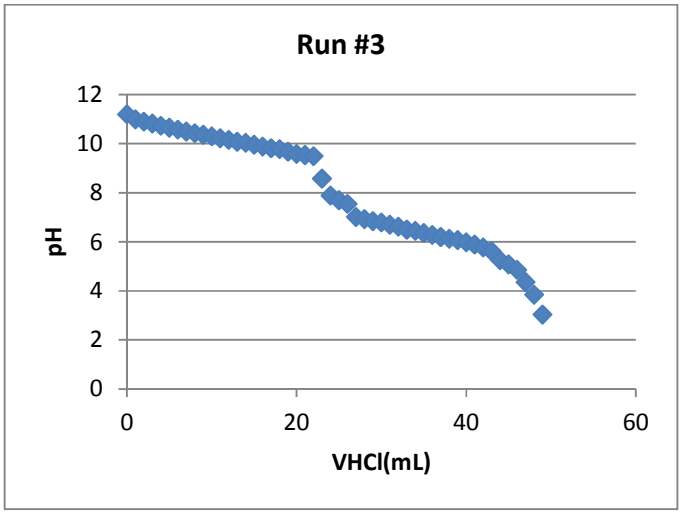


Figure 5.26 Titration curve of experimental run #3

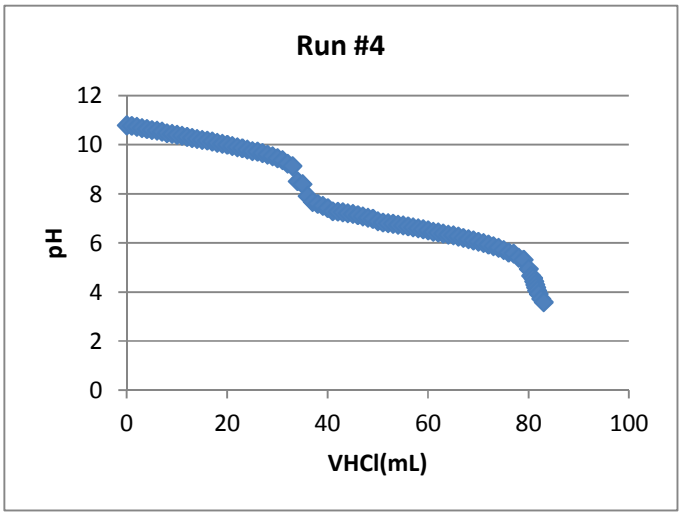


Figure 5.27 Titration curve of experimental run #4

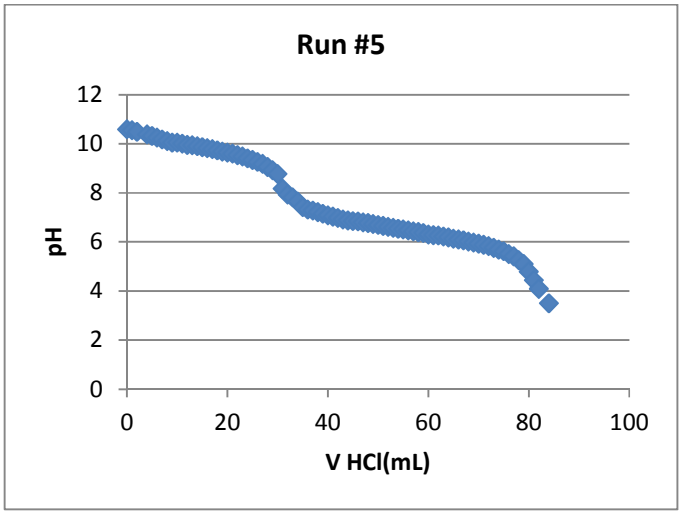


Figure 5.28 Titration curve of experimental run #5

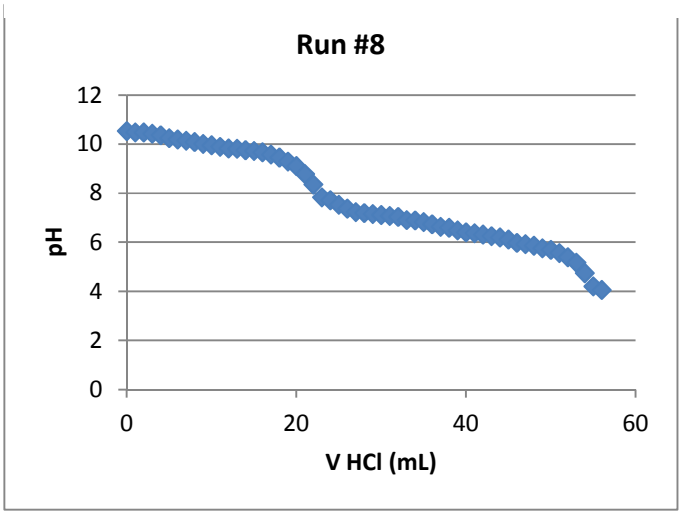


Figure 5.29 Titration curve of experimental run #8

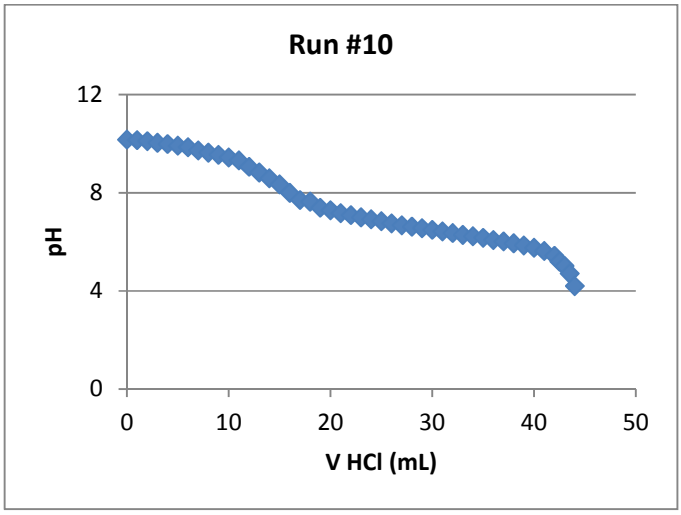


**Figure 5.30 Titration curve of experimental run #10**

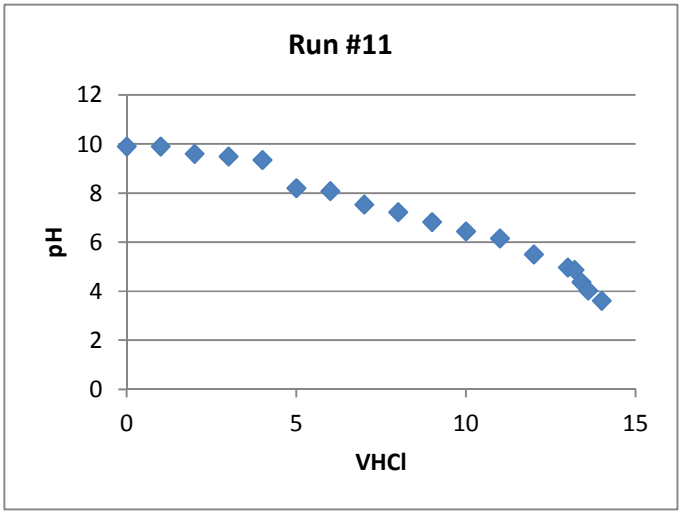


**Figure5.31 Titration curve of experimental run #11**

Table 5.23 collects the results of the composition in moles and % of moles of carbonate and bicarbonate and the conversions of the experimental samples. Notice that all the titration curves gave us mixtures carbonate-bicarbonate, which disagrees with the findings of the pH method.

**Table 5.23 Experiment conditions and results (bicarbonate-carbonate composition and conversion) from the titration curves. All the experiments have been cooled down by immersion in a bucket of cool water. The initial concentration of the bicarbonate of all experiments is 1M. The final solution of all experiments is colorless. Set of experiments #2.**

| Run # | Temperature ($^{o}$C) | $[KHCO_3]_o$ | $t_{exposed}$ (h) | 1st equivalence point (mmoles of HCl) | 2nd equivalence point (mmoles of HCl) | moles carbonate | moles bicarbonate | % carbonate | % bicarbonate | Conversion (%) Based on titration curve |
|---|---|---|---|---|---|---|---|---|---|---|
| 1 | 320 | 1 | 2 | -- | -- | -- | -- | -- | -- | -- |
| 2 | 320 | 1 | 4 | 0.70 | 1.52 | 0.70 | 0.12 | 85.40 | 14.30 | 92.00 |
| 3 | 320 | 1 | 4 | 2.30 | 4.90 | 2.30 | 0.30 | 88.50 | 11.50 | 93.90 |
| 4 | 250 | 1 | 4 | 0.62 | 1.68 | 0.62 | 0.44 | 58.50 | 41.50 | 74.00 |
| 5 | 250 | 1 | 4 | 3.10 | 8.40 | 3.10 | 2.20 | 58.50 | 41.50 | 73.80 |
| 6 | 250 | 1 | 2 | -- | -- | -- | -- | -- | -- | -- |
| 7 | 200 | 1 | 2 | -- | -- | -- | -- | -- | -- | -- |
| 8 | 200 | 1 | 4 | 2.10 | 5.80 | 2.10 | 1.60 | 56.80 | 43.20 | 72.40 |
| 9 | 150 | 1 | 2 | -- | -- | -- | -- | -- | -- | -- |
| 10 | 150 | 1 | 4 | 1.40 | 4.40 | 1.40 | 1.60 | 46.70 | 53.30 | 63.60 |
| 11 | 150 | 1 | 8 | 0.40 | 1.40 | 0.40 | 0.60 | 40.00 | 60.00 | 57.10 |

Table 5.24 compares the results of conversion obtained for the pH-conversion equation based on the final pH measurement and the conversion obtained from the titration curves.

**Table 5.24 Experiment conditions and conversion calculated from conversion-pH equation and from titration curves. All the experiments have been cooled down by immersion in a bucket of cool water. The initial concentration of the bicarbonate of all experiments is 1M. The final solution of all experiments is colorless. Set of experiments #2.**

| Run # | Temperature (°C) | $[KHCO3]_o$ | $t_{exposed}$ (h) | pH initial | pH final | Results Conversion (%) Based on pH eq | Conversion (%)Based on titration curve |
|---|---|---|---|---|---|---|---|
| 1 | 320 | 1 | 2 | 8.10 | 10.66 | 91.46 | -- |
| 2 | 320 | 1 | 4 | 8.02 | 12.42 | >100 % | 92.0 |
| 3 | 320 | 1 | 4 | 8.10 | 13.40 | >100 % | 93.9 |
| 4 | 250 | 1 | 4 | 8.05 | 10.01 | 69.14 | 74.0 |
| 5 | 250 | 1 | 4 | 8.24 | 10.06 | 71.5 | 73.8 |
| 6 | 250 | 1 | 2 | | 10.09 | 72.91 | -- |
| 7 | 200 | 1 | 2 | 8.17 | 9.92 | 64.89 | -- |
| 8 | 200 | 1 | 4 | 8.12 | 10.15 | 75.74 | 72.4 |
| 9 | 150 | 1 | 2 | 8.07 | 9.03 | 22.91 | -- |
| 10 | 150 | 1 | 4 | 8.08 | 9.99 | 68.19 | 63.6 |
| 11 | 150 | 1 | 8 | 8.11 | 9.90 | 63.95 | 57.1 |

The difference of the conversion obtained from the conversion-pH equation and the titration curves is between 2.3 and 6.9 % except for runs #2 and #3. Based on the pH equation, the solutions after runs 2 and 3 consist of a mixture carbonate-hydroxide. While based on the titration curves, the solutions consist of a mixture of carbonate-bicarbonate. The sample pHs when the titrations were made (pH≃11 for both experiments) were different from the final pH measured just after the experiment (pH=12.42 for run #2 and pH=13.4 for run #3). This experiment should be reproduced to determine if the storage of the sample changed the final concentration or if the pH reading was not accurate.

In the next chapter, the thermodynamic properties of the bicarbonate decomposition reaction are determined based on the results thermodynamic properties obtained by the titration method as the analysis of the accuracy of both methods - the titration method and the pH-conversion method- made us rely more in the values of conversion calculated with the titration method than the ones obtained with the pH-conversion method. The relative accuracy of both bicarbonate and carbonate concentrations for the pH method ranged from 5 to 51 %, while the relative accuracy of the titration method of the bicarbonate and carbonate concentrations for the titration method ranged from 0.01 to

11.10 % (for the carbonate) and from 0.82 to 11.97 % (for the bicarbonate).Once the thermodynamic properties of the reaction of decomposition of bicarbonate ($2KHCO_3 \leftrightarrow K_2CO_3 + CO_2 + H_2O$ )are calculated from the experimental results, they are finally compared to literature data and the discrepancies are discussed.

# CHAPTER 6. STUDY OF THE CARBONATE/BICARBONATE CHEMISTRY. THERMODYNAMIC PROPERTIES OF THE BICARBONATE DECOMPOSITION REACTION

This chapter is divided in three sections. In the first one, the thermodynamic properties of the bicarbonate decomposition reaction are determined based on the results of conversion obtained by the titration method. The reason of using the titration curve method is because we rely more on the values of conversion calculated with this method than the ones obtained with the pH-conversion method. The thermodynamic properties are obtained from the Van't Hoff plot and then, compared to literature data in the next two sections. In the second section, data of the Gibbs free energy, enthalpy and entropy of the reaction species at standard temperature and at 300°C from two different sources: Craig (1992)[85] (who gives data at standard temperature) and Barner and Scheuerman (1973) [86] (who gives data at standard temperature and at 300 °C) are collected. The thermodynamic data of the reactions is, therefore, calculated from the thermodynamic data of the reaction species and compared to our experimental values. In addition to this, the third section describes an experimental process of the Bureau of Mines (1962) which consists in the absorption of carbon dioxide into potassium carbonate-bicarbonate solutions at 120 °C. The quasi-equilibrium concentrations of the reaction species are given or can be estimated and consequently, the equilibrium constant of the reaction of the absorption of $CO_2$ in carbonate can be calculated . The reaction the Bureau of Mines studies is $K_2CO_3 + CO_2 + H_2O \leftrightarrow 2KHCO_3$ and its equilibrium constant is defined as $K_{eq} = \frac{[KHCO_3]^2}{[K_2CO_3][CO_2]}$. We can relate the Bureau of Mines reaction with the reaction we are interested, the decomposition reaction of bicarbonate into carbonate and $CO_2$. The reaction of interest is given by expression $2KHCO_3 \leftrightarrow K_2CO_3 + CO_2 + H_2O$ and its equilibrium constant ($K_{eq} = \frac{[K_2CO_3][CO_2]}{[KHCO_3]^2}$) is just the inverse of Bureau of Mines reaction. The two experimental data, Bureau of Mines data and our experimental data , are finally compared.

## 6.1 Estimation of the thermodynamic properties with Van't Hoff plot

The thermodynamic properties (enthalpy and entropy) for the reaction $2\ HCO_3^-(aq) \leftrightarrow CO_3^{2-}(aq) + CO_2(aq) + H_2O$ can be extracted with the Van't Hoff plot. The Van't Hoff equation relates the change in temperature (*T*) to the change in the equilibrium constant at zero ionic strength ($K_{eq}^o$) given the standard enthalpy change ($\Delta H$) for the process [87]. The equation is

$$\frac{dlnK_{eq}{}^{o}}{dT} = \frac{\Delta H}{RT^2} \qquad \text{Equation 6.1}$$

If the enthalpy change of reaction is assumed to be constant with temperature, the definite integral of this differential equation between temperatures $T_1$ and $T_2$ is given by

$$ln\left(\frac{K_2}{K_1}\right) = \frac{\Delta H}{R}\left(\frac{1}{T_2} - \frac{1}{T_1}\right) \qquad \text{Equation 6.2}$$

In this equation $K_1$ is the equilibrium constant at zero ionic strength at absolute temperature $T_1$ and $K_2$ is the equilibrium constant at zero ionic strength at absolute temperature $T_2$.From $\Delta G = \Delta H - T\Delta S$ and $\Delta G = -RTlnK_{eq}{}^{o}$, it follows that

$$lnK_{eq}{}^{o} = -\frac{\Delta H}{RT} + \frac{\Delta S}{R} \qquad \text{Equation 6.3}$$

Therefore, a plot of the natural logarithm of the equilibrium constant versus the reciprocal temperature should give a straight line. The slope of the line is equal to minus the standard enthalpy change divided by the gas constant (*-ΔH/R*) and the intercept is equal to the standard entropy change divided by the gas constant (*ΔS/R)*. The Gibbs free energy depends on the temperature and is calculated as $\Delta G = \Delta H - T\Delta S$.

Table 6.1 displays the values of the equilibrium constant of the experiments ($K_{eq}$) , the activity coefficients of carbonate, bicarbonate and $CO_2$ ($\gamma_{CO_3{}^{2-}}$, $\gamma_{HCO_3{}^{-}}$ and$\gamma_{CO_2}$) and the equilibrium constant at zero ionic strength ($K_{eq}{}^{o}$). The equilibrium constant of the experiments ($K_{eq}$) is calculated from the conversion value with equation 5.15, $\mathrm{K_{eq}} = \left(\frac{\text{Conversion KHCO}_3}{2\cdot(1-\text{Conversion KHCO}_3)}\right)^2$.The equilibrium constants are calculated from both values of conversion (%), the one obtained from the pH equation and the one obtained from the titration curve. However, the titration curve values are the ones used in the Van't Hoff plot. The activity coefficients of carbonate, bicarbonate and $CO_2$ ($\gamma_{CO_3{}^{2-}}$, $\gamma_{HCO_3{}^{-}}$ and $\gamma_{CO_2}$) are calculated from Davies equation $\log\gamma = -0.5z^2 f(I)$ (Chapter 3, equation 3.5), where $f(I) = \left(\frac{I^{\frac{1}{2}}}{1+I^{\frac{1}{2}}} - 0.2I\right)\left(\frac{298}{t+273}\right)^{\frac{2}{3}}$ , *b* is a constant ( a typical value of 0.10 is used [71, 80]) and *I* is the ionic strength and is calculated as:

$$I = \frac{1}{2}\left([K^+]1^2 + [HCO_3{}^{-}]1^2 + \left[CO_3{}^{2-}\right]2^2\right)$$

The bicarbonate, carbonate and $K^+$ concentration depend on the initial concentration of bicarbonate and the conversion of bicarbonate and are given by the following expressions: $[K^+] = [KHCO_3]_o$, $[HCO_3^-] = [KHCO_3]_o(1 - conversion)$ and $\left[CO_3^{2-}\right] = \frac{[KHCO_3]_o \cdot conversion}{2}$. The ionic strength in terms of the conversion and initial concentration is therefore

$$I = \frac{1}{2}\left([KHCO_3]_o + [KHCO_3]_o(1 - conversion) + \frac{[KHCO_3]_o \cdot conversion}{2} 4\right)$$

$$= \frac{1}{2}([KHCO_3]_o(2 + conversion)) \qquad \text{Equation 6.4}$$

The activity coefficients, therefore, depend on the conversion and temperature. The dependence is reflected on *I* and *f(I)* equations. The equilibrium constant at zero ionic strength ($K_{eq}{}^o$) (defined in Butler[66]) is calculated from expression

$$K_{eq}{}^o = K_{eq}\frac{\gamma_{CO_2}\gamma_{CO_3{}^{2-}}}{\left(\gamma_{HCO_3{}^-}\right)^2} \qquad \text{Equation 6.5}$$

The activity coefficients , $K_{eq}{}^o$ and the posterior calculation of the thermodynamic properties are solved based on the conversions of the titration curves.

**Table 6.1 Experiment conditions, conversion and equilibrium constant ($K_{eq}$) calculated from conversion-pH equation and from titration curves, ionic strength (*I*), activity coefficients and equilibrium constant at zero ionic strength ($K_{eq}{}^{o}$). Set of experiments #2.**

| Run # | T (°C) | $[KHCO_3]_o$ | t (h) | Conversion (%) Based on pH eq | Conversion (%) Based on titration curve | $K_{eq}$ Based on pH eq | $K_{eq}$ Based on titration curve | I | f(I) | $\log(\gamma_{CO_2})$ | $\log(\gamma_{CO_3^{2-}})$ | $\log(\gamma_{HCO_3^-})$ | $Keq^o$ | $\ln(Keq^o)$ |
|---|---|---|---|---|---|---|---|---|---|---|---|---|---|---|
| 1 | 320 | 1 | 2 | 91.46 | -- | -- | -- | -- | -- | -- | -- | -- | -- | -- |
| 2 | 320 | 1 | 4 | >100 % | 92 | -- | 33.06 | 1.46 | 0.16 | 0.15 | -0.32 | -0.08 | 31.92 | 3.46 |
| 3 | 320 | 1 | 4 | >100 % | 93.9 | -- | 59.24 | 1.47 | 0.16 | 0.15 | -0.32 | -0.08 | 57.41 | 4.05 |
| 4 | 250 | 1 | 4 | 69.14 | 74 | 1.25 | 2.03 | 1.37 | 0.18 | 0.14 | -0.36 | -0.09 | 1.83 | 0.60 |
| 5 | 250 | 1 | 4 | 71.5 | 73.8 | 1.57 | 1.98 | 1.37 | 0.18 | 0.14 | -0.36 | -0.09 | 1.78 | 0.58 |
| 6 | 250 | 1 | 2 | 72.91 | -- | 1.81 | -- | | | | | | | |
| 7 | 200 | 1 | 2 | 64.89 | -- | -- | -- | | | | | | | |
| 8 | 200 | 1 | 4 | 75.74 | 72.4 | 2.44 | 1.72 | 1.36 | 0.20 | 0.14 | -0.39 | -0.10 | 1.50 | 0.41 |
| 9 | 150 | 1 | 2 | 22.91 | -- | -- | -- | | | | | | | |
| 10 | 150 | 1 | 4 | 68.19 | 63.6 | 1.15 | 0.76 | 1.32 | 0.21 | 0.13 | -0.43 | -0.11 | 0.63 | -0.46 |
| 11 | 150 | 1 | 8 | 63.95 | 57.1 | 0.79 | 0.44 | 1.29 | 0.22 | 0.13 | -0.43 | -0.11 | 0.36 | -1.02 |

Observe that the equilibrium constant at zero ionic strength ($Keq^{o}$ )and the equilibrium constant considering the ionic strength (Keq )are similar at high equilibrium constant, i.e. the activity coefficients does not affect the value of the equilibrium constant significantly. The difference is larger at lower values of the equilibrium constant. In all the cases, the equilibrium constant at zero ionic strength ($Keq^{o}$ ) is lower than the equilibrium constant when the ionic strength is considered .The absolute error ranges from 0.08 when the equilibrium constant is 1 approx. to 1.14 when the equilibrium constant is around 30.

Van't Hoff plot shows the natural logarithm of the equilibrium constants from experiments based on the titration curve calculations ($\ln(Keq^{o})$ in Table 6.1) and the inverse of the temperature in Kelvin.

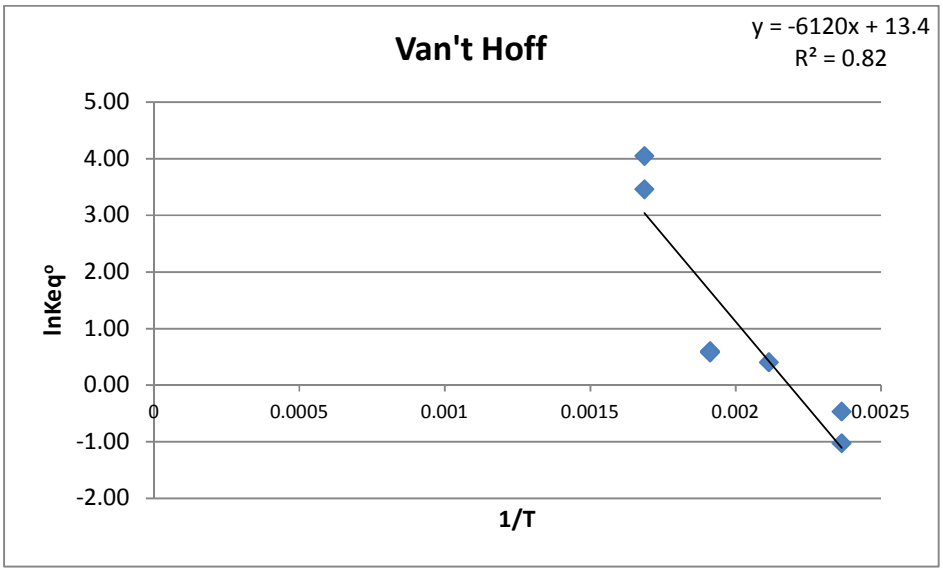


**Figure 6.1 Van't Hoff plot for reaction 2 $HCO_3^-(aq) \leftrightarrow CO_3^{2-}(aq)+CO_2(aq)+H_2O$**

The enthalpy and entropy are obtained from the slope and the y-intercept, $lnK_{eq} = -\frac{\Delta H}{RT} + \frac{\Delta S}{R}$ of the Van't Hoff plot

$$lnK_{eq}{}^{o} = -\frac{6120.}{T} + 13.4 \qquad \text{Equation 6.6}$$

ΔH=6120 K x 8.314 J/mol K=50900 J/mol

ΔS=13.4 x 8.314 J/molK=111. J/mol K

The Gibbs free energy is calculated from the enthalpy and entropy values from equation

$$\Delta G\left(\frac{J}{mol}\right) = \Delta H - T\Delta S = 50900 + 111.T \qquad T \text{ is given in K} \qquad \text{Equation 6.7}$$

## 6.2 Comparison with literature thermodynamic data

### *6.2.1 Craig, N.C. and Barner and Scheuerman*

The thermodynamic values obtained from the Van't Hoff plot are compared to the values calculated from literature data. Barner and Scheuerman [86] and Craig [85] give the values of enthalpy, entropy and Gibbs free energy of the species involved in the reaction of decomposition of bicarbonate, $HCO_3^-(aq) \leftrightarrow CO_3^{2-}(aq)+CO_2(aq)+H_2O$ .At 25°C, the thermodynamic data of the species from two different literature sources are tabulated in tables 6.2 and 6.3

**Table 6.2 Thermodynamic data at 25°C taken from Barner and Scheuerman [86]. Data of the $CO_2$(aq) has been estimated**

| | $OH^-$(aq) | $H_2O$(l) | $CO_2$(g) | $CO_2$(aq) estimated | $CO_3^{2-}$(aq) | $HCO_3^-$(aq) |
|---|---|---|---|---|---|---|
| **$\Delta_f H°$(kcal/mol)** | -55 | -68.3 | -94.1 | | -161.9 | -165.4 |
| **$\Delta_f G°$(kcal/mol)** | -37.6 | -56.7 | -94.3 | -92.29 | -126.2 | -140.3 |
| **$\Delta S°$(cal/molK)** | 2.4 | 16.7 | 51.1 | | -3.6 | 26.8 |
| **$\Delta_f H°$ (kJ/mol)** | -229.9 | -285.494 | -393.338 | | -676.742 | -691.372 |
| **$\Delta_f G°$ (kJ/mol)** | -157.168 | -237.006 | -394.174 | -385.808 | -527.516 | -586.454 |
| **$\Delta S°$ (J/molK)** | 10.032 | 69.806 | 213.598 | | -15.048 | 112.024 |

**Table 6.3 Thermodynamic data at 25°C taken from Craig[85]. Data of the cp° of carbonate and bicarbonate has been estimated**

| | $OH^-$(aq) | $H_2O$(l) | $CO_2$(g) | $CO_2$(aq) | $CO_3^{2-}$(aq) | $HCO_3^-$(aq) |
|---|---|---|---|---|---|---|
| **$\Delta_f H°$(kJ/mol)** | -229.99 | -285.83 | -393.51 | -413.8 | -677.14 | -691.99 |
| **$\Delta_f G°$(kJ/mol)** | -157.24 | -237.13 | -394.36 | -385.98 | -527.81 | -586.77 |
| **$\Delta S°$(J/molK)** | -10.75 | 69.91 | 213.74 | 117.6 | -56.9 | 91.2 |
| **cp°(J/molK)** | -148.5 | 75.29 | 37.11 | | -483.36(estimated) | -94.24(estimated) |

At 300 °C, the thermodynamic data of the species are given by Barner and Scheuerman and are tabulated in table 6.4

**Table 6.4 Thermodynamic data at 300°C taken from Barner and Scheuerman [86]. Data of the $CO_2$ (aq) has been estimated**

| | $OH^-$(aq) | $H_2O$(l) | $CO_2$(g) | $CO_2$(aq) estimated | $CO_3^{2-}$(aq) | $HCO_3^-$(aq) |
|---|---|---|---|---|---|---|
| **$\Delta_f H°_{300°C}$(kcal/mol)** | -68.2 | -65.9 | -94.1 | | -193.7 | -171.6 |
| **$\Delta_f G°_{300°C}$(kcal/mol)** | -17.3 | -46.8 | -94.4 | -86.8 | -82.6 | -114.8 |
| **$\Delta S°_{300°C}$(cal/molK)** | -46.8 | 29.3 | 57.7 | | -11 | -0.1 |
| **$\Delta_f H°_{300°C}$ (kJ/mol)** | -285.076 | -275.462 | -393.338 | | -809.666 | -717.288 |
| **$\Delta_f G°_{300°C}$ (kJ/mol)** | -72.314 | -195.624 | -394.592 | -362.824 | -345.268 | -479.864 |
| **$\Delta S°_{300°C}$ (J/molK)** | -195.624 | 122.474 | 241.186 | | -45.98 | -0.418 |

**Estimation of $CO_2$ (aq) Gibbs free energy for Barner and Scheuerman [86]**

For the $CO_2$ , the Gibbs free energy in aqueous phase infinite dilution is calculated from Henry's law [88]:

$$G_{CO_2}^{\infty,aq}(T) = \Delta_f G_{CO_2}^{ig}(T) + RTln\left(\frac{H_{CO_2,w}}{P^{ref}}\right) \qquad \text{Equation 6.8}$$

Where $G_{CO_2}^{\infty,aq}(T)$ is the mole fraction scale aqueous-phase infinite dilution Gibbs free energy of $CO_2$ at temperature *T*, $\Delta_f G_{CO_2}^{ig}(T)$ is the ideal gas Gibbs free energy of formation of $CO_2$ at temperature *T* , $H_{CO_2,w}$ is the Henry's constant of $CO_2$ in water and $P^{ref}$ is the reference pressure. Based on the work of Versteef and Van Swaaij[89], the Henry's constant is obtained by the following equation

$$H_{CO_2,w}(kPa \cdot m^3 \cdot kmol^{-1}) = 2.8249 \cdot 10^6 \, exp\left(\frac{-2044}{T}\right) \qquad \text{Equation 6.9}$$

Where *T* is the temperature in Kelvin

At T=25°C, $H_{CO_2,w}(kPa \cdot m^3 \cdot kmol^{-1}) = 2.8249 \cdot 10^6 \, exp\left(\frac{-2044}{298}\right) = 2965.9$

$$G_{CO_2}^{\infty,aq}(25°C) = -394.174\frac{kJ}{mol} + 8.314 \cdot 10^{-3}\frac{kJ}{molK}298.15K \; ln\left(\frac{2965.8}{101.325}\right) = -385.81\frac{kJ}{mol}$$

At T=300°C, $H_{CO_2,w}(kPa \cdot m^3 \cdot kmol^{-1}) = 2.8249 \cdot 10^6 \, exp\left(\frac{-2044}{573}\right) = 79761.$

$$G_{CO_2}^{\infty,aq}(300°C) = -394.592\frac{kJ}{mol} + 8.314 \cdot 10^{-3}\frac{kJ}{molK}573.15K \; ln\left(\frac{79761}{101.325}\right) = -362.82 \; kJ/mol$$

At 25°C, the values can be compared with Craig, N.C.[85] and they are similar

- $\Delta_f G°(kJ/mol)_{Craig,}$=-385.95 kJ/mol
- $\Delta_f G°(kJ/mol)_{Barner, et al. estimated}$=-385.81 kJ/mol

**Estimation of heat capacity (cp°) of $CO_3^{2-}$ (aq),$HCO_3^-$ (aq) and $CO_2$(aq) for Craig [85] at 300 °C**

Craig does not give values of the heat capacity (cp°) of $CO_3^{2-}$ (aq),$HCO_3^-$ (aq) and $CO_2$(aq) to estimate the enthalpy and entropy change . An estimation of these values have been made assuming that the heat capacity is a constant between 25 and 300°C, therefore, taking the enthalpy values at 25 and 300°C from Barner et and Scheuerman and applying equation

$$\Delta H_T^o = \Delta H_{298}^o + c_p\,(T - 298) \qquad \text{Equation 6.10}$$

Solving for the heat capacity

$$c_{p,CO_3^{2-}} = \frac{\Delta H^o_{300°C,CO_3^{2-}} - \Delta H^o_{25°C,CO_3^{2-}}}{300°C - 25°C} = \frac{-809.666\frac{kJ}{mol} - (-676.742\frac{kJ}{mol})}{300°C - 25°C}$$

$$= -0.48336\frac{kJ}{molK} = -483.36\frac{J}{molK}$$

$$c_{p,HCO_3^{2-}} = \frac{\Delta H^o_{300°C,HCO_3^{2-}} - \Delta H^o_{25°C,HCO_3^{2-}}}{300°C - 25°C} = \frac{-717.288\frac{kJ}{mol} - (-691.372\frac{kJ}{mol})}{300°C - 25°C}$$

$$= -0.09424\frac{kJ}{molK} = -94.24\frac{J}{molK}$$

$$c_{p,CO_2} = \frac{\Delta H^o_{300°C,CO_2} - \Delta H^o_{25°,CO_2}}{300°C - 25°C}$$

The enthalpy values of the $CO_2$(aq) are not given by Barner and Scheuerman so this value cannot be estimated

**Estimation of the enthalpy, entropy and Gibbs Free energy for reaction 2 $HCO_3^-$(aq)↔$CO_3^{2-}$(aq)+$CO_2$(aq)+$H_2O$ taking Barner and Scheuerman [86] and Craig[85] data**

The final equations to calculate the thermodynamic values would be

**At 25°C**

$$\Delta_r H^o_{25°C} = \Delta_f H^o_{25°C,CO_3^{2-}} + \Delta_f H^o_{25°C,CO_2} - 2\Delta_f H^o_{25°C,HCO_3^-} + \Delta_f H^o_{25°C,H_2O} \qquad \text{Equation 6.11}$$

$$\Delta_r S^o_{25°C} = \Delta S^o_{25°C,CO_3^{2-}} + \Delta S^o_{25°C,CO_2} - 2\Delta S^o_{25°C,HCO_3^-} + \Delta S^o_{25°C,H_2O} \qquad \text{Equation 6.12}$$

$$\Delta_r G^o_{25°C} = \Delta_f G^o_{25°C,CO_3^{2-}} + \Delta_f G^o_{25°C,CO_2} - 2\Delta_f G^o_{25°C,HCO_3^-} + \Delta_f G^o_{25°C,H_2O} \qquad \text{Equation 6.13}$$

**At 300 °C,** Barner and Scheuerman give the values of the entropy and enthalpy of the species at T= 300°C, the equations to calculate them

$$\Delta_r H^o_{300°C} = \Delta H^o_{300°CC,CO_3^{2-}} + \Delta H^o_{300°C,CO_2} - 2\Delta H^o_{300°C,HCO_3^-} + \Delta H^o_{300°C,H_2O} \qquad \text{Equation 6.14}$$

$$\Delta_r S^o_{300°C} = \Delta S^o_{300°C,CO_3^{2-}} + \Delta S^o_{300°C,CO_2} - 2\Delta S^o_{300°C,HCO_3^-} + \Delta S^o_{300°C,H_2O} \qquad \text{Equation 6.15}$$

$$\Delta_r G^o_{300°C} = \Delta G^o_{300°C,CO_3^{2-}} + \Delta G^o_{300°C,CO_2} - 2\Delta G^o_{300°C,HCO_3^-} + \Delta G^o_{300°C,H_2O} \qquad \text{Equation 6.16}$$

Craig does not give the values of the entropy and enthalpy of the species at T= 300°C, so they can be calculated with the entropy and enthalpy values at room temperature and the heat capacities using equations.

$$\Delta_r S_T^o = \Delta_r S_{298}^o + \int_{298}^{T} \frac{\Delta c_p}{T}\, dT \qquad \text{Equation 6.17}$$

$$\Delta_r H_T^o = \Delta_r H_{298}^o + \int_{298}^{T} \Delta c_p\, dT \qquad \text{Equation 6.18}$$

$\Delta c_p = \sum \nu_i c_p(products) - \sum \nu_i c_p(reactants)$ ,i. $c_p = cp^o_{298,CO_3^{2-}} + cp^o_{298,CO_{2(aq)}} - 2cp^o_{298,HCO_3^-}$ and T is the temperature in K. The $cp^o_{298,CO_{2(aq)}}$ is not given and cannot be estimated due to the lack of data. Table 6.5 and 6.6 give the thermodynamic values of the decomposition reaction of bicarbonate calculated from the Van't Hoff plot and from the values of Craig and Barner and Scheuerman (tables 6.2 to 6.4)

**Table 6.5 Comparison of the thermodynamic data at 25°C of our Van't Hoff plot with Barner and Scheuerman [86]and Craig [86]. Barner and Scheuerman is calculated with the estimated value of $CO_2$(aq)**

| **2 $HCO_3^-$(aq)↔$CO_3^{2-}$(aq)+$CO_2$(aq)+$H_2O$** | | | |
|---|---|---|---|
| | **Van't Hoff plot T=25°C** | **Literature values T=25°C Barner et al. [86] (estimated)** | **Literature values T=25°C Craig [85]** |
| **$\Delta_r$G (kJ/mol)** | 17.8 | 22.578 | 22.62 |
| **$\Delta_r$H (kJ/mol)** | 50.9 | | 7.21 |
| **$\Delta_r$S (J/K· mol)** | 111. | | -51.79 |

**Table 6.6 Comparison of the thermodynamic data at 300°C of our Van't Hoff plot with Barner and Scheuerman [86]. Barner and Scheuerman is calculated with the estimated value of $CO_2$(aq)**

| 2 $HCO_3^-$↔$CO_3^{2-}$+$CO_2$+$H_2O$ | | |
|---|---|---|
| | **Van't Hoff plot T=300°C** | **Literature values T=300°C Barner et al. [11]** |
| **$\Delta_r G_{300°C}$ (kJ/mol)** | -12.8 | 56.012 |
| **$\Delta_r H_{300°C}$ (kJ/mol)** | 50.9 | |
| **$\Delta_r$S (J/K· mol)** | 111. | |

While the Gibbs free energy at 25 °C present a similar behavior in the three cases, with differences of 21 % from our values and the literature values; the enthalpy, entropy at 25 °C and Gibbs free energy at 300

°C results present large discrepancies. According to our Van't Hoff plot, at 25 °C the reaction is more endothermic. Our enthalpy ($\Delta_r H$=50.9 kJ/mol) is seven times higher than Craig's data ($\Delta_r H$ =7.21 kJ/mol). The entropy of the reaction present the opposite behavior, according to Craig's data the entropy decreases ($\Delta_r S$=-51.79 J/mol K) while our Van't Hoff plot indicates that it increases ($\Delta_r S$ =111. J/mol K). At 300°C, the difference of the Gibbs free energy obtained from the Van't Hoff plot and Barner et al. is also large. Based on Barner and Scheuerman values, the reaction is not spontaneous ($\Delta G_{300°C}$=56.012 kJ/mol), however, the Van't Hoff plot shows a spontaneous behavior ($\Delta G_{300°C}$=-12.8 kJ/mol). The experiments support our findings as we observed high conversions at temperatures close to 300 °C. The value of the Gibbs free energy of Barner and Scheuerman, nevertheless, has been estimated using Henry's law constant due to the lack of $CO_2$(aq) data and might not be accurate.

Craig (pp. 105-106) analyzes the effect of the Gibbs free energy in terms of enthalpy and entropy. Craig show that there are four possible sign combinations of $\Delta_r H$ and $\Delta_r S$.

| **$\Delta_r H$** | **$\Delta_r S$** | **$\Delta_r G$** |
|---|---|---|
| - | + | -at all T |
| + | - | + at all T |
| - | - | - at low T, + at high T |
| + | + | + at high T,- at low T |

The reactions that switch favorable direction with temperature change are the ones which the signs of $\Delta_r H$ and $\Delta_r S$ are the same. Those reactions with opposite signs are spontaneous in only one direction. It has been observed from our experiments and also by previous researchers the switch in the spontaneity of the reaction which supports the sign of our entropy value. Butler [66], for example, describes the reaction $Na_2CO_3+CO_2+H_2O\leftrightarrow 2NaHCO_3$ as reversible, where lower temperatures and higher $CO_2$ pressures favor the right direction and higher temperatures and lower $CO_2$ pressures favor the left direction.Butler also says that the $K_2CO_3$ presents the same behavior. The Bureau of Mines [67] describes that temperatures of about 100 °F (38°C approx.) favor nearly complete conversion of carbonate to bicarbonate in $K_2CO_3+CO_2+H_2O\leftrightarrow 2KHCO_3$ reaction, while boiling temperature shift the equilibrium to the left. Craig also analyzes the entropy term in a molecular level; he states that a negative value of the $\Delta_r S$ arises from the "freezing" of water molecules around the ions due to ion-dipole attractions. The dipolar water molecules orient themselves in an energetically favorable way around the positive and negative ions. The decreased mobility of these water molecules lowers their entropy because vibrational degrees of freedom take the place of translational and rotational ones. In the reaction $2\ HCO_3^-(aq)\leftrightarrow CO_3^{2-}(aq)+CO_2(aq)+H_2O$, two initial single charged ions go to one double

charged, no clear answer can be made by looking at the reaction but according to the previous reasoning, the degrees of freedom of the water molecules seems to increase and therefore, a positive value of the entropy looks more reasonable. Also the number of molecules increase in the reaction, two molecules of reactants lead to three molecules. This behavior is usually associated to an increase in the entropy of the reaction. If $CO_2$ is a gas , then the increase in entropy is very large.

### *6.2.2 Report Bureau of Mines*

The Bureau of Mines in the Bulletin 597[67] "Pilot-Plant studies of the hot carbonate process for removing carbon dioxide and hydrogen sulfide" develops a purification process for treating synthesis gas by absorption with a hot solution of potassium carbonate. The impure synthesis gas exits from the absorber at elevated pressure and temperature. The purification process removes carbon dioxide and hydrogen sulfide with a hot, concentrated alkaline solution under pressure. In this system the driving force between the partial pressure of carbon dioxide in the gas and its equilibrium pressure above the solution was believed sufficient for absorption to occur without the conventional lowering of temperature. Contrary to usual practice, absorption would then be possible at about the same temperature as regeneration.

The reaction that occurs during absorption is $K_2CO_3 + CO_2 + H_2O \leftrightarrow 2KHCO_3$. Temperatures of about 100 °F, favor nearly complete conversion of carbonate to bicarbonate, while boiling temperature shift equilibrium to the left. However, at high-partial pressures of carbon dioxide such as exist in impure synthesis gas at 20 to 30 atmospheres, there was a strong possibility that considerable formation of bicarbonate could occur at elevated temperatures. We analyzed their published results and calculated equilibrium constant and Gibbs free energy based on their composition data to further validate our model.

Pilot-plant studies are described. The initial work was done in a small pilot plant using inert gas containing carbon dioxide and nitrogen. The flow sheet diagram is shown in figure 6.2

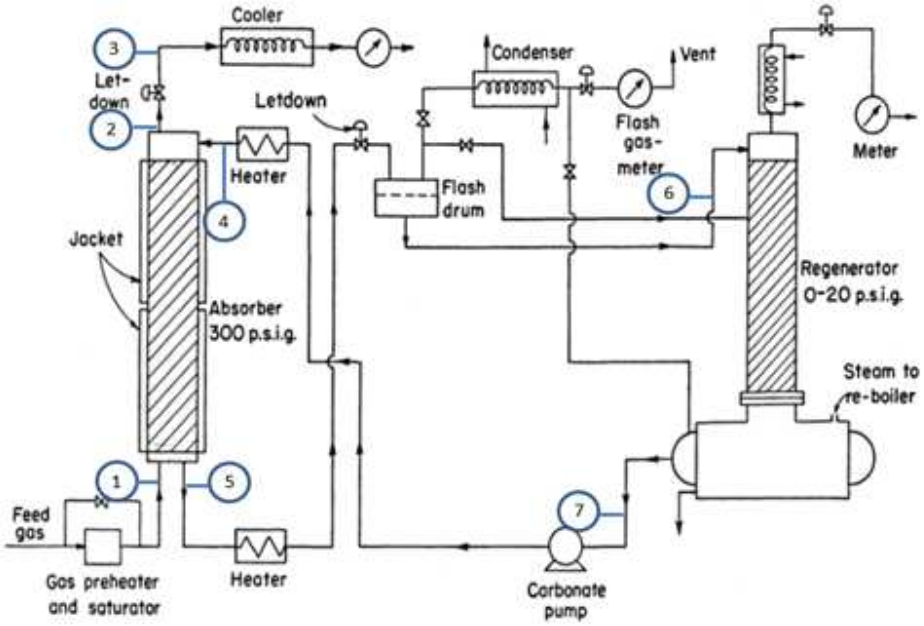


**Figure 6.2 Flow sheet for Hot-Carbonate Scrubbing system**

A compressed gas mixture of nitrogen and carbon dioxide at 300 p.s.i.g was fed into the bottom of the absorber. The gas either entered at ambient temperature or was passed through a heated vessel containing water at the system pressure so that the gas could be heated and saturated with water vapor at the temperature of the entering carbonate solution. For hot absorption the regenerated carbonate flowed through a preheater before entering the top of the absorber.

The scrubbed gas flowing from the top of the absorber was reduced to atmospheric pressure, metered and sampled. Since the absorber was kept in adiabatic condition, when the feed gas was preheated, the spent solution leaving the absorber was hotter than the entering solution by an amount equivalent to the exothermic heat of absorption. The hot, spent carbonate was depressurized in a flash drum, where part of the carbon dioxide and some steam were flashed-usually cooling the solution just below the boiling temperature in the regenerator reboiler.

Sample points were provided to obtain samples of the regenerated and spent carbonate solutions, as well as samples of the feed, scrubbed, regenerated and flashed gases. Gas samples were analyzed for carbon dioxide using an Orsat. The liquid samples were taken at system temperature in a small pressure cylinder half filled with distilled water so that no precipitation occurred on cooling to room temperature. Carbonate and bicarbonate content of these liquids was determined by acid titration, measuring the volume of carbon dioxide liberated on acidification.

Two series of tests were made, the first one uses a gas containing 26 to 30 percent of carbon dioxide, the second using gas containing 9 to 11 percent carbon dioxide. The rest of the gas was principally nitrogen. Concentrations are expressed as percent equivalent concentration of potassium carbonate, which is defined as the concentration referring to a solution of zero conversion with only potassium carbonate and water present. The first series of experimental data are analyzed in this thesis. A feed gas flow of about 500 standard (32 °F, 14.7 psi, dry gas) cubic feet per hour was used in these tests. Cold absorption was carried out in run 5A. The concentration of carbonate (13 percent) is restricted at this temperature because of the limited solubility of potassium bicarbonate. Hot carbonate absorption was investigated in the remaining experiments.

Table 6.7 shows the data taken from the Bulletin. To prove the consistency of the data, we decided to calculate the $CO_2$ absorbed from the data given table 6.7. As the gas and liquid compositions are given, we did calculations based on both liquid and gas data and we compared our results to the Bulletin 597 results in tables 6.8 and 6.9.

**Table 6.7 Liquid and gas compositions for Hot-Carbonate Scrubbing system Data taken from Bureau of Mines in the Bulletin 597**

| Row# | | 6A | 6B | 7A | 7B | 8 | 8A | 8B |
|---|---|---|---|---|---|---|---|---|
| | | 40 pct $K_2CO_3$ hot | 40 pct $K_2CO_3$ hot | 40 pct $K_2CO_3$ hot | 40 pct $K_2CO_3$ hot | 40 pct $K_2CO_3$ hot | 40 pct $K_2CO_3$ hot | 40 pct $K_2CO_3$ hot |
| 1 | **T bottom liquid(°F)** | 244 | 259 | 246 | 267 | 241 | 262 | 264 |
| | **Absorber** | | | | | | | |
| 2 | Feed gas rate...std.c.f/hr | 494.3 | 512.6 | 486.4 | 491.7 | 473.2 | 501.6 | 500.1 |
| | **Flash drum** | | | | | | | |
| 3 | Flashed gas...std.c.f/hr | | | 29.8 | 27 | | | |
| | **Carbon dioxide concentrations(%)** | | | | | | | |
| 4 | Feed gas to absorber | 27.7 | 30.3 | 28.1 | 28 | 27.5 | 28.9 | 28.3 |
| 5 | Scrubbed gas from absorber | 16.3 | 20.3 | 12.9 | 12.8 | 15.5 | 16.8 | 12.5 |
| 6 | Regenerated gas | 95.9 | 98.5 | 96.7 | 96.7 | 98.9 | 98.7 | 96.9 |
| 7 | Flashed gas | | | 93.7 | 93.7 | | | |
| 8 | Volume carbon dioxide scrubbed std.c.f/hr | 61.1 | 74.1 | 80.3 | 86 | 72.4 | 65.5 | 82.1 |
| 9 | Standar cubic feet per hour of carbon dioxide absorbed per gallon | 2.53 | 2.9 | 2.67 | 2.87 | 2.89 | 2.98 | 3.13 |
| | **Liquid compositions** | | | | | | | |
| 10 | Percent equivalent $K_2CO_3$ | 36.2 | 38.9 | 40.5 | | 38.7 | 38.4 | 35.8 |
| 11 | Fraction conv.regenerated | 0.32 | 0.325 | 0.3 | | 0.36 | 0.3 | 0.3 |
| 12 | Fraction conv.spent | 0.56 | 0.57 | 0.51 | | | 0.56 | 0.61 |
| 13 | Carbon dioxide absorbed from gas….lb.moles/hr [1] | 0.179 | 0.207 | 0.223 | 0.239 | 0.202 | 0.183 | 0.228 |
| 14 | Carbon dioxide picked up by liquid….lb.moles/hr [1] | 0.179 | 0.201 | 0.214 | | | 0.186 | 0.239 |

Table 6.8 shows the results of the $CO_2$ measured using the gas composition data and table 6.9 uses the liquid composition data.

**Table 6.8 Gas composition data. The numbers in brackets represent the position in the flow sheet for Hot-Carbonate Scrubbing system**

| Row # | | 6A | 6B | 7A | 7B | 8 | 8A | 8B |
|---|---|---|---|---|---|---|---|---|
| 1 | **Feed gas rate…moles/hr (1)[2]** | 625.26 | 648.41 | 615.27 | 621.97 | 598.57 | 634.50 | 632.60 |
| 2 | **$CO_2$ feed gas to absorber…moles/hr (1)** | 173.20 | 196.47 | 172.89 | 174.15 | 164.61 | 183.37 | 179.03 |
| 3 | **$N_2$ feed gas to absorber…moles/hr (1)** | 452.06 | 451.94 | 442.38 | 447.82 | 433.96 | 451.13 | 453.57 |
| 4 | **$N_2$ scrubbed gas from absorber…moles/hr(2,3)** | 452.06 | 451.94 | 442.38 | 447.82 | 433.96 | 451.13 | 453.57 |
| 5 | **$CO_2$ scrubbed gas from absorber…moles/hr(2,3)** | 88.04 | 115.11 | 65.52 | 65.74 | 79.60 | 91.09 | 64.80 |
| 6 | **$CO_2$ scrubbed calculated…moles/hr(2,3)** | **85.16** | **81.36** | **107.37** | **108.42** | **85.00** | **92.28** | **114.23** |
| 7 | **$CO_2$ scrubbed …moles/hr(2,3) (Value converted from data: Row 7, Table 6.7)** | **77.29** | **93.73** | **101.57** | **108.79** | **91.58** | **82.85** | **103.85** |
| 8 | **$CO_2$ scrubbed …moles/hr(2,3) (Value converted from data: Row 12, Table 6.7)** | **81.27** | **93.98** | **101.24** | **108.51** | **91.71** | **83.08** | **103.51** |

**Table 6.9 Liquid composition data. The numbers into brackets represent the position in the flow sheet for Hot-Carbonate Scrubbing system**

| Row # | | 6A | 6B | 7A | 7B | 8 | 8A | 8B |
|---|---|---|---|---|---|---|---|---|
| 1 | **gal/h (4,7)** | 24.15 | 25.55 | 30.07 | 29.97 | 25.05 | 21.98 | 26.23 |
| 2 | **moles/hr $K_2CO_3$ equivalent/h (4,7)** | 376.33 | 446.77 | 562.22 | | 434.36 | 376.30 | 401.70 |
| 3 | **moles/hr $K_2CO_3$ regenerated (4,7)** | 255.90 | 301.57 | 393.55 | | 277.99 | 263.41 | 281.19 |
| 4 | **moles/hr $K_2CO_3$ spent(5)** | 165.59 | 192.11 | 275.49 | | | 165.57 | 156.66 |
| 5 | **moles/hr $CO_2$ reacted** | **90.32** | **109.46** | **118.07** | | | **97.84** | **124.53** |
| 6 | **moles/hr $CO_2$ (Value converted from data: Row 13, Table 6.7)** | **81.27** | **91.25** | **97.16** | | | **84.44** | **108.51** |

[1] lb.moles/hr is defined as the number of atoms in 12 lb of $^{12}C$. One lb-mol is equal to 453.59237 mol [67]

[2] moles/h refers to g.moles/hr

Based on figure 6.2, the following relations can be established:

$\dot{N}_{K2CO3,4} = \dot{N}_{K2CO3,7}$

$\dot{N}_{K2CO3,5} = \dot{N}_{K2CO3,6}$

$\dot{N}_{CO2,1} - \dot{N}_{CO2,2} = \dot{N}_{K2CO3,4} - \dot{N}_{K2CO3,5}$ as $K_2CO_3+CO_2+H_2O \rightarrow 2KHCO_3$

The sub-index represents the position in the flow sheet for Hot-Carbonate Scrubbing system (figure 6.2). The following equations show the data of tables 6.8 and 6.9 step by step.

**Gas composition Data (Table 6.8)**

Table 6.8 shows the gas feed rate in the absorber , the $CO_2$ and $N_2$ content at the entrance of the absorber (position 1 in figure 6.2) and exit of the absorber (position 2 in figure 6.2). The $CO_2$ absorbed is then calculated from the difference between the $CO_2$ entering and exiting the absorber.

Row #1: The feed gas rate (position 1 in figure 6.2) is given by the Bureau of Mines (Row #2 in table 6.7). The Bureau of Mines gives the feed gas rate in std.c.f/h (standard (32 °F, 14.7 psi, dry gas ) cubic feet per hour) and we converted from std.c.f/h to moles /h

$$Row\ \#1: \quad \dot{N}_1 = Feed\ gas\ rate\left(\frac{moles}{h}\right) = Feed\ gas\ rate\left(\frac{std.c.f}{h}\right)\frac{28.317\frac{L}{c.f}\,1atm}{0.082\frac{atmL}{molK}\,273K} \qquad \text{Equation 6.19}$$

Row #2 and #3: The moles /hr of $CO_2$ $\left(\dot{N}_{CO_2,1}\right)$and $N_2$ $(\dot{N}_{N_2,1})$in the feed gas (position 1 in figure 6.2) are calculated from the feed gas rate in moles/hr $(\dot{N}_1)$ and the $\%CO_{2,feed\ gas}$ given by the Bureau of Mines (Row #4 Table 6.7). The percentage of $N_2$ in the feed gas ( $\%N_{2,feed\ gas}$)

$$Row\ \#2: \quad \dot{N}_{CO_2,1} = CO_{2,feed\ gas}\left(\frac{moles}{h}\right) = Feed\ gas\ rate\left(\frac{moles}{h}\right)\%CO_{2,feed\ gas}/100 \qquad \text{Equation 6.20}$$

$$Row\ \#3: \quad \dot{N}_{N_2,1} = N_{2,feed\ gas}\left(\frac{moles}{h}\right) = Feed\ gas\ rate\left(\frac{moles}{h}\right)\%N_{2,feed\ gas}$$

$$= Feed\ gas\ rate\left(\frac{moles}{h}\right)\left(1 - \%\frac{CO_{2,feed\ gas}}{100}\right) \qquad \text{Equation 6.21}$$

Row #4 and #5: The moles /hr of $CO_2$ and $N_2$ in the scrubbed gas (position 2 in figure 6.2) is given by

$$Row\ \#4: \quad \dot{N}_{N_2,2} = N_{2,scrubbed\ gas}\left(\frac{moles}{h}\right) = N_{2,feed\ gas}\left(\frac{moles}{h}\right) \qquad \text{Equation 6.22}$$

$$Row\ \#5: \quad \dot{N}_{CO_2,2} = CO_{2,scrubbed\ gas}\left(\frac{moles}{h}\right) = \frac{\%CO_{2,scrubbed\ gas}}{\%N_{2,scrubbed\ gas}} \cdot N_{2,scrubbed\ gas}\left(\frac{moles}{h}\right)$$

$$= \frac{\%CO_{2,scrubbed\ gas}}{100 - \%CO_{2,scrubbed\ gas}} \cdot N_{2,scrubbed\ gas}\left(\frac{moles}{h}\right) \qquad \text{Equation 6.23}$$

Rows #6, #7 and #8: Rows 6, 7 and 8 give the moles /hr of $CO_2$ absorbed calculated from different data. Row #6 is calculated as the difference between the moles/hr of $CO_2$ entering the absorber (Row #2 in table 6.8) and the moles/hr of $CO_2$ exiting the absorber (Row #5 in table 6.8). Row #7 gives the moles /hr of $CO_2$ absorbed calculated from data $Volume\ carbon\ dioxide\ scrubbed\left(\frac{std.c.f}{h}\right)$ in table 6.7 and converting the units to moles/hr. Finally, row #8 gives the moles /hr of $CO_2$ absorbed calculated from data $Carbon\ dioxide\ absorbed\ from\ gas\left(\frac{lb.moles}{h}\right)$ in table 6.7 and converting the units to moles/hr. The three values should be the same

$$Row\ \#6: \quad CO_{2,scrubbed,calculated}\left(\frac{moles}{h}\right)$$

$$= CO_{2,feed\ gas}\left(\frac{moles}{h}\right) - CO_{2,scrubbed\ gas}\left(\frac{moles}{h}\right) \qquad \text{Equation 6.24}$$

$$Row\ \#7: \quad CO_{2,scrubbed,calculated}\left(\frac{moles}{h}\right)$$

$$= Volume\ carbon\ dioxide\ scrubbed\left(\frac{std.c.f}{h}\right)\frac{28.317\frac{L}{c.f}1atm}{0.082\frac{atmL}{molK}273K} \qquad \text{Equation 6.25}$$

$$Row\ \#8: \quad CO_{2,scrubbed,\text{from data: Carbon dioxide absorbed from gas}}\left(\frac{moles}{h}\right)$$

$$= Carbon\ dioxide\ absorbed\ from\ gas\left(\frac{lb.moles}{h}\right)\frac{454\ gmole}{lbmole} \qquad \text{Equation 6.26}$$

Both, row #7 and #8 shouldn't differ because both values of $CO_{2,scrubbed,\text{from data}}$ given in table 6.7 by the Bureau of Mines should be merely a conversion of volume to mole. However, the values are tabulated to check it. The $CO_2$ scrubbed calculated and the $CO_2$ scrubbed taken from the data present a small difference but not significant. And this difference does not show a trend.

**Liquid composition data (Table 6.9)**

Table 6.9 shows the liquid flow rate in the absorber , the potassium carbonate content at the entrance of the absorber (position 4 in figure 6.2) and exit of the absorber (position 5 in figure 6.2). The $CO_2$ absorbed is then calculated considering that the $CO_2$ is absorbed by reaction $K_2CO_3 + CO_2 + H_2O \leftrightarrow 2KHCO_3$. The solution entering the absorber is also called the regenerated solution and the solution exiting the absorber is also called the spent solution.

Row #1: The gallons per hour of solution entering the absorber (position 4 in figure 6.2) are obtained from data given by the Bureau of Mines and tabulated in rows #8 and #9 of table 6.7. Row #8 of table 6.7 gives the 'Volume carbon dioxide scrubbed in std.c. f/hr ' and row #9 of table 6.7 gives the 'Standard cubic feet per hour of carbon dioxide absorbed per gallon'. By dividing these two values, we calculate the volume of liquid solution in gal/hr

$$Row\ \#1: \quad \dot{V}_4 = \frac{gal}{hr} = \frac{Volume\ carbon\ dioxide\ scrubbed\ \frac{std.c.f}{hr}}{Standard\ cubic\ feet\ per\ hour\ of\ carbon\ dioxide\ absorbed\ per\ gallon} \quad \text{Equation 6.27}$$

Row #2: The equivalent moles $K_2CO_3$ per hour in the liquid solution at the entrance of the absorber (position 4 in figure 6.2) is calculated from the *percent equivalent of potassium carbonate* given by the Bureau of Mines (Row #10 in table 6.7). The *percent equivalent of potassium carbonate* is defined as the concentration in percentage of mass referring to a solution of zero conversion with only potassium carbonate and water present. Consequently, the equivalent moles $K_2CO_3$ per hour is defined as the concentration in moles/hr of a solution of zero conversion with only potassium carbonate and water present.

$$Row\ \#2: \quad \dot{N}_{K2CO3,eq,4} = \frac{moles\ K_2CO_3\ eq}{h}$$
$$= \frac{percent\ equivalent\ K_2CO_3}{percent\ H_2O} \cdot \dot{V}_4\left(\frac{gal}{hr}\right) \cdot \frac{1mol}{138\ g\ K_2CO_3} \cdot \frac{1000\ g\ H_2O}{1L} \cdot \frac{3.79\ L}{1\ gal} \quad \text{Equation 6.28}$$

Row #3: The molar flow of carbonate entering the absorber (position 4 in figure 6.2), i.e. moles $K_2CO_3$ regenerated/h, is given by the equivalent moles $K_2CO_3$ per hour in the regenerated solution and the fractional conversion in the regenerated solution given in row #11 of table 6.7. The fraction conversion is the fraction of $K_2CO_3$ converted to $KHCO_3$.

$$Row\ \#3: \quad \dot{N}_{K_2CO_3,4} = \frac{moles\ K_2CO_3\ regenerated}{h}$$
$$= \frac{moles\ K_2CO_3\ eq}{h}(1 - Fraction\ conv.regenerated) \quad \text{Equation 6.29}$$

Row #4: The molar flow of carbonate at the exit of the absorber (position 5 in figure 6.2), i.e. moles $K_2CO_3$ spent/h, is given by the equivalent moles $K_2CO_3$ per hour in the regenerated solution and the fractional conversion in the spent solution given in row #12 of table 6.7

$$Row\ \#4: \quad \dot{N}_{K_2CO_3,5} = \frac{moles\ K_2CO_3\ spent}{h} = \frac{moles\ K_2CO_3\ eq}{h}(1 - Fraction\ conv.spent) \quad \text{Equation 6.30}$$

Row #5: The molar flow of $CO_2$ reacted are calculated as the difference of the molar flow of carbonate in the regenerated and spent solutions

$$Row\ \#5: \quad \frac{moles\ CO_2\ \ reacted}{h} = \frac{moles\ K_2CO_3\ regenerated}{h} - \frac{moles\ K_2CO_3\ \ spent}{h} \qquad \text{Equation 6.31}$$

Row #6: The molar flow of $CO_2$ reacted is calculated with data *Carbon dioxide picked up by liquid* given by the Bureau of Mines in lb.moles/hr (Row 14 in table 6.7) and converting the units to moles/hr.

$$Row\ \#6: \quad \frac{moles\ CO_2\ \ reacted}{h} = Carbon\ dioxide\ picked\ up\ by\ liquid \left(\frac{lb.moles}{h}\right) \frac{454\ gmole}{lbmole} \qquad \text{Equation 6.32}$$

If we compare row #5 and row #6, there is a difference in the moles of $CO_2$/hr between 9 to 20 moles but we could not find any trend that explains this difference.

Calculations of run 8A are displayed in the following equations step by step, the rest of the runs are similarly calculated

- **For the gas composition data**

Row #1: Feed gas rate (moles /h)

$$Row\ \#1: \quad \dot{N}_1 = Feed\ gas\ rate\ \left(\frac{moles}{h}\right) = 501.6 \frac{std.c.f}{h} \frac{28.317 \frac{L}{c.f} 1atm}{0.082 \frac{atmL}{molK} 273K} = 634.50 \frac{moles}{h}$$

Rows #2 and #3: Moles /hr of $CO_2$ and $N_2$ in the feed gas

$$Row\ \#2: \quad \dot{N}_{CO_2,1} = CO_{2,feed\ gas} \left(\frac{moles}{h}\right) = 634.50 \frac{moles}{h} \cdot \frac{28.9}{100} = 183.37 \frac{moles}{h}$$

$$Row\ \#3: \quad \dot{N}_{N_2,1} = N_{2,feed\ gas} \left(\frac{moles}{h}\right) = 634.50 \frac{moles}{h} \left(1 - \frac{28.9}{100}\right) = 451.13 \frac{moles}{h}$$

Rows #4 and #5: Moles /hr of $CO_2$ and $N_2$ in the scrubbed gas:

$$Row\ \#4: \quad \dot{N}_{N_2,2} = N_{2,scrubbed\ gas} \left(\frac{moles}{h}\right) = N_{2,feed\ gas} \left(\frac{moles}{h}\right) = 451.13 \frac{moles}{h}$$

$$Row\ \#5: \quad \dot{N}_{CO_2,2} = CO_{2,scrubbed\ gas} \left(\frac{moles}{h}\right) = \frac{16.8}{100 - 16.8} \cdot 451.13 \frac{moles}{h} = 91.09 \frac{moles}{h}$$

Rows #6, #7 and #8: Concerning the moles /hr of $CO_2$ scrubbed , there are three values: the first one calculated from the equations above and the other two taken from table 6.7 and converting the units.

$$Row\ \#6: \quad CO_{2,scrubbed,calculated} \left(\frac{moles}{h}\right) = CO_{2,feed\ gas} \left(\frac{moles}{h}\right) - CO_{2,scrubbed\ gas} \left(\frac{moles}{h}\right)$$

$$= 183.37 \frac{moles}{h} - 91.09 \frac{moles}{h} = 92.28 \frac{moles}{h}$$

$$Row\ \#7: \quad CO_{2,scrubbed,\text{from data: Volume CO2 scrubbed}} \left(\frac{moles}{h}\right) = 65.5 \frac{std.c.f}{h} \frac{28.317 \frac{L}{c.f} 1atm}{0.082 \frac{atmL}{molK} 273K}$$

$$= 82.85 \frac{moles}{h}$$

$$Row\ \#8: \quad CO_{2,scrubbed,\text{from data: Carbon dioxide absorbed from gas}}\left(\frac{moles}{h}\right) = 0.183\frac{lb.moles}{h}\frac{454\ gmole}{lbmole}$$

$$= 83.08\frac{moles}{h}$$

- **For the liquid composition data**

Row #1: The gallons per hour of solution entering the absorber

$$Row\ \#1: \quad \dot{V}_4 = \frac{gal}{hr} = \frac{65.5\ CO_2\ std.c.f/hr}{2.98\ CO_2\ std.c.f/gal} = 21.98\frac{gal}{hr}$$

Row #2: The equivalent moles $K_2CO_3$ per hour

$$Row\ \#2: \quad \dot{N}_{K_2CO_3,eq,4} = \frac{\text{moles } K_2CO_3 \text{ eq}}{\text{h}}$$

$$= \frac{38.4 \text{ g } K_2CO_3}{(100-38.4)\text{g } H_2O}21.98\ \frac{gal}{hr}\frac{1mol}{138\ g\ K_2CO_3}\frac{1000\ g\ H_2O}{1L}\frac{3.79\ L}{1\ gal}$$

$$= 376.30\ \frac{\text{moles } K_2CO_3 \text{ eq}}{\text{h}}$$

Row #3: Moles $K_2CO_3$ regenerated/h

$$Row\ \#3: \quad \dot{N}_{K_2CO_3,4} = \frac{\text{moles } K_2CO_3 \text{ regenerated}}{\text{h}} = 376.30\frac{\text{moles } K_2CO_3 \text{ eq}}{\text{h}}(1-0.3)$$

$$= 281.19\frac{\text{moles } K_2CO_3 \text{ regenerated}}{\text{h}}$$

Row #4: Moles $K_2CO_3$ spent/h

$$Row\ \#4: \quad \dot{N}_{K_2CO_3,5} = \frac{\text{moles } K_2CO_3 \text{ spent}}{\text{h}} = 376.30\frac{\text{moles } K_2CO_3 \text{ eq}}{\text{h}}(1-0.56)$$

$$= 156.66\frac{\text{moles } K_2CO_3 \text{ spent}}{\text{h}}$$

Row #5: Moles $CO_2$ reacted /h

$$Row\ \#5: \quad \frac{\text{moles } CO_2 \text{ reacted}}{\text{h}} = 281.19\frac{\text{moles } K_2CO_3 \text{ regenerated}}{\text{h}} - 156.66\frac{\text{moles } K_2CO_3 \text{ spent}}{\text{h}}$$

$$= 97.84\frac{\text{moles } CO_2 \text{ reacted}}{\text{h}}$$

Row #6: The molar flow of $CO_2$ reacted calculated with data Row 13 in table 6.7 and converting the units to moles/hr.

$$Row\ \#6: \quad \frac{moles\ CO_2\ \ reacted}{h} = 0.186\frac{lb.moles}{h}\frac{454\ gmole}{lbmole} = 84.44\frac{moles\ CO_2\ \ reacted}{h}$$

**Calculation of the equilibrium constant of reaction $2KHCO_3 \leftrightarrow K_2CO_3 + CO_2 + H_2O$ based on Bureau of Mines data**

Equation 6.33 gives the expression of the equilibrium constant

$$Keq = \frac{[HCO_3^-]^2}{[CO_3^{2-}][CO_2(aq)]} \text{ or } Keq = \frac{\dot{N}^2_{HCO_3^-}}{\dot{N}_{CO_3^{2-}}\dot{N}_{CO_2(aq)}} \qquad \text{Equation 6.33}$$

To calculate the equilibrium constant of reaction is $K_2CO_3 + CO_2 + H_2O \leftrightarrow 2KHCO_3$, we need to know the equilibrium compositions of the bicarbonate, carbonate and carbon dioxide in the spent solution as we assumed that the spent solution and the scrubbed gas is in equilibrium. Table 6.11 displays the molar flows of the species at the spent solution. The following equations show the procedure to calculate all the data tabulated in table 6.11.

Row #1 and #2: Row #1 gives the temperature in the absorber in °F. This data has been taken from the Bureau of Mines (Row #1 in table 6.7). The temperature in °F is converted into K and the temperature in K is shown in row #2.

Row #3 and #4: Row #3 gives the equivalent moles $K_2CO_3$ per hour, which is defined as the concentration in moles/hr of a solution of zero conversion with only potassium carbonate and water present (Row #2 in table 6.9). Row #4 gives the molar flow of carbonate in the spent solution (Row # 4 in table 6.9) calculated from equation 6.30, $\dot{N}_{K_2CO_3,5} = \frac{moles\ K_2CO_3\ spent}{h} = \frac{moles\ K_2CO_3\ eq}{h}(1 - Fraction\ conv.spent)$.

Row #5: Row #5 shows the bicarbonate flows in the spent solution calculated from the carbonate flow at zero conversion (Row 2 in table 6.9) and the carbonate flow at the actual conversion(Row # 4 in table 6.9). As in reaction $K_2CO_3 + CO_2 + H_2O \leftrightarrow 2KHCO_3$, 2 moles of bicarbonate are formed per mole of carbonate, the bicarbonate flow is then given by the following equation

$$\text{Row \#5: } \dot{N}_{HCO_3^-} = 2\left(\dot{N}_{K_2CO_3\,o} - \dot{N}_{CO_3^{2-}}\right) \qquad \text{Equation 6.34}$$

Row #6 and #7: Both rows give the Henry's constant in $kPa\ m^3/\ kmol$ (Row 6) and in $psi\ L/mol$ (Row 7). The Henry's constant in the carbonate solution is assumed to be approximately the one in water[90]

$$Row\ \#6:\ H_{CO_2,water}(kPa\ m^3\ kmol^{-1}) = 2.8249 \cdot 10^6 \exp\left(\frac{-2044}{T}\right) \qquad \text{Equation 6.35}$$

$$Row\ \#7: H_{CO_2,water}(psi\ L\ mol^{-1})$$
$$= H_{CO_2,water}(kPa\ m^3\ kmol^{-1})\frac{dm^3\ mol^{-1}}{m^3\ kmol^{-1}}\frac{1MPa}{1000kPa}\frac{142.8\ psi}{1MPa} \qquad \text{Equation 6.36}$$

Row #8 and #9: Row #8 shows the concentration of carbon dioxide in solution ($CO_2(aq)$) and is calculated with the partial pressure of $CO_2$ and the Henry's constant. The partial pressure of $CO_2$ is calculated with the total pressure in the absorber given by the Bureau of Mines (300 psi) and the molar fraction of $CO_2$ in the scrubbed gas (Row # 5 in table 6.7)

$$Row\ \#8:\ [CO_2]\left(\frac{mol}{L}\right) = \frac{P_{CO_2}}{H_{CO_2,water}} = \frac{300psi \cdot \%CO_2, scrubbed\ gas/100}{H_{CO_2,water}(psi\ L\ mol^{-1})} \qquad \text{Equation 6.37}$$

Row #9 gives the molar flow of $CO_2$ in moles $CO_2$/h given by equation 6.38

$$Row\ \#9:\ \frac{moles\ CO_2}{h} = \frac{[CO_2]mol}{L} * \frac{3.79L}{gal} * gal/h \qquad \text{Equation 6.38}$$

Row #10: Once the flows of carbonate, bicarbonate and $CO_2$ are calculated, the equilibrium constant ($Keq$) of the $CO_2$ absorption with carbonate, $K_2CO_3 + CO_2 + H_2O \leftrightarrow 2KHCO_3$, is determined with equation 6.33 ($Keq = \frac{\dot{N}^2_{HCO_3^-}}{\dot{N}_{CO_3^{2-}}\dot{N}_{CO_2(aq)}}$). Consequently, the equilibrium constant at zero ionic strength ($K_{eq}{}^o$) can be calculated ($K_{eq}{}^o = K_{eq}\frac{\gamma_{CO_2}\gamma_{CO_3{}^{2-}}}{\left(\gamma_{HCO_3{}^-}\right)^2}$).However, in the validation of the pH model of the $H_2O$-Carbonate system in chapter 3 (Figure 3.14), we measured the pH vs. concentrations and proved our model using activity coefficients and ignoring them. We observed that the activity coefficients model is valid at concentrations of carbonate lower than 1M. At concentrations over 1M, there is a big deviation between the measured pH- concentration results and the estimated pH –concentration. At high concentrations, ignoring activity coefficients in the calculations gives better results. To check if the activity coefficient model could be used in the Bureau of Mines data, we calculated the concentration equivalent in mol/L (defined as the concentration in mol/L referring to a solution of zero conversion with only potassium carbonate and water present) with the following equation

$$[K_2CO_3]_{,eq} = \frac{moles\ K_2CO_3\ eq}{L} = \frac{percent\ equivalent\ K_2CO_3}{percent\ H_2O}\ \frac{1mol}{138\ g\ K_2CO_3}\ \frac{1000\ g\ H_2O}{1L}$$

The Percent equivalent $K_2CO_3$ data are taken from the Bureau of Mines Bulletin 597 (Row # 9 in table 6.7). Table 6.10 displays the concentration equivalent results

**Table 6.10 Concentration equivalent of carbonate for runs 6A to 8B from Bureau of Mines**

| | 6A | 6B | 7A | 8 | 8A | 8B |
|---|---|---|---|---|---|---|
| **Percent equivalent $K_2CO_3$(Data take from Bulletin 597) Bureau of Mines** | 36.2 | 38.9 | 40.5 | 38.7 | 38.4 | 35.8 |
| **$[K_2CO_3]_{eq}$(mol/L)** | 4.11 | 4.61 | 4.93 | 4.57 | 4.52 | 4.04 |

Based on table 6.10, we didn't take into account the activity coefficients in the equilibrium constant calculations. The bureau of mines works with concentrations around 4-5M and the activity coefficients model used is not reliable at these high concentrations.

Row #11: Finally, row #11 gives the equilibrium constant of the reaction of interest, the decomposition reaction of bicarbonate, $2KHCO_3 \leftrightarrow K_2CO_3 + CO_2 + H_2O$. The equilibrium constant of the decomposition of bicarbonate to give $CO_2$ and carbonate is the inverse of the equilibrium constant of the $CO_2$ absorption with carbonate given in the previous row.

**Table 6.11 Composition data in the spent and regenerated solutions and equilibrium constants of reactions $K_2CO_3 + CO_2 + H_2O \leftrightarrow 2KHCO_3$ and $2KHCO_3 \leftrightarrow K_2CO_3 + CO_2 + H_2O$**

| Row # | | 6A | 6B | 7A | 7B | 8 | 8A | 8B |
|---|---|---|---|---|---|---|---|---|
| 1 | **T bottom liquid(°F)** | 244 | 259 | 246 | 267 | 241 | 262 | 264 |
| 2 | **T liquid (K)** | 390.93 | 399.26 | 392.04 | 403.71 | 389.26 | 400.93 | 402.04 |
| 3 | **moles $K_2CO_3$ eq /h** | 376.33 | 446.77 | 562.22 | | 434.36 | 376.3 | 401.7 |
| 4 | **moles/h $K_2CO_3$ spent** | 165.59 | 192.11 | 275.49 | | | 165.57 | 156.66 |
| 5 | **moles/h $KHCO_3$ spent** | 421.49 | 509.32 | 573.46 | | | 421.46 | 490.08 |
| 6 | **$H_{CO2}$(kPa $m^3$/kmol)** | 15145 | 16891 | 15371 | 17870 | 14809 | 17254 | 17499 |
| 7 | **$H_{CO2}$(psi L/mol)** | 2162.6 | 2412.0 | 2194.9 | 2551.9 | 2114.8 | 2463.9 | 2498.9 |
| 8 | **mol/L $CO_2$ (aq)** | 2.26E-02 | 2.52E-02 | 1.76E-02 | 1.50E-02 | 2.20E-02 | 2.05E-02 | 1.50E-02 |
| 9 | **mol/h $CO_2$ (aq)** | 2.07 | 2.45 | 2.01 | 1.71 | 2.09 | 1.70 | 1.49 |
| 10 | **$K_{eq}$ $K_2CO_3 + CO_2 + H_2O \leftrightarrow 2KHCO_3$** | 518 | 552 | 594 | | | 630 | 1028 |
| 11 | **$K_{eq}$ $2KHCO_3 \leftrightarrow K_2CO_3 + CO_2 + H_2O$** | **1.93E-03** | **1.81E-03** | **1.68E-03** | | | **1.59E-03** | **9.73E-04** |

Observe that the flow of $CO_2$ dissolved mol of $CO_2$ /h(aq) calculated from Henry's law are so low compared to the moles of $CO_2$ reacted (moles/h $K_2CO_3$ regenerated minus moles/h $K_2CO_3$ spent ). The flow of $CO_2$ absorbed from the gas follow two paths, some reacts to produce carbonate and some stays in solution. However, the dissolved mol of $CO_2$ /h(aq) is so small that experimentally, it cannot be possible to see the difference between the moles absorbed from the gas and the moles of $CO_2$ reacted.

**Comparison of Bureau of Mines equilibrium constant with our experimental results**

The Van't Hoff equation obtained from our experiments (figure 5.30) relates ln $K_{eq}$ of the decomposition reaction of bicarbonate with 1/T is, $lnK_{eq} = -\frac{6618.9}{T} + 13.359$ .The equilibrium constant is related to the Gibbs free energy by equation $\Delta G \quad = -RTlnK_{eq}$

Table 6.12 shows the temperature in *K*, the natural logarithm of the equilibrium constant obtained from the Bureau of Mines data (Row #11 in Table 6.11) and the equilibrium constant obtained from the Van't Hoff equation, as well as the Gibbs free energies calculated from both equilibrium constants. Our thermodynamic values and Bureau of Mines values are compared.

**Table 6.12 Temperature in *K*, natural logarithm of the equilibrium constants obtained from the Bureau of Mines data and Van't Hoff equation and Gibbs free energies calculated from both equilibrium constants**

| | **6A** | **6B** | **7A** | **7B** | **8** | **8A** | **8B** |
|---|---|---|---|---|---|---|---|
| **T liquid (K)** | 390.93 | 399.26 | 392.04 | 403.71 | 389.26 | 400.93 | 402.04 |
| **ln $K_{eq}$ $2KHCO_3 \leftrightarrow K_2CO_3 + CO_2 + H_2O$ Bureau of Mines** | -6.25 | -6.31 | -6.39 | | | -6.45 | -6.94 |
| **ΔG $2KHCO_3 \leftrightarrow K_2CO_3 + CO_2 + H_2O$ Bureau of Mines data (kJ/mol)** | **20.32** | **20.96** | **20.82** | | | **21.48** | **23.18** |
| **ln $K_{eq}$ Van't Hoff equation** | -3.57 | -3.22 | -3.52 | -3.04 | -3.64 | -3.15 | -3.10 |
| **ΔG $2KHCO_3 \leftrightarrow K_2CO_3 + CO_2 + H_2O$ Van't Hoff (kJ/mol)** | **11.61** | **10.69** | **11.49** | **10.19** | **11.80** | **10.50** | **10.38** |

The natural logarithm of the equilibrium constant values (ln $K_{eq}$) calculated with the Bureau of Mines data is almost twice as large as our Van't Hoff values, and consequently the Gibbs free energy determined with the Bureau of Mines of $K_{eq}$ is double the Gibbs free energy obtained from the Van't Hoff values. The causes of the discrepancy could be due to assumptions we made: the Henry's constant used is calculated for $CO_2$ in water and we assumed the same value $CO_2$ in carbonate solution. Observe that if the affinity of the potassium carbonate solution is higher and can absorb twice as much $CO_2$, the Bureau of Mines equilibrium constant would be half the value listed in table 6.12. Also, the ionic effect is not taking into account in the Bureau of Mines calculation of the equilibrium constant. The reason of ignoring the ionic effect is the big deviation found in the validation of the activity coefficients model in chapter 3 when working at concentrations over 1M ( the Bureau of Mines work with 4-5 M solutions). In addition to this, Van't Hoff plot range of temperature (150 -320°C) does not cover the temperature of the hot absorption (around 120 °C) but it is close. Observe also that the temperature influence in the

Van't Hoff plot is very big. A small change in the temperature causes a big change in the $K_{eq}$ calculated from the Van't Hoff plot. Both models, nevertheless, predict that reaction $2KHCO_3 \leftrightarrow K_2CO_3 + CO_2 + H_2O$ is not spontaneous at temperatures around 120 °C. And therefore, it predicts that the backward reaction is spontaneous.

### *6.2.3 SUPCRT92*

The thermodynamic properties of reaction $2HCO_3^- \leftrightarrow CO_3^{2-} + CO_2(aq) + H_2O$ is also estimated by running the SUPCRT92 code (J. W. Johnson et al., 1992) developed in 1992 at UC Berkeley and LLNL to calculate standard thermodynamic properties of electrolytes. The temperature and pressure are specified in the code and it displays the thermodynamic properties values of the reaction

**Table 6.13 Thermodynamic properties values of reaction $2HCO_3^- \leftrightarrow CO_3^{2-} + CO_2(aq) + H_2O$ estimated by SUPCRT92 code**

| PRES(bars) | TEMP(°C) | ρH2O(g/cc) | LOG K | ΔG (cal) | ΔH (cal) | ΔS (cal/K) | ΔV (cc) | cp(cal/K) |
|---|---|---|---|---|---|---|---|---|
| 30 | 150 | 0.918 | -3.474 | 6727 | 3536 | -7.5 | -8.7 | 13 |
| 30 | 175 | 0.894 | -3.368 | 6906 | 3829 | -6.8 | -10.2 | 10.4 |
| 30 | 200 | 0.866 | -3.266 | 7071 | 4041 | -6.4 | -12.2 | 6.1 |
| 30 | 225 | 0.834 | -3.171 | 7228 | 4109 | -6.2 | -15.1 | -1.3 |
| 30 | 250 | 0.014 | *** BEYOND RANGE OF APPLICABILITY OF AQUEOUS SPECIES EQNS *** | | | | | |
| 30 | 275 | 0.013 | *** BEYOND RANGE OF APPLICABILITY OF AQUEOUS SPECIES EQNS *** | | | | | |
| 30 | 300 | 0.012 | *** BEYOND RANGE OF APPLICABILITY OF AQUEOUS SPECIES EQNS *** | | | | | |
| 40 | 150 | 0.919 | -3.473 | 6724 | 3539 | -7.5 | -8.7 | 13 |
| 40 | 175 | 0.894 | -3.366 | 6903 | 3834 | -6.8 | -10.2 | 10.5 |
| 40 | 200 | 0.867 | -3.265 | 7068 | 4049 | -6.4 | -12.2 | 6.3 |
| 40 | 225 | 0.835 | -3.169 | 7224 | 4122 | -6.2 | -15 | -1 |
| 40 | 250 | 0.799 | -3.084 | 7382 | 3977 | -6.5 | -19.4 | -10.7 |
| 40 | 275 | 0.018 | *** BEYOND RANGE OF APPLICABILITY OF AQUEOUS SPECIES EQNS *** | | | | | |
| 40 | 300 | 0.017 | *** BEYOND RANGE OF APPLICABILITY OF AQUEOUS SPECIES EQNS *** | | | | | |
| 50 | 150 | 0.92 | -3.472 | 6722 | 3542 | -7.5 | -8.6 | 13.1 |
| 50 | 175 | 0.895 | -3.365 | 6901 | 3839 | -6.8 | -10.2 | 10.5 |
| 50 | 200 | 0.867 | -3.263 | 7065 | 4056 | -6.3 | -12.1 | 6.4 |
| 50 | 225 | 0.836 | -3.168 | 7221 | 4135 | -6.2 | -14.9 | -0.7 |
| 50 | 250 | 0.8 | -3.082 | 7377 | 4000 | -6.4 | -19.3 | -10.2 |
| 50 | 275 | 0.024 | *** BEYOND RANGE OF APPLICABILITY OF AQUEOUS SPECIES EQNS *** | | | | | |
| 50 | 300 | 0.022 | *** BEYOND RANGE OF APPLICABILITY OF AQUEOUS SPECIES EQNS *** | | | | | |
| 60 | 150 | 0.92 | -3.471 | 6720 | 3546 | -7.5 | -8.6 | 13.2 |
| 60 | 175 | 0.896 | -3.364 | 6898 | 3844 | -6.8 | -10.1 | 10.6 |
| 60 | 200 | 0.868 | -3.262 | 7062 | 4063 | -6.3 | -12.1 | 6.6 |
| 60 | 225 | 0.837 | -3.166 | 7217 | 4148 | -6.1 | -14.9 | -0.4 |
| 60 | 250 | 0.801 | -3.08 | 7373 | 4023 | -6.4 | -19.2 | -9.7 |
| 60 | 275 | 0.759 | -3.006 | 7540 | 3699 | -7 | -25.7 | -13.6 |
| 60 | 300 | 0.028 | *** BEYOND RANGE OF APPLICABILITY OF AQUEOUS SPECIES EQNS *** | | | | | |

These results (negative log K) would clearly show the reaction favored to the left (bicarbonate formation), not to the right (bicarbonate dissociation); also, the temperature range (of validity) does not quite extend to 300 °C. However, our observations indicate the opposite behavior.

# CHAPTER 7. CONCLUSIONS

1) Our findings indicate that biocarbon can indeed undergo vigorous oxidation in an aqueous alkaline/carbonate environment at low to moderate temperatures and thus generate power in a fuel cell at efficiencies exceeding 80%.
2) We observed that seasoning of the charcoal before fuel cell operation is needed. The charcoal needs to be immersed in electrolyte under vacuum. The vacuum causes the air to leave the carbon pores and therefore, the electrolyte can penetrate the pore.
3) The electrolyte plays a key role in the carbon fuel cell creating a medium through which carbonate or hydroxide ions can travel from the cathode to the anode. In the aqueous alkaline fuel cell, the electrolyte consists of a liquid mixture that presents a good ionic conductivity.
   We tried different concentrations of hydroxides and carbonates electrolytes. We discovered that an aqueous-alkaline fuel cell working at 200 °C at 700 psi showed the best performance when solutions of high concentrations of potassium carbonate were used as electrolyte.
4) We studied the chemistry of the hydroxide and carbonate electrolyte at room conditions and at the fuel cell conditions. At room conditions, the chemistry of both hydroxide and carbonate electrolytes is governed by the acid-base equilibria. A model using activity coefficients based on Davies activity coefficient model fits the pH –concentration experimental data. The acid-base model is valid from 0 to 3M in the case of hydroxide electrolytes and for 0 to 1M for carbonate electrolytes. At the fuel cell conditions, the acid-base equilibria itself does not fit the pH-concentration for the carbonate electrolyte; the decomposition of bicarbonate reaction occurs, which explains the species concentrations observed.
5) At room temperature, we discovered that carbonate/bicarbonate solutions are very sensitive to the presence of $CO_2$ due to reaction $CO_3^{2-}+CO_2+H_2O\leftrightarrow 2HCO_3^-$. The atmospheric $CO_2$ shifts reaction to the right and acidifies the sample; on the other hand, we also observed that the exposure of the solution to vacuum shifts the reaction to the left as the $CO_2$ escapes to the gas phase and the sample becomes more alkaline. Therefore, the bicarbonate/carbonate solutions storage should be done by capping them in bottles with little dead air space to minimize its exposure to air and preserve the original solution.
6) We observed the decomposition of bicarbonate both in a dry atmosphere and in solution. The dry potassium bicarbonate decomposition was monitored via TG-MS performed by the Hungarian Academy of Science. The dry bicarbonate decomposition occurs between 150 to 240

°C when heating the potassium bicarbonate at a rate of 15 °C/min approx. In solution, we studied the decomposition of bicarbonate at temperatures from 150 to 320°C at its saturation pressure. The final experimental solution, analyzed by titration, showed conversions that ranged from 57.1 % (T= 150 °C) to 92 % (T= 320 °C). The titration analyses are consistent with the pH of the final solution at all temperatures but 320 °C. At 320 °C, the pH measurement indicates even higher decomposition. A Van't Hoff plot based on our experimental titration results shows that the bicarbonate decomposition reaction is endothermic; our Van't Hoff plot gives a reaction enthalpy of 50873. J/mol and shows a positive change in the entropy of the reaction, $\Delta S$ =111.06 J/mol K.

7) Our findings indicate that the carbon dioxide formed as the potassium bicarbonate decomposes in all the temperature range we worked (from 150 to 320 °C) is trapped primarily in an aqueous form instead of released as a gas. This conclusion is evident by the observed lack of pressure increase above the saturation pressure of just water when using $KHCO_3$ electrolyte in the pressure vessel.
8) The high conversions from bicarbonate to carbonate found at around the fuel cell conditions of temperature and pressure indicated the instability of bicarbonate ions and proved that the fuel cell electrolyte should not present any problem during operation.

## 7.1 Further work

The new design of the fuel cell (4th design in chapter 3) is being tested. The new fuel cell shows no mechanical problem and it shows a steady behavior during operation. However, we didn't succeed in getting high potentials. We monitored around 0.3 V at 250 °C and 800 psi working with 5M potassium carbonate and a silver catalyst. Higher temperatures, different catalysts and electrolytes need to be tested. Based on previous research, we are especially interested in using a Nickel catalyst and a mixture of potassium and lithium carbonate as electrolyte.

More work can also be done in the chemistry models. Activity coefficients were calculated based on Davies model, which is limited to low concentrations. The analytical pH-concentration data considering these activity coefficients showed a good fit in the experimental data at low carbonate concentrations. However, we are interested in higher concentrations. The Pitzer activity coefficients model is also going to be examined.

To verify the carbonate/bicarbonate chemistry at fuel cell conditions, we plan to reproduce the experiments in the near future. We need to check small discrepancies between the pH and titration methods. The pH of the final solution was tested right after the experiment. However, the titration of the solutions was performed months later and we cannot be sure that the sample storage changed the initial sample as the bicarbonate/carbonate solutions are very sensitive to the presence of $CO_2$. We expect to present the final results in May in San Francisco at the 10th International Symposium on Supercritical Fluids. A paper in this topic is also planned to be published.

# REFERENCES


1. *World Energy Outlook* OECD's International Energy Agency (IEA) 2009.
2. C J Winter, J Nitsch , and editors, *Hydrogen as an energy carrier: technologies, systems, economy.* New York: Springer-Verlag, 1988: p. 56-78.
3. Appleby, A.J. and F.R. Foulkes, *Fuel cell handbook.* New York: Van Nostrand Reinhold, 1989: p. 199-200.
4. *Carbon trust to explore opportunities to cut carbon and support UK business in China.* http://www.carbontrust.com/EN?CECIC.aspx.
5. Liebhafsky, H.A. and E.J. Cairns, *Fuel Cells and Fuel Batteries*. 1968, New York: J. Wiley & Sons.
6. Vielstich, W., *Fuel Cells.* 1965, London: Wiley-Interscience. 501.
7. Cherepy, N.J., et al., *Direct Conversion of Carbon Fuels in a Molten Carbonate Fuel Cell.* J. Electrochem. Soc., 2005. **152**: p. A80-A87.
8. J.F.Cooper, *Proceedings of the Second International Conference on Fuel Cell Science Engineering and Technology* Rochester, NY, United States, June 14–16 (2004): p. 375–385.
9. *International Energy Outlook.* http://www.eia.doe.gov/oiaf/ieo/coal.html, 2009.
10. Cao, D., Y. Sun, and G. Wang, *Direct carbon fuel cell: fundamentals and recent developments.* Power Sources, 2007. **167**: p. 250-257.
11. Giddey, S., S.P.S. Badwal, and A. Kulkarni, *A Comprehensive Review of Direct Carbon Fuel Cell Technology.* Progress in Energy and Combustion Science, 2011.
12. Nunoura, T., et al., *Performance of a First-Generation, Aqueous-Alkaline Biocarbon Fuel Cell.* Ind. Eng. Chem. Res., 2007. **46**: p. 734-744.
13. Antal, M.J. and G.C. Nihous, *Thermodynamics of an Aqueous-Alkaline/Carbonate Carbon Fuel Cell.* Ind. Eng. Chem. Res., 2008. **47**: p. 2442-2448.
14. Lehman, R.L. and J.S. Gentry *Thermal Stability of Potassium Carbonate Near Its Melting Point.* Thermochimica Acta 1998.
15. Anon., *Grove, Sir William Robert.* Encyclopaedia Britannica Deluxe edition, CD-ROM, 2001.
16. Jacques, W.W., *Method of Converting Potential Energy of Carbon into Electrical Energy*. 1896: U.S.A.
17. Broers, G., *High temperature galvanic fuel cells.* Doctoral thesis, University of Amsterdam, 1958.
18. Selman, J.R., Power Sources 160, 2006: p. 852-857.
19. Weaver, R.D., et al., *Direct Electrochemical Generation of Electricity from Coal*. 1979, SRI: Menlo Park, CA 94025.
20. Vutetakis, D.G., D.R. Skidmore, and H.J. Byker, J. Electrochem. Soc., 1987. **134**: p. 3027.
21. Cooper, J.F., *Direct Conversion of Coal Derived Carbon in Fuel Cells*, in *Recent Trends in Fuel Cell Science and Technology*, S. Babu, Editor. 2006, Anamaya Publishers: New Delhi. p. 246-264.
22. Peelen, W.H.A., et al., Appl. Electrochem, 2000. **30**: p. 1389-1395.
23. Steinberg, M., Hydrogen Energy 31: p. 405-411.
24. Li, X., et al., *Power Sources 186.* 2009: p. 1-9.
25. Li, H., Q. Liu, and Y. Li, *Electrochim.* 2010. **Acta 55**: p. 1958-1965.
26. Chen, M., et al., Hydrogen Energy 35, 2010: p. 2732-2736.
27. Cao, D., et al., Hydrogen Energy 35, 2010: p. 1778-1782.
28. Zecevic, S., E.M. Patton, and P. Parhami, *Carbon-air fuel cell.* Carbon, 2004. **42**: p. 1983-1993.
29. Edison, T.A., US 460,122, 1891.

30. Hackett, G.A., J.W. Zondlo, and S. R, *Power Sources 168.* 2007: p. 111-118.
31. Nakagawa, N. and M. Ishida, Ind.Eng.Chem.Res. 27, 1988: p. 1181-1185.
32. Li, S., et al., *Solid State Ionics 179.* 2008: p. 1549-1552.
33. Gur, T.M., M. Homel, and A.V. Virkar, Power Sources 195, 2010: p. 1085-1090.
34. Liu, R., et al., Power Sources 195, 2010: p. 480-482.
35. Kim, J., et al., Power Sources 160: p. 7578-7573.
36. Ihara, M., et al., *Solid State Ionics 175.* 2004: p. 51-54.
37. Saito, H., S. Hasegawa, and M. Ihara, Electrochem. Soc.153, 2006: p. B443-B447.
38. Hasegawa, S. and M. Ihara, electrochem. Soc.155, 2008: p. B58-B63.
39. Gur, T.M. and R.A. Huggins, *Direct Electrochemical Conversion of Carbon to Electrical Energy in a High Temperature Fuel Cell.* J. Electrochem. Soc., 1992. **139**(10): p. L95-L97.
40. Dubois, J., J. Millet, and S. Palous, Electrochimica Acta, 1967. **12**: p. 241.
41. Plambeck, J.A., *Fused salt systems.* Encyclopedia of electrochemistry of the elements, 10 New York, 1987: p. 283-318.
42. Goret, J. and B. Tremillon, Electrochim Acta, 1967. **12**: p. 1065-1083.
43. Nabae, Y., K.D. Pointon, and J.T.S. Irvine, *Electrochemical oxidation of solid carbon in hybrid DCFC with solid oxide and molten carbonate binary electrolyte.* Energy & Environmental Science, 2008. **1**: p. 148-155.
44. Chuang, S.S.C., *Carbon-based fuel cell.* Akron, 2006.
45. Balachov, I.I., et al., *Presented in Fuel Cell Seminar, Direct Carbon Fuel Cell Workshop.* Proceedings online:http://www.fuelcellseminar.com/pdf/Direct_Carbon_Fuel_Cell_Workshop/Balachov_Iouri.pdf Palm Springs, CA, USA, , 2005: p. 14th November.
46. Lipilin, A.S., et al., US Pat. Appl. No. 20060019132 2006.
47. Bockris, J.O.M. and S. Srinivasan, *Fuel Cells: Their Electrochemistry.* 1969, New York: McGraw-Hill Book Co. 659.
48. Emrich, W., *Handbook of Charcoal Making*. 1985, Dordrecht: Reidel.
49. Mochidzuki, K., et al., *Electrical and Physical Properties of Carbonized Charcoals.* Ind. Eng. Chem. Res., 2003. **42**: p. 5140-5151.
50. Antal, M.J. and M.G. Gronli, *The Art, Science, and Technology of Charcoal Production.* Ind. Eng. Chem. Res., 2003. **42**: p. 1619-1640.
51. Dai, X. and M.J. Antal, Jr., *Synthesis of a High-Yield Activated Carbon by Air Gasification of Macadamia Nut Shell Charcoal.* Ind. Eng. Chem. Res., 1999. **38**: p. 3386-3395.
52. Tam, M.S. and M.J. Antal, Jr., *Preparation of Activated Carbons from Macadamia Nut Shell and Coconut Shell by Air Activation.* Ind. Eng. Chem. Res., 1999. **38**(11): p. 4268-4276.
53. Conesa, J.A., M. Sakurai, and M.J. Antal, *Synthesis of a High-Yield Activated Carbon by Oxygen Gasification of Macadamia Nut Shell Charcoal in Hot, Liquid Water.* Carbon, 2000. **38**(6): p. 839-848.
54. Tam, M.S., et al., *Activated Carbon from Macadamia Nut Shell by Air Oxidation in Boiling Water.* Ind. Eng. Chem. Res., 2001. **40**(2): p. 578-588.
55. Antal, M.J., et al., *Review of Methods for Improving the Yield of Charcoal from Biomass.* Energy Fuels, 1990. **4**: p. 221-225.
56. Antal, M.J., C. DeAlmeida, and W.S.-L. Mok, *A New Technology for Manufacturing Charcoal from Biomass*, in *Proceedings of the IGT Conference on Energy from Biomass & Wastes XV*, D.E. Klass, Editor. 1991, Institute for Gas Technology: Chicago. p. 521-530.
57. Antal, M.J., et al., *High-Yield Biomass Charcoal.* Energy Fuels, 1996. **10**(3): p. 652-658.
58. Antal, M.J., et al., *Attainment of the theoretical yield of carbon from biomass.* Ind. Eng. Chem. Res., 2000. **39**(11): p. 4024-4031.

59. Nunoura, T., et al., *Studies of the Flash Carbonization Process. 1. Propagation of the Flaming Pyrolysis Reaction and Performance of a Catalytic Afterburner.* Ind. Eng. Chem. Res., 2006. **45**: p. 585-599.
60. Antal, M.J., K. Mochidzuki, and L.S. Paredes, *Flash Carbonization of Biomass.* Ind. Eng. Chem. Res., 2003. **42**: p. 3690-3699.
61. Anbar, M., *Methods and Apparatus for the Pollution-Free Generation of Electrochemical Energy*. 1973, Stanford Research Institute: USA.
62. Dickson, A.G. and C. Goyet, *Handbook of methods for the analysis of the various parameters of the carbon dioxide system in sea water; version 2.* ORNL/CDIAC-74, , 1994.
63. Millero, F.J., *Thermodynamics of the carbon dioxide system in the oceans.* Geochim. Cosmochim. Acta, 59, 1995: p. 661-677.
64. Stumm, W. and J.J. Morgan, *Aquatic Chemistry 2d ed.* New York: Wiley, 1981: p. 204-206.
65. http://cdiac.ornl.gov/, *Carbon Dioxide Information Analysis Center.* U.S. Department of Energy, 2012.
66. Butler, J.N., *Carbon dioxide equilibria and their applications*. 1992, Chelsea, MA: Lewis Publishers Inc. 259.
67. Field, J.H., et al., *Pilot-Plant Studies of the Hot-Carbonate Process for removing Carbon Dioxide and Hydrogen Sulfide.* Bureau of Mines Bulletin 597, 1962.
68. Davies, C.W., *Ion Association. London.* Butterworths, 1962: p. 37–53.
69. Sillen, L.G. and A.E. Martell, *Stability constants. Special publ. no.17 (1964) and 25 (1971).* London: The Chemical Society.
70. Ellis , A.J. and R.M. Golding *Am. J. Sci.* 1963. **261**: p. 47-60.
71. Malinin, S.D., Geokhimiya 1959. **3**: p. 235-245.
72. Takahashi, T., et al., *Global sea-air CO2 flux based on climatological surface ocean pCO2 and seasonal biological and temperature effects.* Deep-Sea Research (Part II, Topical Studies in Oceanography), 2002. **49, 9-10**: p. 1601-1622.
73. Cohen, P., *The ASME handbook on Water Technology for Thermal Power Systems.* The American Society of Mechanical Engineers, 1989: p. 442.
74. *Solubility Database - International Union of Pure and Applied Chemistry / National Institute of Standards and Technology.*
75. Bandura, A.V. and S.N. Lvov, *The Ionization Constant of Water over Wide R, anges of Temperature and Density.* http://www.nist.gov/data/PDFfiles/jpcrd696.pdf, 2005.
76. Wiebe, R. and V.L. Gaddy, *The Solubility of Carbon Dioxide in Water at Various Temperatures from 12 to 40° and at Pressures to 500 Atmospheres. Critical Phenomena.* American Chemical Society, 1940. **62 (4)**: p. 815–817.
77. Denbigh, K., *The principles of Chemical Equilibrium.* Cambridge University Press.
78. Ulrich Grigull, J.S., Peter Schiebener, *Steam Tables in SI-Units Wasserdampftafeln.* Springer-Verlag Berlin Heidelberg New York Tokyo, 1984.
79. Butler, J.N., *Carbon dioxide equilibria and their applications.* Chelsea, MA: Lewis Publishers Inc. 259., 1992.
80. Ellis, A.J. and R.M. Golding, Am. J. Sci., 1963. **261**: p. 47-60.
81. Blitz, A., *Experimental Analysis Of An Undesirable Crystal Precipitate In A Developmental Carbon Fuel Cell.* A thesis submitted to the global environmental science undergraduate division in partial fulfillment of the requirements for the degree of Bachelor of Science in Global Environmental Science. University of Hawaii at Manoa, 2011.
82. Lichwa, J., *Determination of Carbohydrates,HMF,and Furfural in Biomass by HPLC.* Renewable Resources Research Laboratory,Hawaii Natural Energy Institute, 1999: p. D-2.

83. Eaton, A.D., L.S. Clescer, and A.E. Greenberg, *Standard Methods for the Examination of Water and Wastewater.* American Public Health Association; American Water Works; Water Environment Federation: Hanover, Maryland, 1995.
84. http://www.titrations.info/acid-base-titration-sodium-hydroxide-and-carbonate.
85. Craig, N.C., *Entropy Analysis*. 1992, New York: Wiley-VCH. 208.
86. Barner, H.E. and R.V. Scheuerman, *Handbook of Thermochemical Data for Compounds and Aqueous Species*. 1973, New York: Wiley-Interscience.
87. Atkins, P. and De Paula, *Physical Chemistry.* W.H. Freeman and Company., 2006: p. 212.
88. Haupin, W.E. and W.B. Frank, *Comprehensive treatise of electrochemistry, Electrochemical processing.* Plenum Press, New York. **2**: p. 301-325.
89. Antropov, A.I. and D.A. Tkalenko, *Elektrokhimiya.* 1970. **6**: p. 595-596.
90. Zhang, Y.C., Chau-Chyun, *Thermodynamic Modeling for CO2 Absorption in aqueous MDEA Solution with Electrolyte NRTL model.* Ind.Eng.Chem., 2010.